

POLITECNICO DI MILANO

Facoltà di Ingegneria Industriale e dell'Informazione

Master Degree in Biomedical Engineering



**Whole-brain analysis of resting state functional networks: a 3T
fMRI twin study**

Advisor:

Anna Maria Bianchi

Co-Advisor:

Eleonora Maggioni

Sergio Cerutti

Paolo Brambilla

Thesis Work by:

Emma Tassi

matr. 899522

Academic Year 2019/2020

*A mia mamma e mio papà,
alle mie sorelle Bianca e Sofia,
a Tiziano.*

Ringraziamenti

La presente tesi è stata svolta presso il Dipartimento di Elettronica, Informatica e Bioingegneria **B³** Lab (Biosegnali-Bioimmagini-Bioinformatica) del Politecnico di Milano. In collaborazione con la Fondazione IRCCS Ca' Granda Ospedale Maggiore Policlinico di Milano.

Vorrei per prima ringraziare la mia Relatrice Prof.ssa Anna Maria Bianchi, per i suoi fondamentali consigli e per l'opportunità che mi ha dato di svolgere questo affascinante lavoro sull'analisi di immagini biomediche, di funzionalità delle reti neurali e di analisi di effetti genetici e ambientali relativi allo studio di gemelli.

Un ringraziamento particolare va alla Dott.ssa Ing. Eleonora Maggioni, correlatrice di questa tesi, senza il suo aiuto non sarei riuscita a raggiungere l'obiettivo di questo lavoro. La ringrazio infinitamente per i suoi consigli, la sua completa disponibilità, il suo entusiasmo e le sue rassicurazioni, ma soprattutto per la passione per la ricerca in questo campo che mi ha trasmesso in questi mesi durante lo sviluppo di questa tesi.

Vorrei inoltre ringraziare il Professor Sergio Cerutti e il Professor Paolo Brambilla, anche loro correlatori di questa tesi, per i loro utili consigli.

Infine vorrei ringraziare la mia famiglia, mia mamma Anna mio papà Sandro ai quali devo la possibilità di aver studiato in questo eccezionale Ateneo. Vi ringrazio per avermi sempre supportato in tutto con tanta pazienza ed aver sempre creduto in me e nella mia tenacia. Ringrazio le mie sorelle Bianca e Sofia per essermi sempre state vicine ed avermi sempre supportato e sopportato anche nei momenti più difficili.

Infine ringrazio il mio ragazzo Tiziano, per i suoi consigli, per la sua pazienza, per credere sempre in me e per il suo infinito incoraggiamento per tutto quello che faccio.

Abstract

In the last two decades, resting-state functional Magnetic Resonance Imaging (rs-fMRI) has become an extremely popular technique in the field of neuroimaging, as it can measure the spontaneous, low frequency fluctuations that appear in the BOLD signal (Blood Oxygen Level Dependent) used to investigate and analyse the functional architecture of the brain. The present thesis deals with the analysis of a big rs-fMRI dataset collected from a unique sample of young Italian twins. The experimental work has involved the implementation of methods for pre-processing and cleaning of the fMRI data and for the subsequent extraction of meaningful information on the brain network topology.

Indeed, BOLD fMRI data are influenced by endogenous and exogenous non-neural processes that can affect the quality of the data obtained during resting-state experiment. Thus, “data denoising” represents a crucial step that influences the reliability of the subsequent fMRI data analyses. Spatial independent component analysis (ICA) has emerged as a valid alternative to regression analyses for fMRI clean up. The issue in the use of sICA for fMRI data cleaning is to accurately classify Independent Components (ICs) into noise and signal components. A classically and still widely used method is the manual classification of ICs. Recently numerous methods, based on different kinds of classifiers, have also been developed to automatically and selectively identify and remove noise-related ICs from fMRI data. Nevertheless, the application of these new tools is not always straightforward and might require big fMRI datasets for training. In this context, one part of this experimental thesis work is related to the development of a novel, fast and easy-to-use tool for subject-level ICA-based identification of fMRI artefacts. This novel tool can be used to advance from a slow, manual labelling of ICs to a fast, semi or fully automatic identification of noise-related ICs.

The newly developed fMRI cleaning tool has been validated on an exemplar dataset and used in the processing pipeline of a big rs-fMRI dataset collected from 43 young couples of twins. Another, relevant focus of the present thesis regards the investigation of the brain mechanisms underlying the “resting state”, from which significant information on brain pathophysiology can be extracted. As has been said, fMRI images acquired during rest can be analysed to extract quantitative measures of the functional connectivity between brain

regions based on temporal synchronization of spontaneous fluctuating rs-fMRI signals. Our understanding of large-scale functional brain networks has been revolutionized by the use of rs-fMRI. Indeed, during resting-state condition is possible to observe the human brain organized in multiple large-scale networks called resting-state networks (RSNs) associated to specific brain function. The human brain is active during rest condition and hierarchically organized into intrinsic functional networks. These functional networks are largely established early in development, then passing from childhood to adolescence is possible to report a more distributed organization. It remains a challenge studying the genetic and environmental influences on these functional brain networks and how such effects dynamically interact during the growth of the subject. In the last years, it has been introduced the idea that the analysis of RSNs and their topological characteristics can potentially be used to investigate functional connectivity changes that occur in the subjects during their development. In this context, the analysis of fMRI datasets from twin samples offers the unique opportunity of studying the heritability associated to RSNs, to evaluate the genetic bases of functional brain networks and the associated topological characteristics.

Heritability represents the quantification of the overall phenotypic variation – in this case brain network functional variability - that is attributable to genetic factors. The application of heritability estimates is a medium for defining boundaries for the ability of genetics to predict disease and determine disease risks that can affect brain function. However, the critical investigation relies also on the examination of genetic and environmental impact on RSNs and their topological parameters. Twin studies provide an excellent platform for the analysis of genetic and environmental impact on a certain phenotype, taking advantage of the assumption that monozygotic twins carry identical genome, while dizygotic twins carry genome approximately 50% in common.

The aim of the present study is to utilize statistical twin methods to investigate the cerebral function “in vivo” and provide insights into the extent of genetic and environmental effects on brain functional characteristic. After the optimized pre-processing and cleaning of the entire rs-fMRI dataset, we apply a Seed-based Functional connectivity analysis to estimate the functional connectivity established between brain regions. Firstly, is applied the parcellation of fMRI volumes based on AAL atlas, obtaining the region of interests (ROI) of the brain to be analysed. The ROIs that we extract, behave as nodes of the dynamic

brain networks. Then, follows the ROI BOLD signal extraction by which we obtain the time series of the BOLD signal associated to each ROI. The BOLD time series of each ROI represents the dynamics of the voxels within the ROI. Subsequently, we use the BOLD time series of each ROI to obtain the Functional Connectivity matrices of Cross-Correlation, by applying the Pearson's linear correlation coefficient between ROIs time series, and the Mutual Information matrix, obtained by calculating the Mutual information shared between ROIs time series. These two Functional Connectivity matrices represent the link-level parameters of the brain network, whose matrix elements indicate the functional connectivity links between couple of ROIs. Subsequently, a set of network-level and node-level topological parameters of the functional brain networks is estimated from the functional connectivity matrix of Cross-Correlation, for all subjects across monozygotic (MZ) and dizygotic (DZ) twin pairs. Then, the similarity of each topological parameter - extracted at the level of network, node or link between nodes – within each couple of twins was evaluated. This similarity analysis was separately performed on MZ and DZ couples separately by extracting the correlation between the values of the topological parameter across MZ/DZ couples at net of Age and Sex of the twin couples. This results in the estimation of intra-pair correlation values for MZ and DZ couples, r_{MZ} and r_{DZ} , which are used to estimate the rates of genetic and environmental influences on the considered topological parameter using twin models. Based on the comparison between r_{MZ} and r_{DZ} values, the most appropriate twin model was selected and if possible, used to estimate the genetic and environmental contributions, including also measures of heritability for each functional brain network parameter. The Fisher's z-test was employed to assess the heritability significance starting from the correlation difference between MZ and DZ couples, associated to each topological parameter.

In parallel, we evaluated possible effects of sex and age on the level of intra-pair similarity of the topological parameters at net of zygosity effect. Using multiple linear regression models, the intra-pair difference of each topological parameter was modelled in terms of zygosity, age and sex. This last analysis wants to capture whether age and sex can influence the difference of each topological parameter in the twin couples.

From the intra-pair similarity analysis, we notice that the intra-pair correlation of each topological parameters between MZ couples results always higher than the intra-pair correlation evaluated between DZ couples. The higher intra-pair correlation differences

between MZ and DZ couples have been found associated to the Mutual Information value between ROIs. This result suggests the hypothesis that functional connectivity between ROI based on non-linear interactions was characterized by a high genetic influence.

Regarding the analysis of genetic and environmental influences, we couldn't analyse Epistatic Effect or apply any twin model to the network-level parameter, due to the fact that all associated rDZ result negative, probably due to the low sample size.

Otherwise, the genetic effects created by Epistasis result to be present in almost all functional connectivity links of the matrix of Mutual Information and Cross-correlation. On the other side, functional connectivity links between ROI couples, based on Mutual Information, result to be more suitable for genetic and environmental analysis based on the application of twin model and also to be associated to higher value of heritability, with respect to functional connectivity links of Cross-Correlation matrix.

The genetic and environmental analysis is also applied on node-level parameters. For the majority of the nodes of node-level parameters that result suitable for twin model's application, we notice an influence of the non-shared environment higher than 70%.

From the quantitative analysis on the intra-pair correlation difference between MZ and DZ couples, we found a higher number of significant intra-pair correlation differences for the nodes and functional connectivity links associated to an Epistatic effect. In addition, functional connectivity links based on Mutual Information show higher number of significant intra-pair correlation difference with respect to Cross-Correlation links.

From the last analysis related to the significant effect of sex and age on the intra-pair difference of each topological parameter, we do not find a significant effect of age or sex on the intra-pair difference of the network-level and link-level parameter. On the contrary, we have seen a significant effect of age and sex on the intra-pair similarity of node-level parameter. For the majority of the nodes we have found a negative correlation value between the age of the twin couple and the intra-pair difference of the node-level parameter, indicating a rise of intra-pair similarity for most of the node-level parameter by increasing the age of the twin couple.

In conclusion, this experimental work of thesis has addressed the main technical challenges associated with both pre-processing and analysis of rs-fMRI data. A complete analysis

pipeline has been implemented for the quantitative investigation of functional connectivity networks that have emerged to be active in the brain during the resting state condition, based on the extraction of a high number of network-, node- and link-level parameters. We consider this work of thesis an improvement for brain functional connectivity and topological parameter analyses applied to twin studies.

We believe also that the obtained results can provide interesting insights into genetic and environmental effects on the functionality of brain networks that can be of great impact in clinical settings, unveiling important mechanisms underlying the onset of psychiatric and neurological illnesses.

Keywords - *twins, monozygote (MZ), dizygote (DZ), resting-state fMRI, brain functionalities, ICA, heritability, genetic influence, environmental influence, functional brain networks, network topological parameter*

Sommario

Negli ultimi anni le tecniche relative all'acquisizione di immagini funzionali del cervello (fMRI) ottenute durante la condizione di resting-state del paziente, hanno acquisito popolarità nel campo del Neuroimaging. Grazie a queste tecniche è stato possibile misurare le oscillazioni spontanee a bassa frequenza che compaiono nel segnale BOLD (Blood Oxygenation Level Dependent) utilizzate per indagare e analizzare l'architettura funzionale della rete cerebrale. Tuttavia, i dati ottenuti tramite tecniche fMRI sono influenzati da processi non-neuronali endogeni ed esogeni che possono incidere sulla qualità delle immagini acquisite. Pertanto, l'eliminazione delle componenti artefattuali dai dati rappresenta un passaggio cruciale che influenza l'affidabilità e la correttezza dei successivi passaggi di elaborazione dei dati. Una valida alternativa ai metodi di regressione applicati per la pulizia dei dati fMRI è risultata essere l'analisi spaziale delle componenti indipendenti (ICA). Un punto chiave nell'uso della tecnica sICA per la procedura di pulizia dei dati, è la classificazione accurata delle componenti indipendenti (ICs) in componenti artefattuali o componenti di effettivo segnale. Il metodo classico, e ancora ampiamente utilizzato, è la classificazione manuale delle ICs. Recentemente sono stati sviluppati numerosi metodi, basati su diversi tipi di classificatori, per identificare e rimuovere selettivamente le ICs associate a componenti artefattuali presenti nei dati fMRI. Tuttavia l'applicazione di tali metodi non è sempre semplice e potrebbe richiedere l'utilizzo di grandi set di dati fMRI. A questo proposito, una parte di questo lavoro di tesi sperimentale è stata dedicata allo sviluppo di un nuovo, facile e intuitivo metodo di identificazione di componenti artefattuali nei dati fMRI, basandosi sulla tecnica ICA. Questo nuovo tool può essere utilizzato per progredire da un'etichettatura manuale, lenta delle ICs ad una identificazione più rapida, che può essere semi- o completamente automatica, delle ICs che non rappresentano un effettivo segnale neuronale di interesse.

Il nuovo metodo di pulizia dei dati fMRI è stato validato su un dataset di esempio e successivamente utilizzato per l'elaborazione di un dataset rs-fMRI raccolto da 43 giovani coppie di gemelli.

Un'altra parte rilevante da sottolineare in questo lavoro di tesi è relativa alla condizione di resting-state assunta dal paziente utilizzata per acquisire i dati fMRI, tenendo conto che da questa condizione è possibile estrarre informazioni significative. Come è stato

precedentemente detto, le immagini funzionali del cervello acquisite durante la condizione di resting-state sono associate a misure di connettività funzionale tra regioni cerebrali caratterizzate dalla sincronizzazione temporale di segnali resting-state fMRI spontanei e oscillanti. La conoscenza delle reti cerebrali funzionali su larga scala è stata rivoluzionata dall'uso della risonanza magnetica funzionale acquisita in tali condizioni di riposo del paziente.

Infatti, durante lo stato di resting-state è possibile osservare l'organizzazione cerebrale in più reti su larga scala chiamate reti dello stato di resting-state (RSNs), ognuna delle quali associata a specifiche funzioni cerebrali. Il cervello umano è quindi attivo durante le condizioni di riposo (resting-state) del paziente, e tende ad assumere un'organizzazione gerarchica formando reti funzionali intrinseche (RSNs). Queste reti funzionali sono formate in gran parte nella fase iniziale dello sviluppo del soggetto. Il passaggio dall'infanzia all'adolescenza in genere segna un cambiamento fondamentale nell'organizzazione di tali reti, che risultano infine avere un'organizzazione più solida. Un passo importante nella ricerca rimane lo studio delle influenze genetiche e ambientali legate a tali reti di connettività funzionale e del loro possibile sviluppo durante la crescita del soggetto. Negli ultimi anni è stata introdotta l'idea che l'analisi delle RSNs e delle loro caratteristiche topologiche possa essere potenzialmente utilizzata per studiare il cambiamento di connettività funzionale che si verifica nei soggetti durante lo sviluppo.

In questo contesto, l'analisi dei dataset fMRI ottenuti da campioni di coppie di gemelli offre l'opportunità unica di studiare l'ereditarietà associata alle RSN, di valutare le basi genetiche delle reti funzionali cerebrali e le caratteristiche topologiche associate.

L'ereditarietà indica la stima quantitativa della variazione fenotipica complessiva che è attribuibile a fattori genetici. Le stime di ereditabilità rappresentano un mezzo per definire i limiti della genetica nel prevedere una determinata malattia e determinare il rischio di un possibile effetto alle funzionalità cerebrali creata da tale malattia. Tuttavia, la parte critica dell'indagine si basa sull'analisi dell'impatto genetico e ambientale sulle RSNs e sui relativi parametri topologici. Gli studi relativi ai gemelli ci forniscono una ottima base per l'analisi dell'impatto genetico e ambientale su un determinato fenotipo, sfruttando il presupposto che i gemelli monozigoti sono caratterizzati da un genoma identico, mentre i gemelli dizigoti presentano un genoma equivalente al 50%. Lo scopo di questo lavoro di tesi è di utilizzare i metodi statistici applicati nello studio dei gemelli per studiare "in vivo"

le funzioni cerebrali e approfondire l'entità degli effetti genetici e ambientali sulle caratteristiche funzionali del cervello. Dopo la pre-elaborazione e l'ottimizzazione della pulizia dell'intero dataset rs-fMRI, è stata applicata un'analisi di connettività funzionale basata su tecniche Seed-based per stimare la connettività funzionale stabilita tra regioni del cervello. In primo luogo, viene applicata la parcellizzazione dei volumi fMRI utilizzando l'atlante AAL, che permette di ottenere le regioni d'interesse (ROI) del cervello da analizzare. Le ROI che estraiamo rappresentano i nodi delle dinamiche reti cerebrali. Alla parcellizzazione dei volumi fMRI, segue l'estrazione del segnale ROI BOLD con cui otteniamo le serie temporali associate a ciascuna ROI. Le serie temporali del segnale BOLD associata a ciascuna ROI rappresentano la dinamica associata a tutti i voxel che compongono la ROI. Successivamente, abbiamo utilizzato le serie temporali del segnale BOLD estratte per ogni ROI, per ottenere le matrici di connettività funzionale della Cross-Correlation, stimata calcolando il coefficiente di correlazione lineare di Pearson tra le serie temporali di coppie di ROI, e la matrice di Mutua Informazione, ottenuta calcolando la mutua informazione (informazione condivisa) tra le serie temporali di una coppia di ROI. Queste due matrici di connettività funzionale rappresentano i parametri a livello di link tra regioni della rete cerebrale. Gli elementi della matrice indicano le connessioni di connettività funzionale tra coppie di ROI. Successivamente, sono stati estratti dalla matrice di connettività funzionale di Cross-Correlazione una serie di parametri topologici a livello di rete e a livello di nodo della rete cerebrale, per tutti i soggetti e per tutte le coppie di gemelli monozigoti (MZ) e dizigoti (DZ). È stata poi valutata la somiglianza di ciascun parametro topologico - estratto a livello di rete, nodo o collegamento (link) tra nodi - all'interno di ciascuna coppia di gemelli. Questa analisi di somiglianza è stata eseguita separatamente su coppie MZ e DZ separatamente estraendo la correlazione tra i valori del parametro topologico attraverso le coppie MZ / DZ al netto di età e sesso delle coppie. Dopo tale analisi abbiamo ottenuto una stima dei valori di correlazione intra-coppia per coppie MZ e DZ, r_{MZ} e r_{DZ} , che vengono utilizzati per stimare le influenze genetiche e ambientali che agiscono sul parametro topologico considerato, utilizzando modelli statistici gemellari. Sulla base del confronto tra i valori r_{MZ} e r_{DZ} , è stato selezionato il modello gemellare più appropriato e, se possibile, utilizzato per stimare i contributi genetici e ambientali, comprese anche le misure di ereditabilità per ciascun parametro funzionale della rete cerebrale. Il test z di Fisher è stato impiegato per valutare la significatività

dell'ereditarietà a partire dalla differenza di correlazione tra coppie MZ e DZ, associata a ciascun parametro topologico.

Parallelamente, abbiamo valutato i possibili effetti del sesso e dell'età sul livello di somiglianza intra-coppia dei parametri topologici, al netto dell'effetto della zigosità della coppia di gemelli. Utilizzando più modelli di regressione lineare, la differenza intra-coppia di ciascun parametro topologico è stata modellata in termini di zigosità, età e sesso.

Quest'ultima analisi vuole capire se l'età e il sesso della coppia possono influenzare la differenza di ciascun parametro topologico nelle coppie gemelle.

Dall'analisi di somiglianza intra-coppia, notiamo che la correlazione intra-coppia di ciascun parametro topologico tra coppie MZ risulta sempre superiore alla correlazione intra-coppia valutata tra coppie DZ. Le differenze di correlazione intra-coppia più elevate tra le coppie MZ e DZ sono state trovate associate al valore di Mutua Informazione calcolata tra ROI. Quest'ultimo risultato suggerisce l'ipotesi che la connettività funzionale tra ROI, basata su interazioni non lineari, fosse caratterizzata da un'alta influenza genetica.

Per quanto riguarda l'analisi delle influenze genetiche e ambientali, non siamo stati in grado di analizzare l'effetto epistatico o applicare alcun modello statistico gemellare al parametro a livello di rete, a causa della negatività dei valori r_{DZ} di ciascun parametro a livello di rete. La negatività dei coefficienti r_{DZ} può essere dovuta alla ridotta dimensione del campione di analisi.

Invece, gli effetti genetici creati dall'epistasi risultano essere presenti in quasi tutti i link di connettività funzionale della matrice di Mutua Informazione e di Cross-Correlazione. I link di connettività funzionale tra coppie ROI, basate su Mutua Informazione, risultano essere più adatti all'analisi genetica e ambientale basata sull'applicazione dei modelli statistici gemellari e associati ad un valore più elevato di ereditarietà, rispetto ai link di connettività funzionale della matrice di Cross-Correlazione.

L'analisi genetica e ambientale viene anche applicata ai parametri nodali della rete. Per la maggior parte dei nodi che risultano adatti per cui risulta applicato un modello statistico gemellare, notiamo un'influenza dell'ambiente non condiviso superiore al 70%.

Dall'analisi quantitativa sulla differenza di correlazione intra-coppia tra coppie MZ e DZ, abbiamo trovato un numero maggiore di differenze di correlazione intra-coppia

significative per i nodi e per i link di connettività funzionale associati ad un effetto epistatico. Inoltre, i link di connettività funzionale basati su Mutua Informazione mostrano un numero maggiore di differenze di correlazione intra-coppia significative rispetto ai link della matrice di Cross-Correlazione.

Dall'ultima analisi di correlazione relativa all'analisi dell'effetto significativo del sesso e dell'età sulla differenza intra-coppia di ciascun parametro topologico, non abbiamo ritrovato un effetto significativo dell'età o del sesso sulla differenza intra-coppia per quanto riguarda i parametri di nodali e di link. Al contrario, abbiamo visto un effetto significativo dell'età e del sesso sulla somiglianza intra-coppia dei parametri nodali della rete. Per la maggior parte dei nodi abbiamo trovato un valore di correlazione negativo tra l'età della coppia di gemelli e la differenza intra-coppia del parametro nodale. Questa correlazione negativa indica un aumento della somiglianza intra-coppia, per la maggior parte dei parametri nodali, all'aumentare dell'età della coppia di gemelli.

In conclusione, questo lavoro di tesi è rivolto inizialmente all'introduzione di un nuovo metodo di pulizia dei dati fMRI, a cui sono seguite analisi di pre-elaborazione e analisi dei dati rs-fMRI ottenuti da coppie di gemelli. Abbiamo implementato un'analisi completa rivolta all'indagine quantitativa delle reti di connettività funzionale, risultate attive a livello cerebrale durante lo stato di riposo del paziente. Tale analisi è basata all'estrazione di un numero elevato di parametri a livello della globale della rete, a livello di nodo e a livello di link tra nodi. Questo lavoro di tesi è per noi un miglioramento nello studio della connettività funzionale cerebrale e un passo avanti per quanto riguarda le analisi dei parametri topologici applicati a studi di coppie di gemelli.

Per concludere, riteniamo che i risultati ottenuti intendono fornire interessanti spunti sugli effetti genetici e ambientali delle reti cerebrali. Tali risultati possono avere un impatto importante nei contesti clinici, in quanto si ha a disposizione un'analisi approfondita di diversi tipi di parametri topologici della rete funzionale.

Parole chiave: *gemelli, monozigoti (MZ), dizigoti (DZ), resting-state fMRI, ICA, ereditabilità, influenza genetica, influenza ambientale, rete cerebrale funzionale, parametri topologici della rete*

Contents

Abstract	I
Sommario	VII
Contents	XIII
List of Tables	XVII
List of Figures	XIX
Chapter 1: Introduction	
1. Magnetic Resonance Imaging	1
1.1 Magnetic Resonance Imaging: principle	1
1.2 Functional Magnetic Resonance Imaging	11
1.2.1 Echo Planar imaging sequence.....	14
1.2.2 Task-based fMRI.....	17
1.2.3 Resting state fMRI.....	19
1.2.4 ICA Analysis in fMRI study	22
1.2.5 Limitation of standard noise-free ICA and pICA.....	32
1.2.6 Application of pICA: Artefacts and data denoising	40
2. Analysis of resting-state fMRI data	42
2.1 Spatio-temporal characteristics	43
2.2 Spectral characteristics	44
2.3 Acquisition and pre-processing of resting-state BOLD fMRI data.....	45
2.4 Methods for RSNs identification.....	46
3. Methods for functional connectivity study	47
3.1 Model-based methods.....	47
3.2 Data-driven methods	51
3.2.1 Independent Component Analysis	52
3.3 Dynamics and Graph-analysis of Brain's Networks	53
4. Twins study: Heritability of brain development	58
4.1 Monozygotic and Dizygotic Twins	59

4.2	The Twin Method.....	61
4.2.1	Assumptions of Twin Method.....	63
4.3	Statistical tools and measures of Twin Models.....	64
4.3.1	Concordance measure.....	66
4.3.2	Correlation measure.....	66
4.3.3	ACE, ADE Twin model and Epistatic Effect.....	67
4.3.4	Heritability estimation in case of ACE or ADE Twin model.....	70
Chapter 2: Experimental Data.....		71
Aim of the research.....		72
1. Subjects and Data Acquisition.....		74
2. MRI Data Pre-processing.....		75
2.1	Pre-processing with SPM.....	76
3. ICA analysis and Denoising tool.....		79
3.1	Melodic Toolbox: Extraction of ICs.....	79
3.2	Automatic Tool for ICs' Classification.....	82
3.2.1	Tool development, test and validation.....	82
3.2.2	Application of the Tool on rs-fMRI data of Twins dataset.....	86
3.3	FSL cleaning tool: fsregfilt.....	87
4. SCA: Seed-based functional connectivity analysis.....		88
4.1	Anatomical Parcellation of the brain.....	90
4.2	Functional connectivity adjacency matrix.....	91
5. Topological parameters estimation and Intra-pair Similarity analysis.....		98
5.1	Node-level parameters estimation and Intra-pair similarity analysis.....	99
5.2	Network-level parameters estimation and Intra-pair similarity analysis.....	101
6. Analysis of Genetic and Environmental Influences of Topological Parameters.....		103
6.1	ACE Twin model and Heritability Estimation.....	104
6.2	ADE Twin model and Heritability Estimation.....	105
7. Quantitative analysis on the difference $r_{MZ} - r_{DZ}$ based on the Fisher test.....		106
8. Effect of Sex and Age on Intra-pair phenotypic difference.....		108

Chapter 3: Results and Discussion	114
1. Automatic tool for classification of noise-related ICs	116
1.1 Test and validation on a training fMRI dataset	116
1.2 Tool application to the entire twin rs-fMRI dataset.....	120
2. Intra-pair similarity analysis on FC matrix links	123
2.1 Intra-pair Similarity analysis on Cross-Correlation matrix	123
2.2 Intra-pair Similarity analysis on Mutual Information matrix	127
3. Intra-pair Similarity analysis on network-level and node-level topological parameters	131
3.1 Intra-pair similarity analysis based on Intra-pair difference of network-level and node-level parameters	131
3.2 Intra-pair similarity analysis based on correlation values of r_{MZ} and r_{DZ} of network-level and node-level parameters	135
4. Analysis of Genetic and Environmental Effect on each Topological parameter	141
4.1 Topological Parameter associated to Epistatic Effect.....	141
4.2 Heritability analysis, ACE and ADE model results	146
5. Quantitative analysis on the difference $r_{MZ} - r_{DZ}$ based on the Z Fisher test	156
6. Effects of Age and Sex on the intra-pair difference of the parameters	160
Chapter 4: Conclusion and Further Developments	165

List of Tables

3.1 Method performances	118
3.2 Nodes that result associated to significant correlation values for MZs and DZs	132
3.3 Epistatic Effect evaluated in each node-level parameter.....	139
3.4 Nodes for node-level parameters for which is applied ADE model and the corresponding heritability estimates	144
3.5 Nodes for node-level parameters for which is applied ACE model and the corresponding heritability estimates	145
3.6 Nodes for node-level parameters for which we obtain a significant Z transformed value	154
3.7 Significant partial correlation values and probability values associated to the effect of age on intra-pair difference of the node-level parameters.	158
3.8 Significant partial correlation values and probability values associated to the effect of sex on intra-pair difference of the node-level parameters	158

List of Figures

1.1 Spinning nuclei with odd number of protons or/and neutrons characterized by precession motion s	2
1.2 Single spin magnetic moment μ precession around external magnetic field B_0 single and Spin states α and β for a single nuclear spin of spin up and spin down condition	3
1.3 Precession motion of the magnetization M with flip angle ϕ around B_0 axis that proceeds at Larmor frequency Magnetization, RF field B_1 and flip angle ϕ in the rotating frame x_1, y_1 and $z_1 = z$ spinning at Larmor frequency	4
1.4 Response due to a RF pulse with flip angle $\phi = 90^\circ$	5
1.5 Elicited signal named Free Induction Decay (FID)	6
1.6 Total magnetic field B varying linearly along r direction in which we apply the gradient magnetic field $G(r)_t$ the total Larmor frequency $\omega(r)$ at r position is also varying linearly along r direction.....	7
1.7 Example of saturation recovery of spin echoes used to obtain T_1 and T_2 weighting contrast by combining the setting of T_E and T_R	10
1.8 Concentration of Hb and HbO2 molecules in capillaries and surrounding tissue during Baseline condition and during the Activation condition	12
1.9 The standard canonical Hemodynamic Response function (HRF) used in fMRI data analysis representing BOLD signal	13
1.10 Spin Echos EPI sequence: phase encoding along y direction using blipped gradient pulse G_y , frequency encoding along x direction using strong switched gradient pulse G_x , RF pulse pair of 90° - 180° pulses.....	15
1.11 Zig-Zag traversal of k space: is the k -space trajectory obtained using SE EPI sequence.	16
1.12 Block design for a task-based fMRI experiment: acquisition process and analysis to obtain the activation map.	18

1.13 Decomposition of each ICs in component map and relative time course of activation	25
1.14 IC maps thresholding associated to each IC component IC1 and IC2	26
1.15 Decomposition of fMRI dataset using spatial ICA (sICA).	28
1.16 Differences between Group-ICA temporal concatenation and Single-subject ICA (sICA)	31
1.17 Probabilistic ICA framework.....	37
1.18 Effect of variance normalization on the mixture-model based thresholding. results for non no variance normalized data and for variance normalized data.	40
1.19 Differences in PCA and ICA reference directions	52
1.20 Example of cortical parcellation of the brain used to extract the BOLD signals in each ROIs, computation of correlation matrix and functional brain network to be analysed in graph-analysis	55
1.21 Development Monozygotic and Dizygotic twins	59
1.22 Univariate twin analysis using on ACE model.	68
1.23 Univariate analysis on twins using ADE model	69
2.1 fMRI data pre-processing scheme	75
2.2 Single-subject ICA via MELODIC: inputs and outputs of melodic command from FSL	78
2.3 Spatial ICA performed by MELODIC toolbox and the consequent ICs classification and Denoising of the rs-fMRI data.	81
2.4 Matrix of spatial correlation with positive and negative values; on the right the matrix of spatial correlation thresholded by for example 0.1	83
2.5 Pipeline for identification of artefactual independent components and schematic diagram of tool development and testing	84
2.6 FSL command fsl_regfilt: inputs and outputs	86

2.7 Steps of Seed-based correlation analysis SCA	88
2.8 Correlation between each point of the matrix of each subject, between all Twin 1 and all Twin 2 of the couple, repeated for all MZ and DZ couples	94
2.9 Correlation between node-level parameter of all Twin 1 and Twin 2, for each node, in MZ and DZ couples.	99
2.10 Correlation between the network-level parameters of all Twin 1 and Twin 2 in MZ couples and DZ couples.	101
2.11 Diagram scheme of the Application of partialcorr function to network-level, node-level and link-level parameter to estimate if exist an effect of Age and Sex on intra-pair difference of the parameter.....	111
3.1 ROC curves: ROC curve used to evaluate the optimal SC threshold; ROC curve used to evaluate optimal SP threshold	115
3.2 Results of the fMRI cleaning procedure: the red and blue clusters emerged from the activation analysis of the original and cleaned fMRI datasets, respectively	117
3.3 Boxplots of number of ICs removed from total dataset of 92 subjects and in 13 over-threshold head movement subjects	120
3.4 Intra-pair cross-correlation averaged difference across MZs and DZs	122
3.5 Difference between the two averaged intra-pair cross-correlation difference matrices of MZ and DZ twins	123
3.6 Two correlation matrices obtained after applying partialcorr on each element of the Cross-Correlation matrix to evaluate the similarity of this parameter between twins.	124
3.7 Intra-pair Mutual Information averaged difference across MZs and DZs	126
3.8 Difference between averaged matrices of intra-pair MI difference of MZs and DZs	126
3.9 Two correlation matrices obtained after applying partialcorr on each element of the Mutual Information matrix to evaluate the similarity of this parameter between twins ..	127
3.10 Boxplot of intra-pair difference in MZs and DZs, for the network-level parameters of Total negative and Total positive weight	130

3.11 Boxplot of intra-pair difference in MZs and DZs, for the network-level parameters of Maximized Modularity and Global Efficiency of the network	130
3.12 Boxplot of intra-pair difference in MZs and DZs, for the network-level parameters of Network Degree and Network Density	130
3.13 Boxplots of the distribution of the intra-pair difference of the network-level parameter of Characteristic path length of the network, across MZs and DZs	131
3.14 Boxplots of the distribution of intra-pair difference for the nodes suitable for ADE, ACE or associated to Epistatic Effect, calculated for the parameter of Node Degree	132
3.15 Correlation values of node-level Parameter of Total positive weight associated to specific nodes that results positive and significant.....	135
3.16 Correlation values of node-level parameter of Node Strength associated to specific nodes that results positive and significant	135
3.17 Correlation values of node-level Parameter of Node Strength associated to specific nodes that results positive and significant	136
3.18 Correlation values of node-level Parameter of Total negative weight associated to specific nodes that results positive and significant	136
3.19 Correlation values of node-level Parameter of Clustering Coefficient associated to specific nodes that results positive and significant	137
3.20 Correlation values of node-level Parameter of Local Efficiency associated to specific nodes that results positive and significant	137
3.21 Correlation values of node-level Parameter of Betweenness Centrality associated to specific nodes that results positive and significant	138
3.22 CC links that are associated to Epistatic Effect	142
3.23 MI links that are associated to Epistatic Effect	143
3.24 Nodes with unique environment influence lower than 50% and Dominant genetic effect higher than 20%.	148

3.25 Nodes with unique environment influence lower than 50% and Additive genetic effect higher than 40%	148
3.26 Nodes in which the Common environmental influences are higher than 20%	149
3.27 Nodes in which the Common environmental influences are higher than 20%	149
3.28 Links of functional connectivity between ROIs in which is applied ACE or ADE model for the MI matrix.	150
3.29 Links of functional connectivity between ROIs in which is applied ACE or ADE model for the CC matrix.	151
3.30 Matrix of heritability when ACE or ADE model is suitable for link-level parameter of MI	152
3.31 Matrix of heritability when ACE or ADE model is suitable for link-level parameter of CC	152
3.32 Significant Z-fisher values for ROI couples with Epistatic Effect, suitable for ADE model, suitable ACE model in MI matrix	152
3.33 Significant Z-fisher values for ROI couples with Epistatic Effect, suitable for ADE model), suitable ACE model in CC matrix	153
3.34 Significant Effect of Age, for the node-level parameter of Node efficiency, on the intra-pair difference evaluates in the “Putamen_L”.	160
3.35 Boxplot of intra-pair differences in the region of “Lingual_L” for the parameter of LE, which shows a Significant Effect of Sex	161

Chapter 1: Introduction

1. Magnetic Resonance Imaging

Magnetic Resonance Imaging (MRI) is a medical imaging technique used in radiology to picture and analyse the anatomy and physiological processes of the body in patient characterized by healthy or disease conditions. This kind of imaging technique is non-invasive and is used to extract quantitative and anatomical information in any plane or volume with a relatively high resolution.

Over the years, MRI has become the main modality used in neuroimaging studies to discriminate among grey matter, white matter, cerebrospinal fluid, blood vessel and tumor by measuring the density of water molecules in these specific areas.

The main components that are used in MRI are a strong, homogeneous external magnetic field, a gradient field created by 3 gradient coils and a transmitting and receiving radiofrequency antennas. Hydrogen nuclei that are present in water molecules are able to absorb and emit radio frequency (RF) waves if are placed in a strong external magnetic field. A high concentration of hydrogen atoms can be detected in water and fat tissues. MRI scans provide a map of the location of the water and fat tissue in the patient's body.

Instead of Computerized Tomography (CT), based on the use of ionizing radiation (X-rays) which can create a damage of the cell of the body, MRI technique uses strong magnetic field, gradient field and RF waves that does not apply damaging radiations.

1.1. Magnetic Resonance: Basic Principle

The nucleons are represented by both protons and neutrons, these nucleons can bond together by nuclear force and create atom nuclei. *Hydrogen nuclei* is an isotope characterized by a single proton and atomic mass number equal to 1.

The standard MRI creates an image of the body in terms of density of those nuclei which are exhibited in the specific analysed region of the body. Hydrogen nuclei that are present in water and fat tissue represent a charged particle that create a spinning around its internal

axis of rotation with an angular momentum J . When these nuclei are subjected to an external magnetic field, they can create the signal used to obtain an MRI image.

Nuclei that contain an odd number of protons and/or neutrons are characterized by the property of “spin”, which means that can create a precession motion around its axis. This particular property depends on the number of protons of the analysed isotope.

The spinning nucleus that rotates around its own axis can induce a small magnetic moment μ (magnetization) along its axis, behaving like a rotating bar magnet as shown in Figure 1.1.

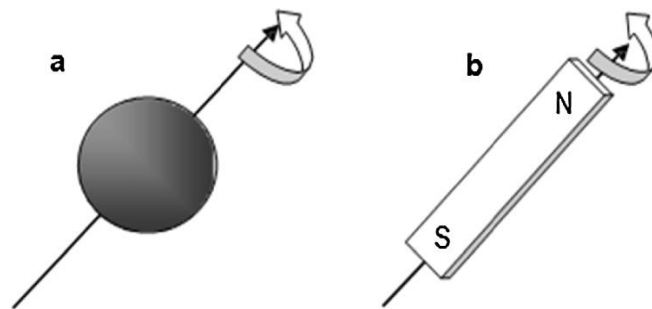


Figure 1.1, a) Spinning nuclei with odd number of protons or/and neutrons characterized by precession motion and creating small magnetic moment along spin axis (b) rotation of magnetic bar creating magnetic field along rotational axis

When the nuclei are placed inside a strong magnetic field B_0 they tend to align their small magnetic moments along the direction of the strong magnetic field. In the case of a strong magnetic field B_0 applied on fat or water tissue, characterized by high amount of hydrogen nuclei, the effect that is obtained is that each nuclei create a small magnetic moment μ that try to align in the direction of B_0 , producing consequently a net magnetization M_z^0 , parallel to B_0 , along the z axis.

However, the angular momentum J of the nuclei, which depends on the spinning velocity and their mass, has the role to prevent the perfect alignment of the small magnetic moment of each spin with B_0 , due to the gyroscopic effect creating by the application of B_0 . The final result is the **precession motion** of each nuclear spins around the z axis, along which we apply B_0 .

The velocity of the rotation around the direction of B_0 is called the Larmor frequency of the spinning nuclei and is defined as the product between the field strength B_0 and the gyromagnetic ratio γ :

$$\omega = \gamma B_0 \quad (1.1)$$

The gyromagnetic ratio γ represents the ratio between the modulus of the magnetic moment of the nuclear spin and the modulus of the angular momentum:

$$\gamma = \mu/J \quad (1.2)$$

The Hydrogen nuclei is characterized by a gyromagnetic ratio of 42.58 MHz/T.

A tissue composed by many nuclear spins and subjected to an external field B_0 , is characterized by two possible values of magnetic quantum number (m) associated to each nuclear spin. These values of m represent two possible conditions of the nuclei: spin up or spin down condition. These particular conditions indicate two possible orientation of the small magnetic moment μ with respect to the direction of the external magnetic field B_0 . If the nuclear spin is oriented close to the B_0 field's direction is reached the minimum energy state associated to the spin up condition. On the contrary, a nuclear spin distant from the field direction is characterized by maximum energy state related, to the spin down condition.

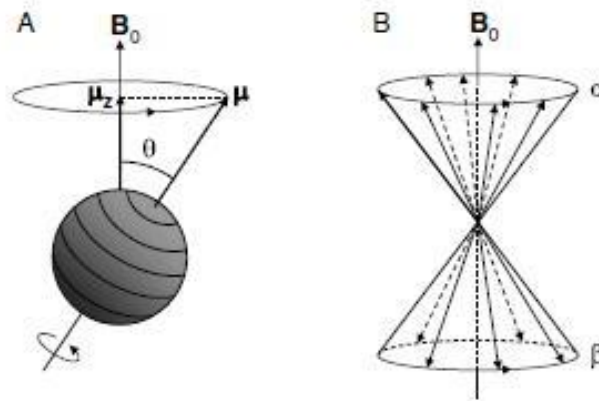


Figure 1.2,(A) single spin magnetic moment μ precession around external magnetic field B_0 single, with an axis inclination θ due to the gyroscopic effect, (B) Spin states α and β for a single nuclear spin of spin up and spin down condition.

One of the main components of the MRI scanner is the main magnet that has to create a strong and homogeneous field in a range between 0.2-3 Tesla, conventionally directed along the z axis of the scanner frame. As has already been mentioned, the application of

the magnetic field B_0 creates the precession motion of hydrogen nuclei around the same B_0 and a net magnetization $M = M_z^0$, parallel to B_0 , along the z axis [1].

Next, a Radiofrequency pulse (RF pulse), B_1 is applied along the transverse plane (x,y) perpendicular to B_0 , directed along z. This RF pulse is oscillating at a Radio frequency tuned to the Larmor frequency, turning the initial longitudinal magnetization $M = M_z^0$, creating by the nuclei, into a moving magnetization subjected to a progressive flip angle φ . The net result is the **precession motion** of the magnetization M .

At macroscopic level, the evolution of the magnetization M start parallel to B_0 with a component $M = M_z^0$, representing the small longitudinal magnetization in the baseline condition, without applying RF pulse.

If is applied a RF pulse, with a frequency tuned with Larmor frequency of the hydrogen nuclei, the net result is a moving magnetization by a flip angle φ , proportional to the RF pulse duration τ_p and the gyromagnetic ratio γ :

$$\varphi = \gamma\tau_p B_1 \quad (1.3)$$

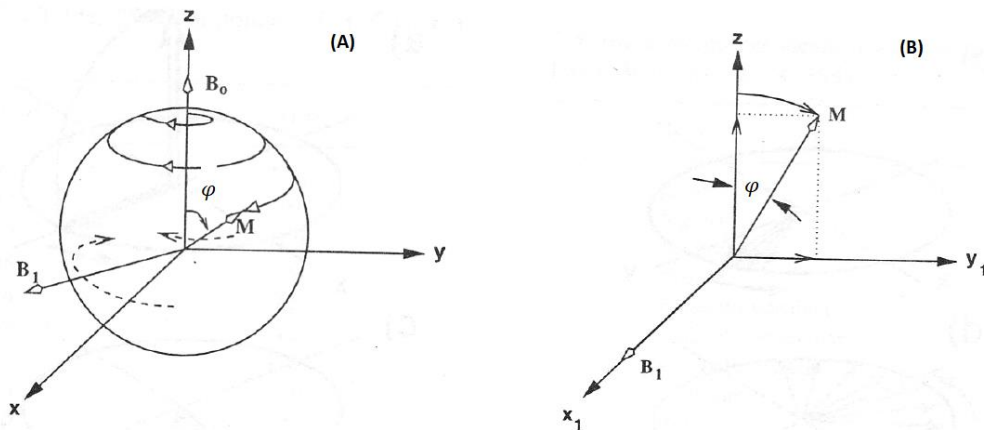


Figure 1.3,(A) Precession motion of the magnetization M with flip angle φ around B_0 axis that proceeds at Larmor frequency (B)Magnetization, RF field B_1 and flip angle φ in the rotating frame $x_1, y_1, z_1 = z$ spinning at Larmor frequency.

At microscopic level, is possible to analyse the response after the application example of RF pulse with flip angle $\varphi = 90^\circ$. First, the process begins with the flip of the phased spins, that correspond to the flipping of M from longitudinal to transverse plane, associated to the changing from longitudinal component M_z^0 to transverse component M_{xy} .

Next, transverse relaxation begins with time constant T_2 that describes the progressive dephasing of the spins and the progressive decay of M_{xy} to zero. Subsequently, the longitudinal relaxation starts with time constant T_1 to progressively phase the spins and restore the longitudinal magnetization M_z^0 since is reached the equilibrium condition, without no more influences of the RF pulse.

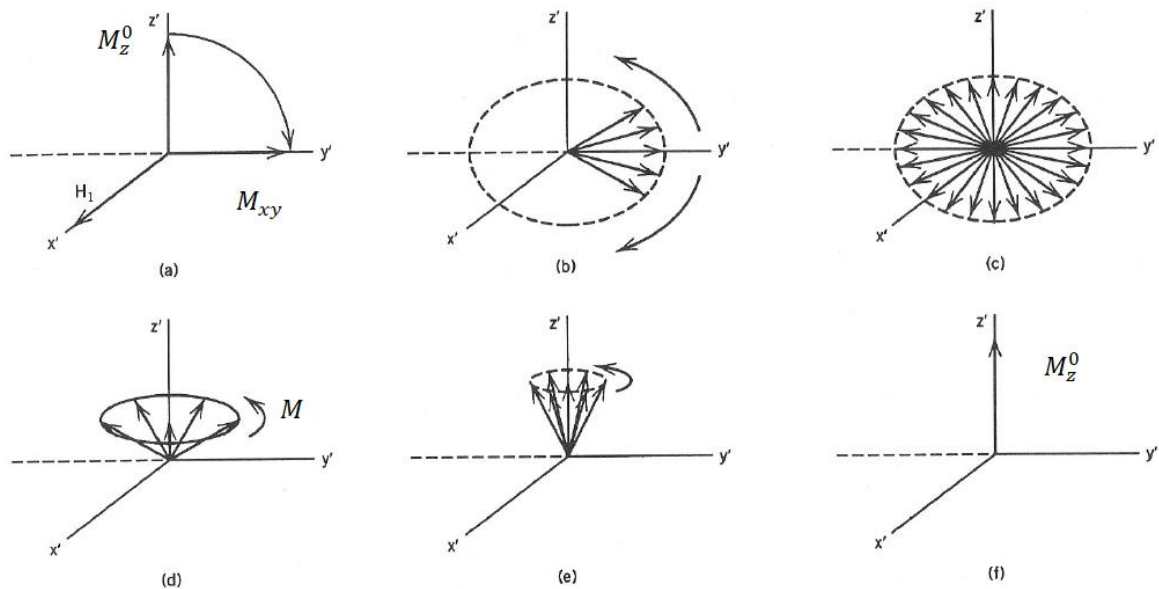


Figure 1.4, Response due to a RF pulse with flip angle $\varphi = 90^\circ$

The condition of a RF pulse tuned with the Larmor frequency describe the ***in-resonance condition***, in which the movement of the magnetization M can be described in a rotating frame spinning at Larmor frequency $\omega = \omega_0 = \omega_{RF}$, that results in a precession of M_{rot} , rotating magnetization, around the apparently fixed RF field $B_{1,ROT}$. The most important effect to be measured is the transverse magnetization component:

$$M_{xy} = M_z^0 \sin \varphi \quad (1.4)$$

M_{xy} can be represented as a dipole rotating at a radiofrequency $\omega_{RF} = \omega_0$ that emits, during the transverse relaxation, a RF signal called ***Free Induction Decay*** (FID). This

response signal emitted by the hydrogen nuclei, rapidly decay and can be measured by a conductive field coil placed around the object to be imaged. The extracted measure of FID is processed in the next step and used to reconstruct the 3D image grey scale of MRI images.

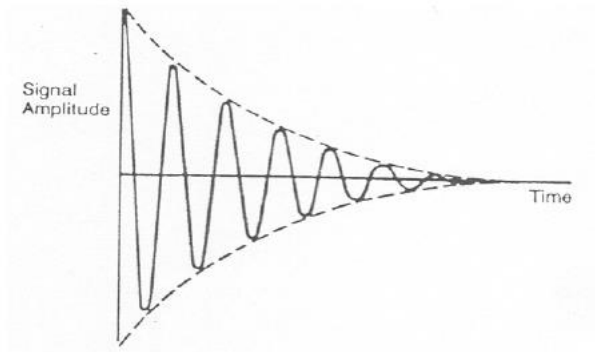


Figure 1.5, Elicited signal named Free Induction Decay (FID)

The FID signal that we obtain represent the sum of the local signals from all the parts of the object, to obtain the 3D MRI image is necessary to encode/localize each local signal in each direction x, y and z.

The spatial localization method used to encode/localize the signal in a certain direction \mathbf{r} consist in adding a gradient magnetic field $\mathbf{G}_r(\mathbf{t})$ (created by gradient coils) to the background magnetic field B_0 , resulting in a linear variation of the local Larmor frequency of the nuclei in that direction \mathbf{r} .

The resulting total magnetic field B is increasing in \mathbf{r} direction in which is applied \mathbf{G}_r :

$$B(\mathbf{t}) = B_0 + r\mathbf{G}_r(\mathbf{t}) \quad (1.5)$$

Considering that ω_0 is called **nominal Larmor frequency** of the MRI scanner, which depends only on B_0 and the gyromagnetic ratio γ . These two parameters of B_0 and γ are considered to be constant, thus ω_0 is maintained constant as well. The nominal Larmor frequency can be estimated and is equal to:

$$\omega_0 = \gamma B_0 \quad (1.6)$$

The **local Larmor frequency** $\omega_l(\mathbf{r})$ along \mathbf{r} **direction** varies linearly along the direction in which we apply \mathbf{G}_r :

$$\omega_l(r) = \gamma r G_r(t) \quad (1.7)$$

The result of the application of $G_r(t)$ along r direction is that the **total Larmor frequency** $\omega(r)$ at r position is also varying linearly along r direction:

$$\omega(r) = \omega_0 + \omega_l(r) \quad (1.8)$$

$$\omega(r) = \omega_0 + \gamma r G_r(t) \quad (1.9)$$

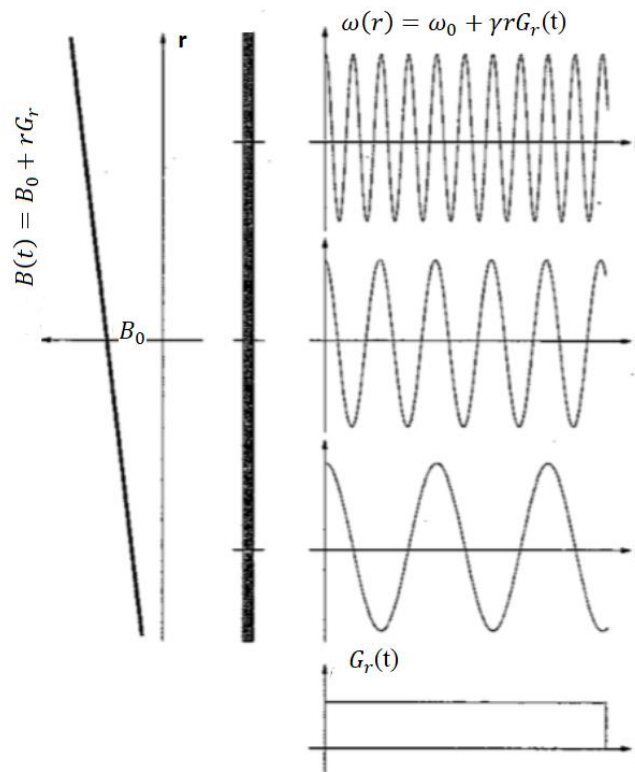


Figure 1.6, Total magnetic field B varying linearly along r direction in which we apply the gradient magnetic field $G_r(t)$; the total Larmor frequency $\omega(r)$ at r position is also varying linearly along r direction.

After the encoding of the FID signal in each direction, is necessary to associate a certain voxel intensity to each 3D voxel creating the image contrast of the MRI image. The voxel intensity of a certain tissue (for example white matter, grey matter, cerebrospinal fluid...) is given by the proton density in that tissue. The signal intensity is also connected to the proton density: stronger is the FID and higher is the proton density in the analysed tissue.

The ***MRI image contrast*** is an important imaging parameter, directly connected to parameters of the proton density and relaxation times of the tissues. Differences in these parameters, observed in two distinguished tissues, have conflicting effects on the image contrast. Different types of image contrast can be obtained by designing different pulse sequences to emphasize differences in one parameter and to minimize the effects of the other parameters.

The three-primary types of image contrasts are: ***proton density, T_1 weighted contrast*** and ***T_2 weighted contrast***.

1. As has been already introduced, the proton density ρ is the main determinant of signal intensity. We use the proton density to differentiate different image contrasts created by different tissues.
2. The T_1 weighted contrast is related to the longitudinal relaxation with a longer time constant T_1 . This time constant represents the time that is necessary to the magnetization M to restore the longitudinal magnetization M_z^0 and the thermodynamic equilibrium of the tissue.
3. The T_2 weighted contrast is related to the transverse relaxation with time constant $T_2 \leq T_1$. T_2 indicates the time necessary to the FID response signal of a certain tissue to decay since $FID=0$ is reached.

Proton density contrast is always present in the MRI image, T_1 weighted and T_2 weighted contrast can be mutually excluded.

T_1 - and T_2 -weighted contrasts are used in the case of two soft tissues characterized by the same proton density. The contrast between the tissues is obtained using the relaxation time constants T_1 and T_2 relative to the analysed tissues. T_1 weighted images are characterized by contrast and the brightness of the image are predominantly determined by T_1 properties of the tissue. On the contrary, T_2 weighted images have a contrast and brightness predominantly determine by T_2 properties of the tissue.

The imaging parameter that need to be changed to obtain T_1 and T_2 weighted contrasts, are:

- T_R , representing the **repetition time**: the time in which we applied the RF field B_1 using a repetitive excitation cycle.
- T_E , representing the **echo delay time**, the time between two subsequent RF pulse.

To obtain T_1 weighted contrast is necessary to shorten the repetition time T_R , magnifying the effects of longitudinal relaxations and the echo time T_E in made as short as possible to reduce the effects of transverse relaxation. Because the minimum imaging time is proportional to the repetition time T_R , the T_1 weighted images can be made quickly.

The T_1 -MRI image technique superimpose the T_1 weighting contrast on the Proton density contrast. This technique applies a shorter T_R , avoids T_2 weighted contrast of the tissue considering a shorter T_2 and at the same time respects the saturation condition for the n-RF pulse (M_{xy} for n-1 RF pulse was over).

The sequences used to obtain a T_1 weighted images are: **Saturation recovery sequences**, consists in multiple 90-degree RF pulses applied at relatively short repetition times, and **Inversion recovery sequences**, consists in a preparatory 180-degree pulse and 90-degree read-out pulse. Due to the 180-degree preparatory pulse Inversion recovery differently from Saturation recovery technique, is characterized by a longer repetition time lengthen by this preparatory pulse.

The latter technique is used to selectively null the signal for certain tissues (e.g fat or fluid) and the time between the preparatory pulse and the 90-degree pulse is called *time to inversion*. By choosing the appropriate *time to inversion* is possible to obtain the suppression of different tissues.

Two possible techniques of Inversion recovery are **Short Time Inversion Recovery sequence (STIR)** or the **Fluid Attenuation Inversion recovery (FLAIR)**.

STIR sequence is used to suppress the fat longitudinal magnetization by exploiting the shorter T_1 that characterize the fat tissue. FLAIR sequence is used to suppress cerebrospinal fluid magnetization (signal) by exploiting the longer T_1 of the cerebrospinal fluid. In this type of MRI contrast the T_2 weighted contrast is avoided due to the short T_R that is applied. The small interval of T_R that is considered in Inversion Recovery and Saturation Recovery technique, forces the FID with time constant T_2 to accelerate such that

the FID is fitted in the short interval of T_R . The acceleration of the FID to fit in T_R interval is obtained by considering smaller time constants of T_E and T_2 .

Differently, to produce T_2 weighted images, the effects of T_1 differences are usually minimized by making $T_R \gg T_1$, $T_E \cong T_2$ [2].

Shorter is the T_2 time constant, faster is the FID decay to reach the value of zero. The T_2 -MRI superimposes the T_2 weighting contrast on the Proton density contrast, considering a longer T_E and longer/tuned T_2 for the tissue to be enhanced/contrasted. T_1 weighting contrast of the tissue is avoided due to considering a longer T_1 time constant.

The technique used to obtain T_2 weighted contrast is the *Saturation recovery spin echo* (illustrated in Fig.1.7) and *Inversion recovery spin echo*, in which is considered a longer T_E to observe the FID of the echos.

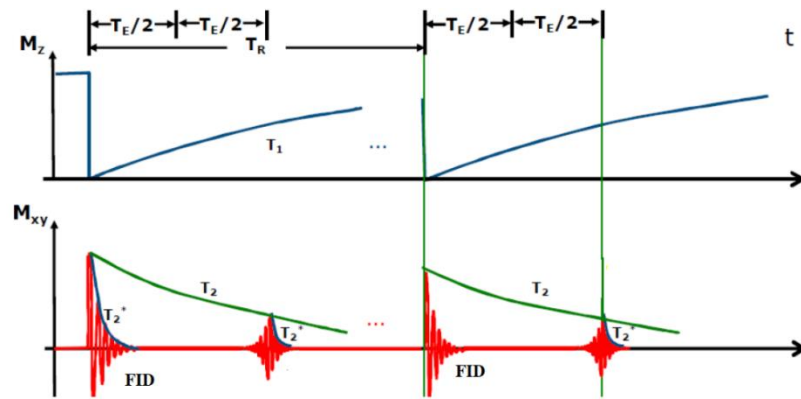


Figure 1.7, Example of saturation recovery of spin echoes used to obtain T_1 and T_2 weighting contrast by combining the setting of T_E and T_R .

The last type of contrast is T_2 * *weighted contrast*. Each tissue is characterized by an inherent T_2 time constant and is subjected to magnetic field inhomogeneities that can reduce the T_2 value.

T_2 * weighted contrast includes additional effects due to macroscopic and microscopic inhomogeneities of the magnetic field. These inhomogeneities can be caused by a changing in blood flow in the arteries or in the vein, or changing in oxygenation level of the vessel.

The formula describing T_2 * weighted contrast is (Eq. 1.10):

$$\frac{1}{T_2^*} = \frac{1}{T_2} + \gamma \Delta B_0 \quad (1.10)$$

Where ΔB_0 represents field inhomogeneities due to the inhomogeneities of the object that need to be scanned. Inhomogeneities of the object create microscopic inhomogeneities between tissue within a voxel.

Both T_2 and T_2^* *represents transverse relaxation* (decay of MRI signal induced by the precession of the transverse magnetization); T_2 describes the decay observed in the Spin Echo(SE) (signal obtain after the application of two RF pulse), differently T_2^* describes the decay creating in Gradient Echos (GE).

The T_2^* weighted contrast is obtained by applying the *Gradient Echo (GE) sequences*, in which the FID signal is continuously activated and deactivated by a strong gradient field applied with alternated sign. GE sequences permit fast imaging, fast scans due to the continuous inversion of the sign of the gradient field that is applied. This inversion of the sign is used to obtain the continuous refocusing of the signal into a Gradient Echos.

Functional MRI provide a T_2^ weighted image*, this means that fMRI is sensitive to neurovascular changes related to physiological and behavioural function and changing in oxygenation and blood flow in brain area.

1.2 Functional Magnetic Resonance Imaging

Functional Magnetic Resonance Imaging (fMRI) has become an important tool for studying cognition and in both healthy and dysfunctional condition in patient's brain.

The fMRI is used to monitor and measure the brain activity of the subject, by detecting the changes associate with blood flow and oxygenation of the brain tissue. These changes are created by altered the metabolism due to a task-based evoked neural response (task-based fMRI) or to spontaneous changes in neural activity, obtained while the subject is resting in the absence of conscious mentation. This latter condition of the subject is called resting state and is used to acquire resting-state fMRI (rs-fMRI) image [3].

Functional Magnetic Resonance Imaging is a neuroimaging tool that use the image created by MRI, representing the anatomic image of the brain of the patient, to superimpose the dynamic changes in neural metabolism and activity. The images created by fMRI use

Blood Oxygenation Level Dependent (BOLD) contrast, obtained by measuring the voxel-wise intensity changes in time of the T2* weighted images. When the subject is performing a cognitive task (to target a specific cognitive process), or is resting, it is possible to obtain alteration of neuronal activity. This alteration creates, in specific brain region, the variation of oxygen consumption levels, used to regularize the metabolic activity in these areas. The net results of this processes are BOLD changes recorded in the brain tissue [4]. In the case of a subject performing a specific task, neurons in a precise region of the brain become more active, increasing the firing rate, indicating a local raising of the neural activity in that region. If this area of the brain is more active, its metabolism changes and increase aerobic and anaerobic oxygen consumption. The amount of Cerebral blood flow (CBF) that arrives to this region of the brain increases and consequently de-oxygenated blood is replaced by oxygenated blood.

The raising of oxygen consumption and blood flow triggers an increased delivery of fully oxygenated haemoglobin (that transports the oxygen to the specific brain region) using vasodilatory processes. Subsequently, the deoxygenated haemoglobin (Hb) is dynamically replaced with oxygenated haemoglobin (HbO₂).

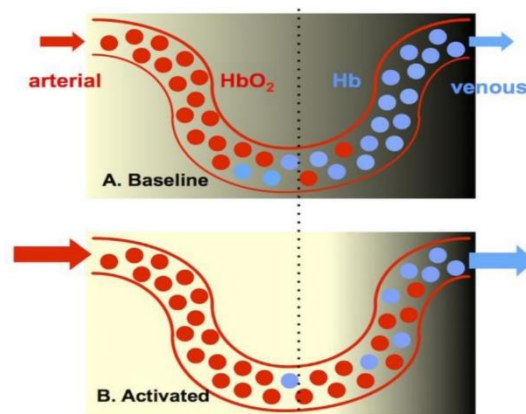


Figure 1.8, Concentration of Hb and HbO₂ molecules in capillaries and surrounding tissue at (A) Baseline condition, (B) Activation: increasing of neural activity create an increase blood oxygenation, rising concentration of HbO₂.

fMRI imaging use **Oxyhaemoglobin (HbO₂)** and **Deoxyhaemoglobin (Hb)** as natural contrast agent. HbO₂ exhibits diamagnetism, which means showing a weak repulsion from magnetic field. On the contrary Hb, that is a form of oxygenated haemoglobin characterized by the absence of oxygen bound, is more magnetic (paramagnetic) than oxygenated haemoglobin. Paramagnetic molecules are related to a weakly attraction to magnetic field. The main effects created by these two forms of haemoglobin can be

observed by considering the MR signal: the diamagnetic blood, composed by oxygenated haemoglobin, creates less disturbance to the MR signal; paramagnetic blood, with Hb, creates MR field inhomogeneities and interference with MR signal that results in a less intense MR signal [3], [5].

The specific active region of the brain is composed by a high amount of oxygenated haemoglobin than deoxygenated haemoglobin and characterized by less field inhomogeneities. As the magnetic field increases, the of T2* weighted contrast raises leading to a slower decay of the MR signal, representing less signal loss. The net result is a local enhancement of the BOLD signal [6].

The different variations in the MR signal, created by neural activity, contribute to creating the *Hemodynamic Response (HDR)*, associated to the Hemodynamic Response Function (HRF) created by a neural event. The HRF represents the percentage of MR signal change and its intensity is indicated by % MR signal change.

The HRF is describe by a specific mathematical function, elicited after the rise of a neural activity in a brain's region. Figure 1.9 shows the standard canonical HRF in fMRI analysis.

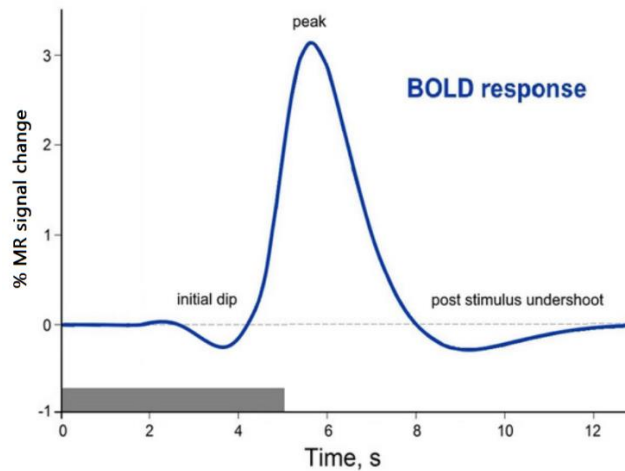


Figure 1.9, The standard canonical Hemodynamic Response function (HRF) used in fMRI data analysis representing BOLD signal.

At time $t=0$ is emitted the stimulus to the patient, used for the specific cognitive task that is applied. Before the neuronal activation is present a *signal drop*, representing the transient of the signal. This transient step is associated to an initial increasing of deoxygenated haemoglobin in the specific brain region. Next, neurons are activated: metabolic demand due to neural activity raises, increasing the inflow of oxygenated blood and concentration

of oxygenated haemoglobin. The net result is represented by an increasing of the HRF. After the onset of the neural activity, the *rise of the HRF* end into a HRF's peak at time $t=5-8$ s. This rise of HRF represents specifically the "BOLD effect" and is proportional to the neuronal activity presents in the brain region. The HRF increase can reach a plateau of the order of 0.5-3%. After the BOLD peak of the HRF, the signal returns to the baseline condition.

1.2.1 Echo Planar Imaging Sequence

The Echo Planar Imaging sequence (EPI) is the most common pulse sequence used for fMRI acquisitions to study the brain activity.

EPI is the *fastest acquisition method* in MRI and allows the acquisition of a brain image, MR slice, in a time frame of 20-100 ms, obtaining a high temporal resolution. On the other side, this technique is characterized by limited spatial resolution due to the sensitivity to susceptibility effect and main magnetic field inhomogeneities. A high spatial resolution of the image acquired with EPI sequence also requires a high-performance gradient field.

The higher temporal resolution of this technique allows to use EPI sequence to analyse the rapidly changing of physiologic processes. The main applications of this sequence are the imaging of the brain, used for fMRI, but also include imaging applications used for analyse anatomic region as heart and abdomen. This fast imaging technique is used to acquired raw data in k-space, representing spatial-encoding data of the signal emitted by the body. The k-space represents a graphic matrix of digitized MR imaging data, that represents the image before applying Fourier Transform data analysis. Each point in k-space contains data from a specific location in the MR image. Applying the Fourier transform of the k-space we can obtain the image by acquiring different brain volumes in few seconds, using as fast imaging sequence the EPI sequence.

Echo Planar Imaging sequence encounters the fMRI necessity. fMRI required the application of a fast sampling of the BOLD signal, obtaining fMRI images with high temporal resolution. Fast imaging technique are essential to acquire hundreds of brain volume in one fMRI scan such that is possible to increase the sensitivity of the image acquisition process.

In one interval of repetition time equals to $T_R = 2 - 3 \text{ sec}$, which indicates the sampling period of the BOLD signal, is acquired one 3D volume of the brain. One fMRI scan acquisition takes $T_{acq} = 5 \text{ min}$ in which are acquired around 100 3D volumes of the brain.

The EPI sequence can be performed by using a single or multiple excitation pulses (“shots”). The number of shots represents the numbers of repetition time T_R necessary to conclude the acquisition process.

In a *single shot EPI* is used a single Radio Frequency RF excitation pulse to obtain the spatial-encoding data of an image, means all k-space data are acquired in one shot and after one repetition time interval T_R is concluded the acquisition process of the one brain volume image. The image acquisition matrix typically is not larger than 128x128.

Is possible to use different kind of *single RF excitation* in the single shot EPI. For example, is conventionally used Spin-Echos SE sequence characterized by 90° followed by 180° pulse, obtaining the *Spin Echo EPI sequence*. Is possible to use also the Gradient-Echos GE sequence, *GE EPI sequence*, characterized by a single RF pulse of 90° with no preparatory pulses.

For example, in the case of using *SE EPI sequence* (Figure 1.10) is necessary to use the pair of 90° - 180° pulses. After 180° pulse is applied a strong switched readout or frequency encoding gradient G_x and simultaneously an intermittent “blipped” low-magnitude phase-encoding gradient G_y . The oscillation of the frequency encoding gradient from positive to negative amplitude, after 180° pulse, create Gradient Echos each with a different degree of phase encoding.

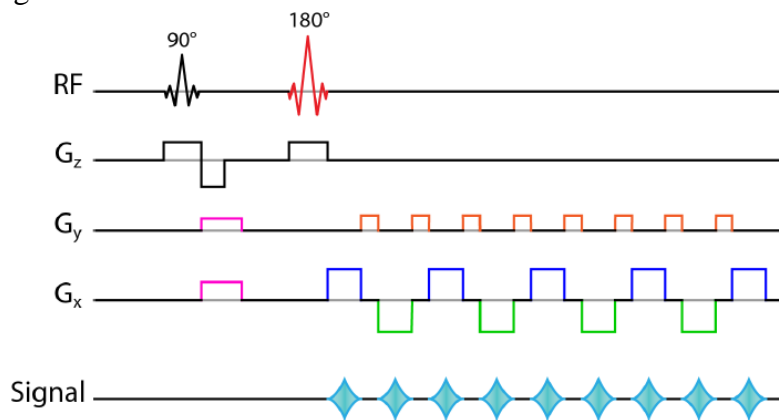


Figure 1.10, Spin Echos EPI sequence: phase encoding along y direction using blipped gradient pulse G_y , frequency encoding along x direction using strong switched gradient pulse G_x , RF pulse pair of 90° - 180° pulses.

Each echo is phase encoded differently by the phase encoded blips on the phase encoding axis y . Each oscillation of the frequency encoding gradients is used to obtain one line of the k -space matrix, and each “blips” represents a transition from one line to the next in k -space [7].

The result in k -space (Fig.1.11) is called “**Zig-Zag**” traversal of k -space. First, is created a negative frequency and phase encoding lobe of the gradient G_x and G_y , such that the trajectory in k -space is moving from the middle of k -space to the bottom left corner $(-k_{x,max}, -k_{y,max})$. Then, the switching frequency encoding gradient G_x swept k -space from left to right and from right to left in the trajectory. Simultaneously, the phase encoding gradient pulses create a step-wise increasing along k_y axis of phase encoding. As result, all data from k -space matrix are scanned in a time frame of 100 ms using a single shot of 90° - 180° pulses (SE sequence), achieving a brain image that represents an MR slice.

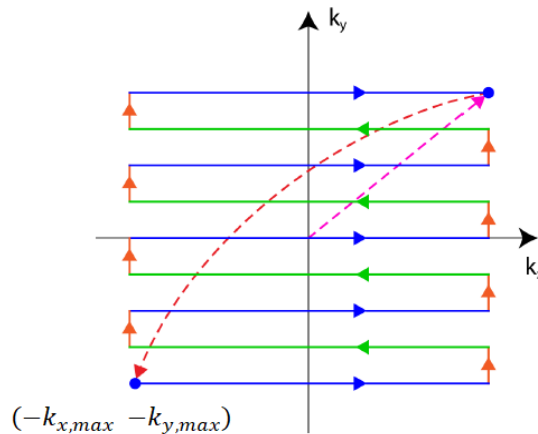


Figure 1.11, Zig Zag traversal of k space: is the k -space trajectory obtained using SE EPI sequence. Different colours of the trajectories refer to G_x and G_y gradients.

To increase the resolution of brain images obtained by EPI sequence are necessary two conditions. First, is necessary to use an intense, **high performance gradient** (to obtain a fast signal readout) achieved with short high phase encoding blips. Secondly, is required a **short rising time** achieved by continuously switched the frequency encoding gradients. In addition, the time scale of the complete process needs to be characterized by a **time scale on the order of $T2^*$** .

However, brain images acquired with Echo Planar imaging technique are characterized by a low spatial resolution, affected by several artifacts. *Artifacts in EPI sequence* are linked to:

1. *Sensitivity to magnetic susceptibility.*
2. *Sensitivity to magnetic field inhomogeneity.*
3. *Magnetic Gradient imperfections*, which can interfere with spatial encoding in phase encoding direction, leading to ghost images in the final result, representing motion artefact effect. To obtain better result in terms of spatial resolution is necessary a high-performance magnetic gradient.
4. *Narrow readout bandwidth in the frequency encoding direction*: this effect can create a chemical shift artefact in that direction, that need a suppression of echoplanar fat signal.

Otherwise, the *high temporal resolution* obtained by a short acquisition time makes EPI sequence ideal for an fMRI acquisition. The high number of brain images acquired are averaged to increase the sensitivity of the acquisition and decreased motion artefact, using this averaging over repeated acquisition.

For example, if is used an EPI sequence to obtain a task-based fMRI are acquired multiple echo-planar images, of the brain while the patient is performing a simple task for a short period. Considering that fMRI cannot capture the absolute activity in the brain but only differences in brain activity between different conditions, a *task-based fMRI acquisition* is composed by *task-condition* and *rest condition*. The subject interrupts and starts performing the task again for a short period, while imaging of the brain is continuously acquired. The net result of these process is a task-on and a task-off phase created during several cycle of acquisition. The fMRI acquisition data are processed to generate map of different region of the brain that are active or non-active, connected to a raise or a drop of blood oxygenation during the task-on and task-off phase.

1.2.2 Task-based fMRI

In task-based fMRI the global aim is to evaluate brain activation relative to a specific function. During the MRI acquisition is asked to the subject to perform a specific task, planned to test one or more functions: motor, cognitive, or sensorial function. The result

that is achieved is a map of the patterns of neuronal activation in the subject's brain. In a typical fMRI experiment can be used visual, auditory or other kind of stimuli, depending on the function of the brain to be tested in the patient. Each stimulus is separated to each other by a reference condition and induces a BOLD response in a specific area of the brain.

Task-based fMRI block design consider two conditions: one state is called *experimental condition*, in which is applied the stimuli, and the other state is known as *control condition*. The control condition is used to establish a baseline associated with BOLD signal. Using this condition are obtained periods of rest in which the stimuli created during the task is turned off. The main aim in a task-based fMRI experiment is to compare the BOLD signal obtained in these two states, based on the following hypothesis: if no task is performed during the rest period the *baseline/control condition* can be connected to “zero-activity” condition with respect to *experimental condition*, in which will be achieved higher activity during the task performance. Based on this assumption, if the neuronal activity in a particular region of the brain is comparable to the activity in the *control condition*, is supposed that this specific region is not involved/active during the task. On the other side, higher is the neuronal activity, in a specific region, with respect to the *control condition*, higher is the involvement of that brain region during the task.

Typically, is used a *Block design* for task-based fMRI experiment (shown in Figure 1.12) in which each trial can take usually a time around 5 min and is composed by design blocks, organized in *task blocks* interleaved by rest period of 10-30 sec *blocks of rest or fixation*. In each trial of the fMRI experiment is measured the range of BOLD contrast elicited between the two conditions (*experimental and control condition*).

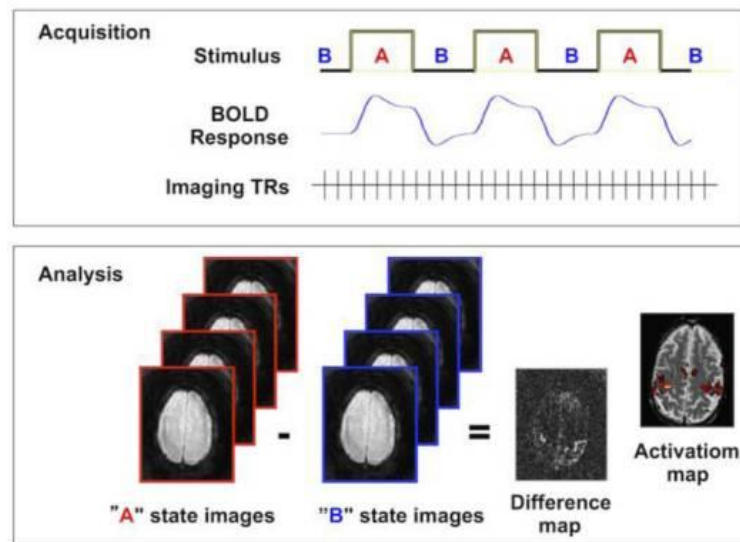


Figure 1.12, Block design for a task-based fMRI experiment: acquisition process and analysis to obtain the activation map.

As result, is measured the neural response in the state A and in the state B, acquiring “A” and “B” state images, while is performed a continuous acquisition of MR images. Using a block design is observe a change between brain states A and B that represents a BOLD signal changes between the two conditions. Then, is performed the average BOLD signal difference between the two states for each scan, creating the *contrast map*. In the end, is created the *activation map* by establish a threshold on a statistical test to evaluate the significant signal difference in each voxel. Each activation map represents the probability of activation in any voxel given an uncertainty due to noise or a small BOLD signal difference between the two states [8].

1.2.3 Resting-state fMRI

Resting state fMRI measures spontaneous fluctuations in neural activity in the state of absence of conscious mentation, when the subject is in a rest condition and the activation in different brain region can occur spontaneously without performing a task. As in task condition, even in a resting-state condition of the subject is impossible to eliminate the sensory and cognitive activation events of neurons.

The main aim of resting-state fMRI (rs-fMRI) experiment is to assess the common variance of the BOLD signal in different region of the brain to evaluate the synchronous neural activity in the brain when the subject is in a rest condition. The hypothesis is based

on the fact that if two regions of the brain are characterized by two similar BOLD signals means that these regions are in communication and create a functional network between spatially distinct region of the brain [9].

During a rs-fMRI acquisition, spontaneous neural fluctuations can be observed in low frequency range. Physiological signals are associated with a very large amplitude and in a very low frequency range ($<0.1\text{Hz}$) [10].

However, is currently unknown the reason why the neural fluctuations are present at low frequency range creating low frequency BOLD fluctuations. Many studies demonstrate that, analysing the hemodynamic response function during a rest condition, spontaneous power fluctuation (representing physiological activity) was positively correlated with localized brain activity with alpha power (8-12Hz) and beta power (17-23Hz) [11].

A recent fMRI analysis on resting state data studies correlation map between different regions of activation in rest condition, showing that the correlation coefficient evaluated between different functional areas depends exclusively on low frequency components. There is, therefore, a contribution of 90% of the low frequency fluctuation ($<0.1\text{Hz}$), related to the frequency spectrum of resting state data, to the correlation coefficient created between functional areas of the same functional network in the brain [12].

These important results can demonstrate that *low frequency fluctuations* in resting state fMRI represent spontaneous neural activations in connected functional areas.

Rs-fMRI acquisition is characterized by a *high spatial resolution* with respect to use EEG or MEG, due to the fact that can spatially localize different functional/resting state networks that activate simultaneously during the resting period.

On the contrary, rs-fMRI is characterized by a *low temporal resolution* (time to complete a scan is 2-3 sec, related to a frequency of 0.5Hz). Low temporal resolution is limited by a *finite signal to noise ratio (SNR)* and *blurred intrinsic hemodynamic response*. The hemodynamic response imposes a fundamental limit on the time-precision of the measurement. The main problem is that the neuronal response we want to measure is extended over time. The temporal smoothing that is created makes it difficult to detect the precise moment of neuronal activity. Therefore, the fMRI image that we obtain as result

reflects an average of acquisitions over many seconds. This makes very difficult to study highly dynamic neural process obtaining blurred fast neural processes.

The lack of temporal resolution causes a high frequent respiratory and cardiac oscillations to be aliased back into the lower resting state frequencies (0.01-0.1Hz). These high frequency cardiac and respiratory patterns can shape, as result, the BOLD-time series of anatomically separate brain regions in a similar way, introducing artificial correlations between time series of these region [13].

Other weakness of resting state fMRI is based on the relevant difference between analysed BOLD signals created by a cognitive task or spontaneous fluctuation in resting condition of the patient.

In a task-based fMRI the brain areas that would be activated, using a certain cognitive or sensorial task, are known a priori; if spatial location of neural activation is already known also the noise can be detected easily in the areas that present a high difference in BOLD signals. Differently, in resting state fMRI is not to possible to known a priori and specifically where the neural activation would be, due to the fact that are measured spontaneous fluctuations. This fMRI technique uses synchronous low-frequency BOLD fluctuations, created during rest condition from distinct regions. This low-frequency BOLD fluctuation represents an indicator of synchronous neural activity to create a functional network.

Resting state fMRI used to analyse functional connectivity, is based first on achieve a ***temporal correlation between fMRI signal changes*** in the different functional areas: cross-correlating an active brain region with all other voxel time coursed in the brain, discovering which area has the highest temporal correlation with the active one.

Next, is necessary to ***spatially localize the functional area*** that are connected, in communication, by establishing a threshold on the voxel correlation coefficient (temporal similarity) of BOLD signal in different regions of the brain. Over threshold voxel correlation coefficient result in the areas that are functionally connected.

As has been said before, low frequency- BOLD fluctuation can be confounded by many processes also low in frequency but not related to neural activity. ***Resting state confounds*** can be for example motion artefacts, cardiac and respiratory physiological noise, changing

in concentration of CO₂ in venous vasculature, the autoregulatory response of the vasculature to blood pressure change or cerebral autoregulation.

The interpretation of neural activation in resting state can be difficult if these confounds are not removed. Although it is not possible to entirely removed all the possible confounds and artefacts but is possible to remove the ones that affect more the data to increase the confidence of fMRI results and interpretation. One of the most important issue to be considered in the clean-up strategy of the data is that the confounding processes/artefact can have time series that are coupled with neural activations to be studied. If the variance of the confounding is removed is also removed the signal of interest.

One method could be use physiological recordings to clean up the data, these recordings contain also cardiac, respiratory, and other confounding processes. This technique uses a linear regression of these physiological recordings to clean up each voxel time series of resting state data. The influence on BOLD signal of each confounding process is modelled and using a linear regression is removed the interference of each physiological recordings [9].

The other approach uses only resting state fMRI data to clean up the acquisition. This technique is used whenever is not possible, or there is lack, of physiological recordings. The strategy is based on applying a band pass filter on the data such that the fluctuations in the frequency range outside of 0.01-0.1 Hz are eliminated and cannot affect connectivity measures [9].

1.2.4 ICA analysis in fMRI study

ICA analysis is a data-driven method, based on the decomposition of fMRI signal and used to analyse the activity in visual, auditory and cognitive domains and even in spontaneous fluctuation recorded in rs-fMRI. ICA technique is applied in many task-based and resting-state studies, used to determine functional connectivity networks created within brain regions [14]. (*data driven method will be described in particular in Paragraph 3 of the introduction*).

In addition, this technique is used to analyse the transient and randomly occurring neurophysiological events, and even the complex dynamic created by neural activation: ICA can distinguish differential response of several systems [15].

Furthermore, *ICA* is also used as an effective tool for *denoising fMRI data*, with respect to random noise or confounding signals, that could be for example respiratory artefacts or pulsation artefacts. This denoising is useful to isolate the brain activation of interest, that represents the source signal to be extracted, from the complex mixtures of sources that can be obtained in the fMRI data. Considering that the expected time course of the brain activation is difficult to be specified a priori, the main benefit of ICA technique, as data-driven method, is the fact that is not based on a priori information of the source signal, but is related to spatial and temporal patterns of activation in different brain regions.

In fMRI analysis is recorded for each voxel of the brain the neural activation and voxel time courses in the brain, then is achieved an HRF for each voxel. Considering fMRI data X , with T number of time points $\times N$ voxels, the ICA model applied can be expressed as:

$$X = AC = \sum_{i=1}^N A_i C_i \quad (1.11)$$

In which X is defined as the space-time data matrix of fMRI measurements, C_i represents the i th source signal, called independent component *IC*. A represents the mixing matrix with dimension $T \times N$: this matrix specifies the relative contribution of each IC at each time point as is represented in Figure 20. The columns of A represent the component maps, and the rows of C represent the time courses of the respective component maps. A and C are formed by i independent components of the process.

The main *hypothesis of ICA for blind source separation* is the linearity and independence of the source signals, considering that the joint probability distribution of N components is:

$$P(C_1, \dots, C_n) = \prod_{i=1}^N P(C_i) \quad (1.12)$$

$P(C_i)$ represents the probability of the i th underlying signal source. The *problem to be solved by ICA method* is find the unmixing matrix W , that is a pseudo reverse matrix of A , such that are obtained ICs as much independent as possible:

$$\hat{C} = WX \quad (1.13)$$

In which X is related to fMRI data, W is the *unmixing matrix* to be estimated by the algorithm and \hat{C} is the estimation of underlying source signal [14]

When ICA is applied to fMRI data, the independent source signals are interpreted as signals belonging to the same network, related to similar BOLD activity. If W is correctly estimated is possible to reconstruct the original fMRI data X and we consider to solve in a proper way the Blind Source separation problem estimating the correct and real Source signal.

Considering X , the original fMRI signal data matrix, and X' the reconstructed fMRI data obtained by using the estimated *unmixing matrix* W and *ICs*. The original data X can be perfectly reconstructed only if:

$$X' = W^{-1}C = AC = X \quad (1.14)$$

Generally, X' (reconstructed original data) is an estimation of the real measured fMRI data X . The application of this algorithm consists in the reconstruction of original fMRI data. To obtain this data reconstruction were introduced different separation methods that can separate modes that were task-related, transiently task related, and also confounding modes, represented by different kind of artefact as head motion, physiological pulsation, or machine noise [16].

Referring to Eq. 1.14, in practical application, the *unmixing matrix* W can be determined using statistical method based on *Infomax principle* [17]. Infomax principle is based on the information maximization, used to provide a unifying framework of components that solved the Blind Source Separation. Infomax algorithm is based on minimizing the Mutual Information between C_i source signals.

Another algorithm, that use high order statistics, is called *FastICA* [18] This algorithm represents a fixed-point for practical optimization of contrast functions. Fast ICA introduces new objective (contrast) functions, whose enable at the same time the estimation of the whole decomposition of the data by minimizing mutual information, and the estimation of individual independent component sequentially (one-by-one) as project pursuit directions.

All the ICA technique's algorithm, in summary, can separate processes related to signal of interest and processes related to artefacts that can be raised in fMRI experiment. Each of these processes may be represented by one or more independent components C_i .

Each **Independent Component** (IC) produced by ICA algorithm consists of a spatial distribution of voxel value ("component map") and the associated time course of activation. It is assumed that the *component maps*, each one specified by a spatial distribution of fixed value (one at each voxel), represent possibly overlapping brain areas of statistically dependent fMRI signal influence. In Fig.1.13 A) are shown the voxels identified in each of the four ICs, participating more actively in the measured signal. The measured fMRI signal is the linear sum of the contributions of each IC to the neural process, measured at each voxel, as is shown in Fig.1.13.

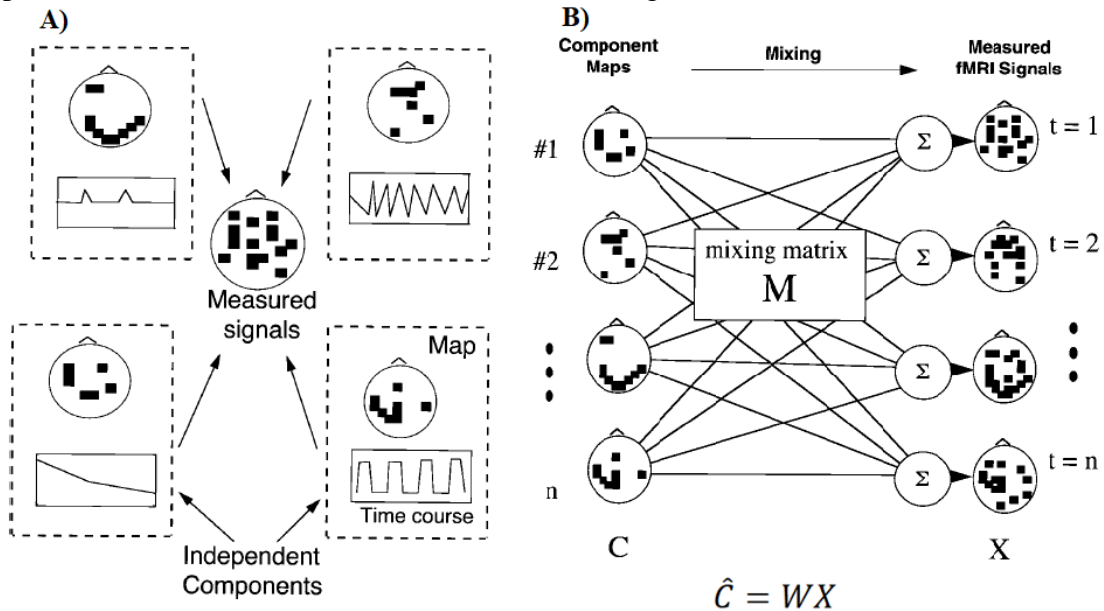


Figure 1.13, in the right figure A) is illustrated the decomposition of each ICs in component map and relative time course of activation. Each measured signal is given by the sum of the contribution of each ICs. The left figure B) represents fMRI as a mixture of independent component. ICA algorithm has to find the unmixing matrix W to obtain the estimation of IC component characterized by component map and time course

Each component C_i contributes to the magnitude of the original data. The contribution of each component is defined as γ_i . The contribution γ_i can be considered as the root mean square error RMS of the data set reconstructed only from this component or the RMS error introduced per data point when the data is reconstructed without this component [19], is defined as:

$$\gamma_i = \frac{1}{TN} \left(\sum_{j=1}^N \sum_{k=1}^T A_{jk}^2 \right)^{1/2} \quad (1.15)$$

Where N is the number of brain voxel and T is the number of time points. A_{jk} is an N by T matrix, obtained as outer product between the i th component map and i th column of W^{-1} .

Each IC is described by a distribution of values. Each value of the distribution, associated to each voxel, indicates how much that voxel is influenced by the activation of that component.

The aim is to find the group of voxels that are more active and contribute significantly to a certain component map. To do this, is necessary to transform the IC map value into z-scores (the number of standard deviations from the map mean). In the end is achieved a z-score for each voxel value in the IC map. If the z-score of a certain voxel is higher than a fixed threshold this *voxel* is considered to be *active for that component*. Each IC is associated to a group of active voxels in specific brain regions.

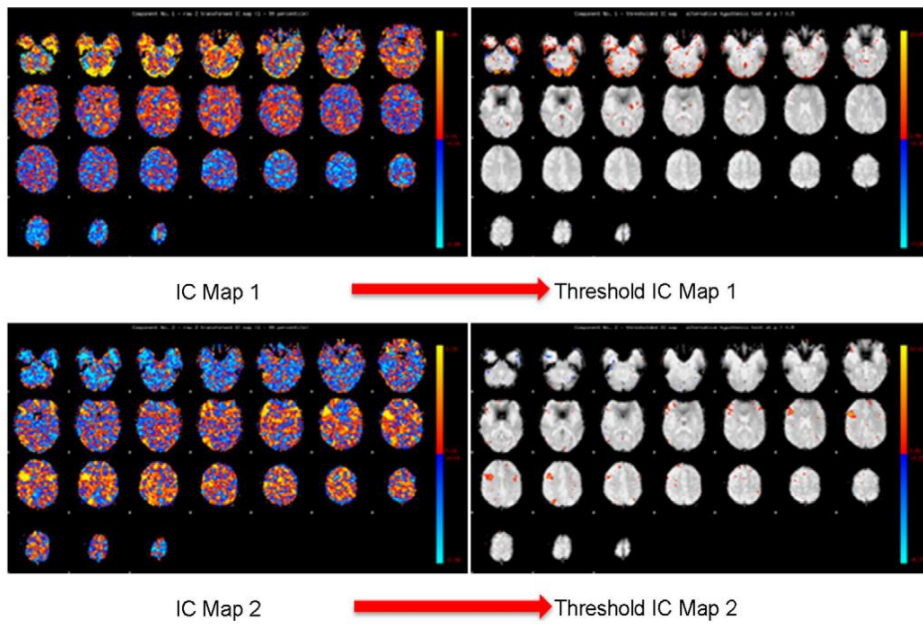


Figure 1.14, IC maps thresholding associated to each IC component IC1 and IC2.

By thresholding IC maps (Fig.1.14) can be obtained the *connectivity maps* with the corresponding underlying sources. The thresholded maps reveal the connectivity of brain regions composed by active voxels, associated to a high z-score value.

Ordering of the Independent Components

Independent component extracted from ICA can be ordered, as PCA, according to the amount of variance explained by that component.

The total signal variance can be expressed as the sum of the component variances. The ICs ordered by the explained variance create an ordering that is natural. Differently, the ICs can be ordered according to the features of interest. Other studies, for example *Moritz et al.* [20] ordered the components based on the frequency content, called power-spectrum ranking method. This method is use for separation of task-related component from the component associated to confounding factors.

ICA classification in sICA and tICA

ICA method can be distinguished in two subcategories depending on which kind of decomposition of the fMRI data is applied: *spatial ICA* (sICA) and *temporal ICA* (tICA). The former decomposes the original time sources into spatial independent components and spatially independent time courses. The latter is used to obtain temporal independent components and temporally independent time courses.

As has been said, to apply the standard, noise-free, ICA technique on fMRI dataset first is necessary to obtain the 2D matrix X of dimension $T \times N$, representing the observed samples used to obtain the underlying sources. This 2D matrix is estimated from 4D data array resulting from fMRI analysis (this 4D array represents the concatenation of 3D functional volumes in time). This decomposition can be performed in two ways [21]:

1. Considering data consist in the realization of t_l random variables, each one measured (sampled) on each v_l voxel. The results are a number of t_l 3D maps of activation (component map). Each 3D map is unrolled to get a matrix X of dimension $v_l \times t_l$.
2. Considering data consist in realization of v_l random variables each one measured at t_l time points. This result in v_l number of time courses each one of length t_l , collected in a matrix X of dimension $t_l \times v_l$.

The problem to be solved is the one expressed in Eq. (1.13).

First case corresponds to *sICA* in which the rows of the matrix C, composed by the underlying source, contain the spatially independent source signal of length v_l (unrolled spatial maps). The second case correspond to *tICA* and the rows of matrix C contain temporally independent source signal of length t_l (time courses associated to the source).

The assumption made in standard ICA is that the mixing matrix A is square [22], such that the number of sources is equal to t_l in sICA, and equal to v_l in tICA.

A matrix in the first case has dimension $t_l \times t_l$, in the second case $v_l \times v_l$.

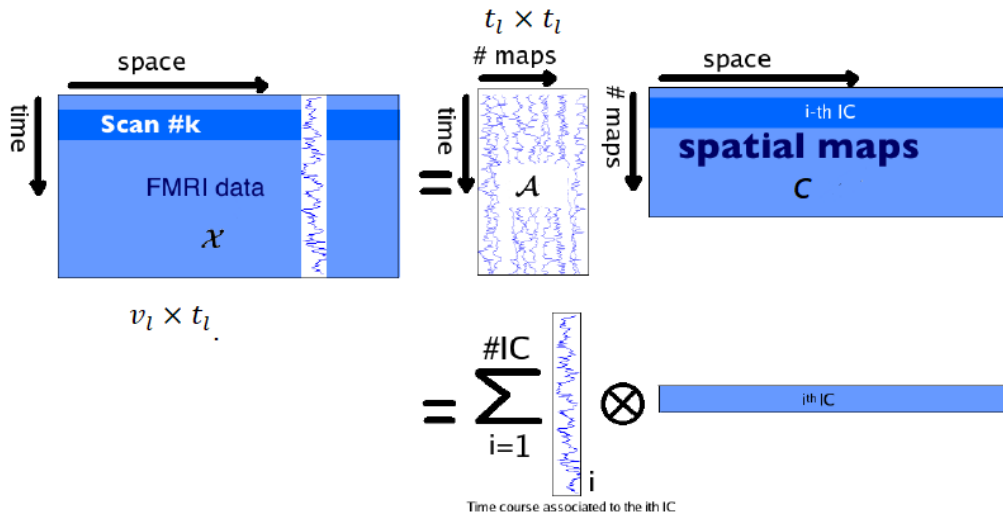


Figure 1.15, Decomposition of fMRI dataset using spatial ICA (sICA).

In Fig.1.15 is represented an example of decomposition of fMRI data operated by spatial ICA. In fMRI study both spatial and temporal ICA are widely used. There is not a direct comparison between spatial ICA and temporal ICA in literature, although the first application of ICA in fMRI study is based on spatial ICA [19].

In literature can be observed an abrupt switch from the use of temporal ICA to spatial ICA for fMRI studies. One of the most important reason of this abrupt change is that in fMRI data the *spatial dimension results larger than the temporal dimension*, as consequence is better to use sICA that solve Blind Source Separation considering a mixing square matrix A of dimension $t_l \times t_l$, where the number of source to be estimated is consider equal to t_l (t_l random variables, each one sampled on each v_l voxel). So, if the spatial dimension is larger than temporal dimension, is less computational heavy the estimation of the matrix A

then the unmixing matrix W . The spatial dimension is considered to be larger than temporal dimension due to the large number of voxels in fMRI experiments, it means that it is not computationally tractable to fully diagonalize the correlation (“mixing”) matrix A in the temporal case (that in this case has size $v_t \times v_t$).

Differently, in EEG studies the *temporal dimension is larger than source dimension* and it is better to use tICA.

However, these two ICA techniques can obtain different results depending on the characteristics of the underlying source signals to be estimated [23].

In the study of *Calhoun et al.* are designed four visual activation paradigms, each one consisting of two spatiotemporal components that were either spatially dependent, temporally dependent, both spatially and temporally dependent, or spatially and temporally uncorrelated. fMRI data were acquired using these paradigms and analysed with regression analysis, used as a “check” if the signal was occurring as expected. sICA and tICA were applied on these data, with the result that ICA can find the component only where expected.

In particular, *where the signals are highly spatially or temporally dependent (where independence is strongly violated)* ICA results do not agree with regression and “failed” for paradigms. Regression in this case is used to “check” these data, but in real application of ICA, the strong hypothesis on the location of activation pattern, are not always available. However, ICA is not completely free of assumption: it is important and necessary to make the correct choice (between spatial and temporal independence) to obtain the correct signal.

If the underlying signals are spatially correlated (dependent) but not temporally, it is better to apply tICA instead of sICA because it would probably estimate the correct activation pattern. *sICA yields not to the correct activation pattern if the null spatial correlation is strongly violated, and vice versa for tICA* [23].

As results, sICA and tICA could be applied if it is considered the correct hypothesis on the experimental condition (between spatial or temporal independence). Based on the appropriate assumption, the proper signals can be estimated and the activation pattern localized.

Single-subject ICA and Group-ICA

In a multi-subject applications of ICA technique, are applied typically two main approaches. Firstly, can be applied **Single-Subject ICA (Individual-subject ICA)** to each subject's data. Each subject data will be represented as a 2D time x space matrix. Each matrix is separately decomposed ICA into pairs of time courses and spatial maps. Original fMRI data is displayed as the sum of outer products of time courses and spatial maps. This process is illustrated in Fig. 1.16. To establish correspondence of ICs across subjects, with this single-subject ICA approach, is used subjective identification [19], spatial matching with a pre-defined template [24], clustering or cross-correlation. Nevertheless, using this approach is difficult to establish a direct correspondence of functional networks across subjects due to the fact that many networks that are identified from different subject are not similar enough and cannot be match directly. The problem can be solved by applying the alternative approach called **Group-ICA**, which introduce a group-level ICA considering fMRI data from all the subjects. This approach establishes a direct correspondence between ICs across subjects, overcoming the difficulties to obtain the matching of the components. Group-ICA can be applied using spatial concatenation, temporal concatenation or tensor organization. The type of Group-ICA widely used is based on *temporal concatenation* or *on tensor organization*. **Multi-session Tensor-ICA** represents all the individual datasets as a 3D single matrix *time x space x session/subject* block of data. Tensor-ICA decompose this block of data in triplets of time courses, spatial maps and session/subject modes. Differently, **Multi-session temporal concatenation** concatenates all individual datasets temporally to form a 2D space x concatenated-time data matrix, and perform the a single 2D ICA run on the concatenated matrix. Differences between Group-ICA and Single-Subject ICA is illustrated in Fig.1.16.

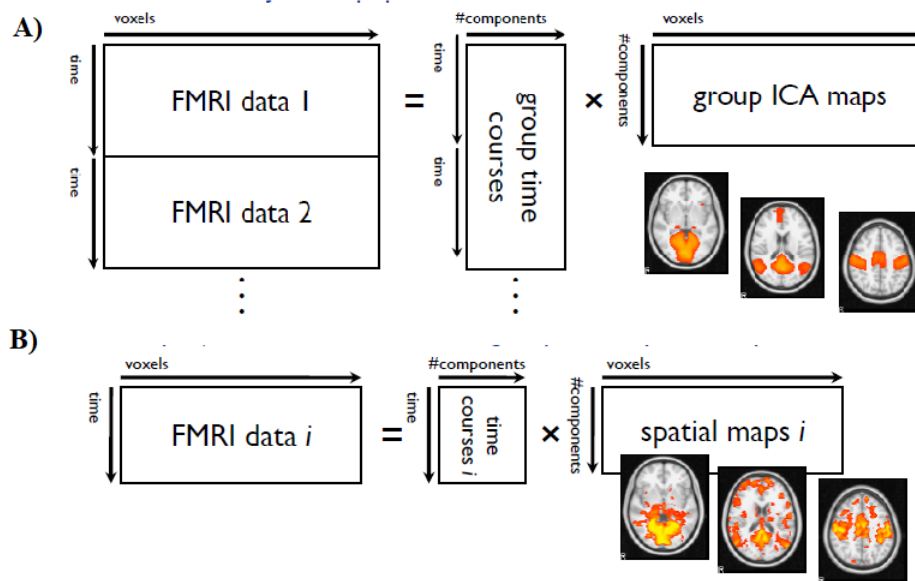


Figure 1.16 Differences between A) Group-ICA temporal concatenation and B) Single-subject ICA (sICA).

sICA application on task-based and resting state fMRI

ICA algorithm can be applied to study functional connectivity both in task-based and resting-state fMRI studies. One of the first practical *application of sICA to analyse task-induced brain activation* was introduced by MacKeown *et al* [19]. In this study is applied spatial ICA, used to decompose fMRI data in spatially independent components, with the main aim of distinguish between task or non-task related signal component and movements artifacts component. In total are extracted 144 ICA components for each trial, and rank-ordered by contribution size. For each trial is created a rank of the consistently task-related ICA components.

Considering that ICA technique is based on no prior knowledge regarding spatial and temporal pattern of brain response, it can be applied to analyse resting state fMRI, which is characterized by a very limited prior knowledge of activation (analyse spontaneous fluctuation created by brain region when subject is resting).

One of the first *application of ICA in resting-state fMRI* study was reported by Kiviniemi *et al.* [25]. This research analyses the ability of ICA to separate spontaneous physiological signal sources measured in 15 anesthetized child patients. The spontaneous physiological fluctuations created during rest condition can be studied by considering nondeterministic signal sources and reduced artifacts in the data. The study examines the activations in

anesthetize patient since they represent a *stable model* for analysing the ability of ICA to separate nondeterministic physiological signal sources from fMRI data.

Differently from *Mackeown et al.*, the study of *Kiviniemi et al.* applies ICA using FastICA algorithm, which corresponds to a faster and more robust method than classical ICA algorithm [18]. FastICA has to find the sources that are maximally independent and whose distribution is more non-Gaussian as possible (far from the normal). The most important step of FastICA is the application of the pre-processing step, in which is applied PCA (Principal Component Analysis) to reduce the dimension of the original data. In this research are considered 40 principal components to explain the higher percentage of the signal variance. Using FastICA, from these 40 components are calculated 40 ICs, associated to 40 ICA component localization maps.

1.2.5 Limitation of standard noise-free ICA and pICA

The fMRI data obtain from fMRI study are present in the form of *intricate mixtures* of the initial signal sources of interest. To process this signal sources is necessary to solve the ***BSS (Blind Source Separation) problem*** since is essential to separate the signal sources from the other signals present in the mixtures. The mixtures of signals are associated to different sources of variability in the signal as motion artefacts, physiological pulsation, head movement or hemodynamic changes that can be created at the time of the image acquisition.

As has been already said, to analyse the expected BOLD signal in voxel location and analyse interregional connectivity in the brain can be used *Model-based Method* or *Data-driven Method*.

In this section will be described the ***benefit introduced by ICA algorithm*** with respect to other analytical technique used for fMRI data. Next, ***ICA's limitations and drawbacks*** - and which technique is used to overcome them - will be examined.

The majority of analytical technique applied to process fMRI data can be mainly divided in Generalized Linear Model (GLM) methods or ICA algorithms. ***GLM methods*** applied strong hypothesis related to the expected BOLD signals that can be recorded in each voxel locations. The expected signals are considered as regressors in the GLM framework constituted by a multiple linear regression. The aim is to obtain the significant regressors

by applying a voxel-wise test statistic. The regressors are tested against a null hypothesis, which consider that these values are distributed according to some known null-distribution. For this kind of statistics are created statistical parametric maps to assess the statistical significance of each voxel under null-hypothesis (obtained using a certain cluster of regressors).

The **main drawbacks of GLM** is that is used strong prior assumptions about the spatio-temporal characteristics (patterns) of the signals included the data. This strong hypothesis leads to obtain suboptimal results, because are included into the model signals and noise that respect the prior assumption about spatio-temporal characteristics. Structured noise, orthogonal to the design, won't be consider in the model. This means that the model is characterized by a rising residual error that create a bias in the parameter estimation.

The other method that is applied, to overcome the limitation of GLM is ICA algorithms. **ICA technique** is free of strong prior hypothesis about the characteristics of the signals contained in the fMRI data. As was already introduced, the goal of these ICA algorithms is solved BSS problem by separating various source of the fMRI signal, by maximizing the statistical independence and non-Gaussianity of the source signals. Each Independent Component, in sICA for example, are represented by spatially independent component map and time course of the underlying signal. Each component map is then transformed in z-map with Gaussian distribution. Z-map are used to identified the “*active voxel*” (most significant voxel) in each IC.

ICA technique differs from GLM method under other aspects. For example, the mixing of sources to be estimated, is considered to be *square*, this means that the signals included in fMRI data are not constrained within a lower dimensional subspace, contrarily to the GLM methods in which data are limited by the number of the regressors of the GLM [26].

However, **ICA** algorithm is characterized by some **drawbacks**. Firstly, ICA techniques are not based on specific modelling hypothesis referred to signal patterns, but nevertheless is not completely free of assumptions. The correct source signals to be estimated, associated to a certain number of ICs, need to be spatially (sICA) or temporally (tICA) independent. It is necessary to iteratively optimize the *unmixing matrix* $W = A^{-1}$ so that $C = WX$ (in which C contain estimated source signal) contains mutually independent rows. If the

correct assumption, on spatial or temporal independence, is violated it can lead to decreasing the effectiveness of ICA technique [23].

Secondly, the effectiveness of ICA is influenced also by the *number of ICs estimated* and by the *method used to threshold the IC maps*. The study of *Ma et al.* investigated the influence of the *number of ICs on the results of ICA*. These results can be affected if this number is too small. By analysing the relationship between the size of the functional connectivity networks and the number of ICs they discover that when the number of ICs was greater than the number of source signals, the results of ICA were not affected by the number. On the contrary, if the number of ICs extracted was smaller than the number of source signals, ICA results show a high dependency on the number [27]. However, it is shown that this influence of number of IC extracted is not clearly observable when the number of ICs is lower than a critical number (found to be 9 ICs when consider in-vivo fMRI data).

The other problem of ICA is that is difficult to *associate thresholds with significant levels for ICA*. Since the amplitude of separated source signal is arbitrary, it results challenging to obtain the *correct statistically significant level of IC maps* to apply the thresholding. In common practice to threshold IC maps is necessary to convert the non-Gaussian independent maps of ICA into z maps with a Gaussian distribution [19]. Then, the significant level can be assigned based on the z map.

The conversion of IC map to z map is necessary to display the voxels contributing significantly to a particular component map. As result, the IC map values are scaled to z-scores, representing the number of standard deviations from the mean. Voxels whose absolute z-scores are greater than son threshold can be considered as an *active voxel* for that component. These z maps are thresholded using a specific z-score threshold (e.g $|z| > 2$). From this thresholding result ICA component maps representing maps of active voxels.

The study of *Ma et al.* analyses the applicability of this z-conversion of the IC maps, by evaluating the effect of z-maps conversion and investigating the consistency between the measured of False Positive Rate (FPRs) and the estimated False Positive Rate (FPRs), related to the results obtained using the z-map conversion. In the experiment, it has been shown that the z map conversion tends to overestimate the FPRs [27]. However, this overestimation is not very severe and may be acceptable in many cases of study.

At last, another drawback of ICA standard algorithm is the *noise-free generative model* that is used. The equation that need to be solved, using Classical ICA to find source signals is defined as:

$$X = AC \tag{1.16}$$

The main assumption used by classical ICA considers that the observed fMRI data are completely characterized by the *estimated source signals* (contained in matrix C) and the mixing matrix A . This means that the model of (Eq.1.16) does not include a noise model [26]. In turn, this *precludes the assessment of statistical significance of the source estimates* within the framework of null-hypotheses testing.

Both problems are strongly connected if we relax the *assumption of a square mixing matrix*. If we relax this assumption by considering a smaller number of source signals that can represent the dynamics in the data, we automatically introduce a mismatch between best linear model fit and original data.

Considering these problems connected to the Classical ICA based on noise-free generative model, is important to analyse *how the absence of a noise-model creates limitations for ICA technique*. As has been introduced, the noise-free generative model of classical ICA excludes either any test for significance and threshold techniques like converting the IC map to z map or statistical significance of source estimates within GLM framework.

To understand this problem is considered GLM and ICA spatial maps, that differ substantially. Activation patterns estimated by GLM technique and the one obtained in the ICA spatial maps can be characterized by important difference. Some activation patterns capture by GLM technique can be visualized in the ICA spatial maps by dramatically increase the number of voxels classified as active. This inflation of active voxels leads to a spatial activation clusters that are well localized, but characterized by ambiguity of interpretation. This represents the classical problem *overfitting of the noise-free generative model* to noisy observation [26].

The overfitting represents a situation in which is raised up the amount of “real effect” of interest, indicating the signal patterns, present in the noise-free generative model. These “real effect” of interest, however, is associated to both signal of interest and noisy

component that biased the results. Is necessary a *probabilistic model* that controls the balance between what is attributable to “real effects” of interest and what is related to observational noise.

Beckmann et al. developed a new model called *probabilistic ICA*, or pICA. This model assumes *non square mixing process* and *observed data characterized by additive Gaussian noise*.

pICA is formulated as a *generative linear latent variables model*. This model assumes that the observed p -dimensional time series are generated from a set of q ($q < p$) statistically independent non-Gaussian sources signal by using a linear and instantaneous “mixing” process characterized by additive Gaussian noise $\eta(t)$:

$$X_i = AS_i + \mu + \eta_i \quad (1.17)$$

In which X_i represent a p -dimensional column vector ($px1$) of individual measurement obtained at each voxel location i . A represents the mixing matrix of dimension $p \times q$, S_i is the q -dimensional column vector that represent the non-Gaussian sources contained in the original fMRI data. μ indicates the constant part of the model and η_i is defined as the Gaussian noise with a normal distribution $\eta_i \sim \mathcal{N}(0, \sigma^2 \sum_i)$. It is made the assumption that $q < p$, the number of sources to be estimated are fewer than the number of observation process in time.

The vector defined as μ is constant and represents the mean of the observation x_i , in which each i represents a certain voxel location. A , as we said, is considered *non-square, non-degenerate* (i.e. of rank q , is full column rank that means all columns of the matrix are linearly independent). The BSS problem can be solved by estimating an *unmixing* matrix W such that we can obtain a good *approximation of the real source signals* \hat{S} inside the original mixtures:

$$\hat{S} = WX \quad (1.18)$$

pICA differs from Classical ICA because consider a non-square mixing process and data confounded by an additive Gaussian noise. However, the objective of these two techniques, *pICA* and Classical ICA (related to noise-free generative model), is to estimate source signals that non-degenerative statistically independent.

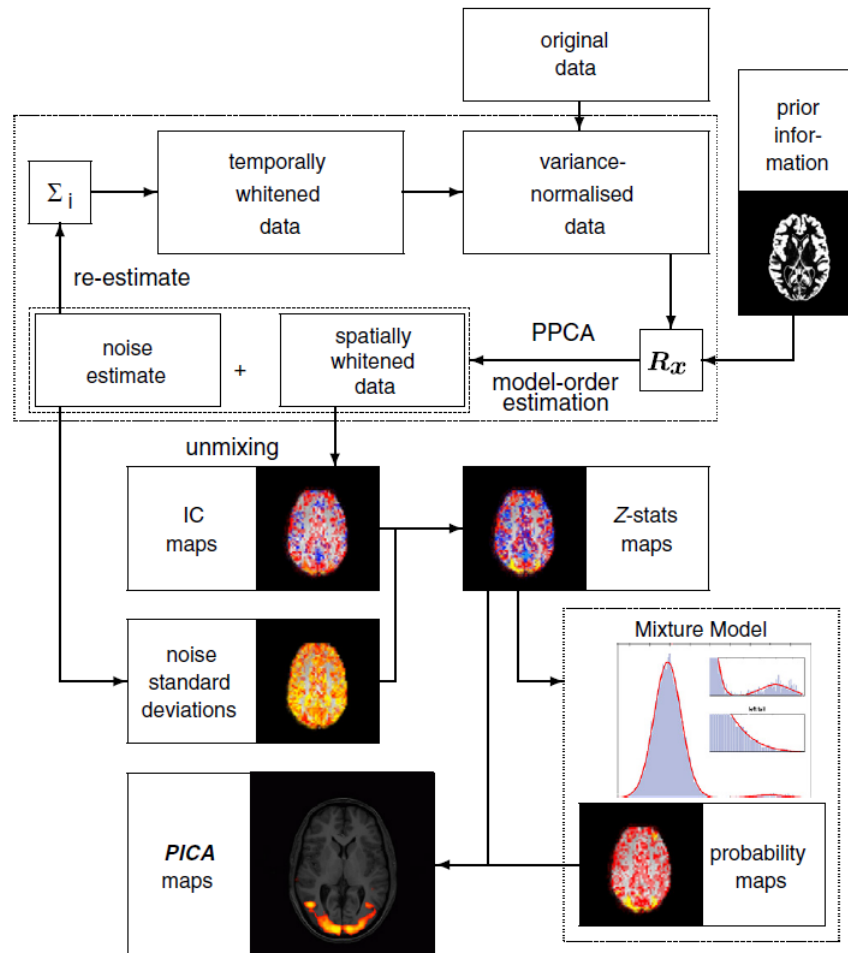


Figure 1.17, Illustration of Probabilistic ICA framework.

In addition, *pICA differs* (as standard ICA) *from GLM* because unlike the design matrix created in GLM, the mixing matrix A is not defined a priori in the model fitting, but is estimated as part of the model fitting during the model estimation. The single step that compose the *pICA* model is illustrated in Fig.1.17.

The original data are firstly demeaned and normalized to obtain *unit noise variance across the space, in all the voxels*, this process is called Variance Normalization (VN). This step is used to ensure that in absence of non-Gaussian signals the ICA decomposition does not consider the uninterested, Gaussian distributed, strong signals that can be characterized by

having a lot of associated variance (for example the signal for cerebrospinal fluid that is bright, related to high variance).

To obtain this homogeneity of noise variance across space, is necessary to have prior knowledge about the signal and the noise, such that can be forced in all the voxels the same noise variance. In the study *Beckmann and Smith (2004)* is introduced a solution: is ***iteratively perform normalization*** and ***probabilistic pICA (PPICA)***, such that the total original data are splitted into initial noise and signal subspaces. The initial noise is used as refinement of normalization step.

The first step begins with de-meaned data, that are firstly temporally pre-whitened, using prior knowledge about the noise covariance, defined as $\sum i$, at each voxel. Then is performed the normalization of voxel-wise standard deviation (VN). In the next step is calculated the sample covariance matrix \mathcal{R}_x . If some a priori spatial information is available, this information is used in conjunction with VN step to obtain \mathcal{R}_x . The output of this step are the *estimated noise* and a set of *spatially whitened observations*, that represents noise estimate and signal split in different sub spaces. Is possible to re estimate the noise covariance $\sum i$ from the residuals and re-iterate the entire cycle to refine the normalization step.

From the spatially whitened observations, the individual component maps (ICs map) can be obtained using FastICA algorithm, that use a fixed-point iteration scheme. FastICA is apply to obtain the *unmixing matrix* to estimate the source signals and ICs.

The final step of ICA is concerned with statistical inference. The estimated IC maps are transformed in voxel-wise Z- statistics, by dividing the *raw IC maps*, estimated by ICA in the step before, by standard deviation of the residuals from initial step of PPICA. The Z maps, differently from raw IC estimates, depend on the amount of variability explained by each voxel location in a decomposition (IC). In the end, Gamma/Gaussian mixture models are fitted to the individual Z maps (associated to the *individual component histogram*), such that can be obtained thresholded maps in order to infer the voxel location that are significantly modulated by the component time course. Gamma/Gaussian distribution are intended to model the “active class”. The resulting thresholded maps are called *PICA maps*.

To obtain the thresholding of ICA maps, is necessary to test an alternative hypothesis (“statistical effect of test condition within the voxel”, that means “voxel activated”) explicitly against a modelled null hypothesis (“No statistical effect of test condition within the voxel”, voxel is not active). After creating the statistical parametric map is established a statistical threshold, and evaluate for each voxel the statistical significance of the component time course in that voxel location. The null hypothesis is not respected for all the voxel that has a threshold level of 0.5. These voxels “survive” the thresholding as soon as the probability of being in the “active” class (using a Gaussian/Gamma mixture model) exceeds the probability of being in the “background” noise class. This threshold level assumes that there is an equal loss on false-positive and false-negative. If these rates are not equivalent the threshold level can be changed.

We may conclude that *thresholding techniques* should allow for explicit *control of the personal loss function*: it should be possible to control the identification of the balance between false-positive and false-negative case.

Another important topic *useful to obtain a correct thresholding of IC map and a good quality of fit (regarding the mixture model)* is the performance of *Variance Normalization step*. The normalization of voxel-wise residual noise (VN) is important for assuring that the voxels which do not contain any signal end up being modelled well by a single Gaussian distribution, to distinguish them by the signal [28].

Without variance normalization the “background” noise histogram is characterized by a more sharply peak with respect to a simple Gaussian bell curve. This can create a fit of the mixture model that is poor, and the Gamma/Gaussian distribution, that is supposed to model activations and deactivations in the tail of the distribution, also include the tails of the background noise class. If the variance normalization is applied in the pre-processing, each voxel’s time course is normalized to the same background variance, creating a better fit of the model. The effect of this better fit, is the decreasing number of false positive rate, that means decreasing the statistical threshold use to threshold IC map, representing an increasing of the “active class” [28].

In Fig.1.18 is illustrated the effect of variance normalization on the mixture-model based thresholding.

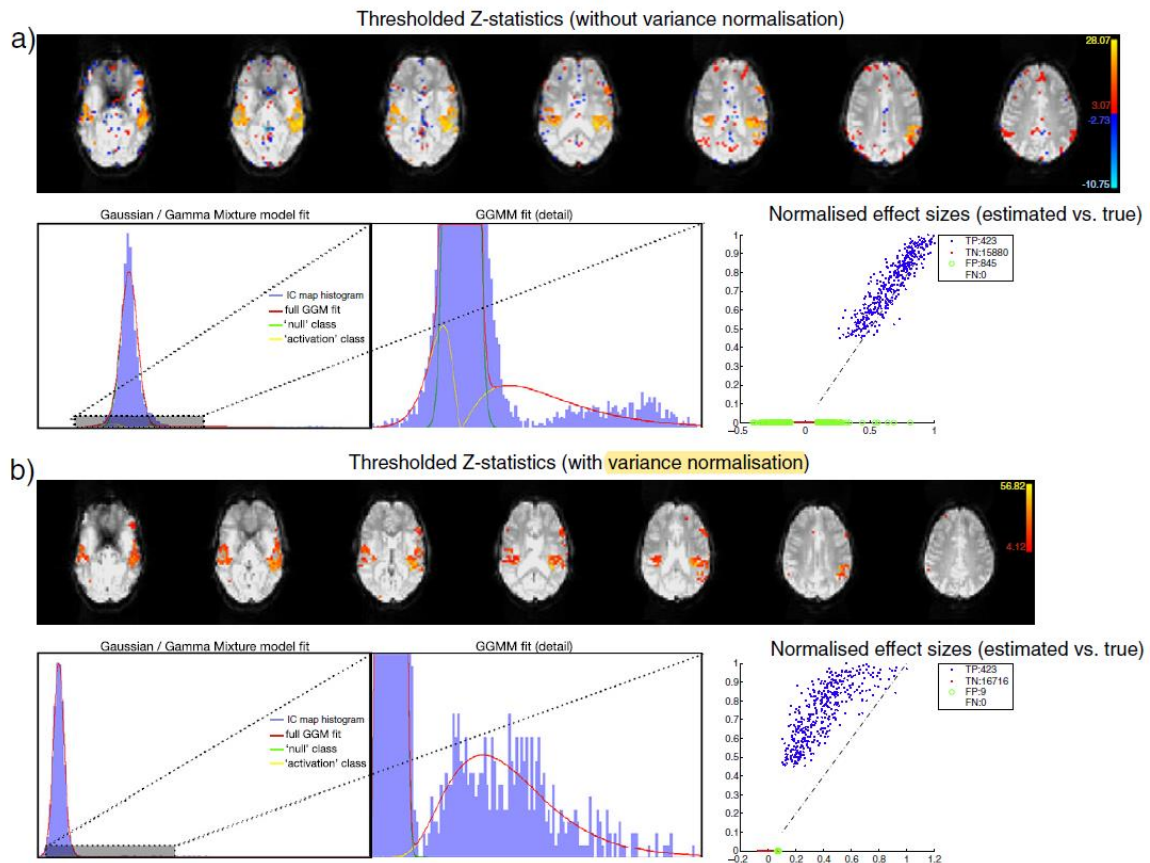


Figure 1.18, Illustration of the effect of variance normalization on the mixture-model based thresholding. a) results for non no variance normalized data and b) for variance normalized data. On the top right and bottom right panel is represented the FP,TP,FN,TN rates.

To conclude, pICA overcome the limitations of the standard noise-free generative model of ICA, introducing an analysis technique that is useful to ensure the extraction of Independent Component from ICA, taking into account also artefacts that can be present in the fMRI original data.

1.2.6 Application of pICA: Artefacts and data denoising

The main applications of pICA are related to the accurate *Artefacts classification and characterization*, followed by *fMRI data denoising*, which works considering the extracted spatial and temporal characteristics of the noise present in the data.

To remove the worst noise present in fMRI data is used *data pre-processing* that consists in spatio-temporal filtering of the data prior to the analysis, correcting motion created by the subject and other distortion, and lastly expressing the model of the outliers as part of the statistical procedure.

pICA can be used to **remove the residual noise present in fMRI data** that survive to the data pre-processing. *pICA* can separate *noise* and *signal*-related pattern of activity by considering that artefactual components can often be recognized based on specific spatial and temporal features. fMRI can be associated to different kind of Artefacts [28]. Firstly, artefacts can be connected with *problem of the scanning hardware*, that affect the measurements and the expected performance of the individual component due to issues of technical components involved in the image generation. The images can be corrupted by slice dropouts, caused by small gradient waveform corruption, that consist in ghosting of the object in the diagonal direction of the image. Other hardware artefacts are connected to the instability of the timing of the slice select gradient and RF pulse, creating spiking of intensity over the brain volume. IC can be also affected by artefact related to *head motion* of the subject during the acquisition, that results in ghost images in the phase encoding direction. Other motions are related to *brain motion*, caused by physiological pulsation created by cardiac and respiratory cycle. This artefact results in rim-like effect at brain/non brain boundary. Then, some images can show up N/2-ghosting that is due to the incorrect timing between image acquisition and gradient switching, representing a high frequency noise that cause ghosting in the image. Another high frequency noise is the high intensity rapid variation of the CSF in the ventricular system, create ventricular pulsation.

A classical but widely used method is related to **manual classification of ICs**. The drawbacks of this approach are that is time consuming and require expertise, therefore is necessary a proper study of IC classification guidelines. To overcome these limitations, **fully automated classified methods** have been proposed, which have the purpose to classified noise IC component based on spatial, temporal and frequency characteristic. The main difference between these methods is in terms of the classifiers that is used e.g. global decision tree [29], SVM [30] or hierarchical fusion of classifier [31]. Other differences between these methods, are related to the number and types of features necessary to correctly classify *signal* from *noise*. As examples, *Pruim et al. 2015* develop ICA-AROMA that use four spatial and temporal features to classify ICs. Differently, FIX toolbox [31] uses 180 features extracted from spatial maps, time course and power spectrum of ICs to classify between *noise and signal*. However, the application of this fully automated methods to new datasets is not always easy and advisable. For example, ICA-AROMA results to be not versatile because detect specifically motion artefacts. On

the other side, to achieve a good FIX performance now new dataset it is recommended to re-train the tool, that is computationally expensive and requires a minimum number of subjects. The main difficulty of automatic classification relates the requirement of much larger and better sets of hand classified ICA decomposition across different MR sequences, to obtain better train sensitive and specific classifiers.

Subsequently to the use of pICA for *artefact characterization*, ***pICA model is then applied for data denoising***. The main aim of this application is to use information represented in the decomposition, extracted in the step of *artefact characterization*, to obtain an IC decomposition denoised by the effects of artefacts. There are various number of possible approaches to be used: can be used information about spatial maps, or time course information to remove certain voxels or identify time points of interests. Likewise, can be use both time course or spatial maps to verify the correction of the artefacts. Differently, other approaches introduce the idea to use ICA as an “intelligent filter” that use the characterization of the artefacts to identify the non-Gaussian structured noise in the data and then subtract it from the original data.

To conclude, pICA applications permit to obtain, in parallel with standard data pre-processing, denoised ICs devoid of the most important effect of artefacts present in IC maps and associated time course.

2. Analysis of resting-state fMRI data

As was introduced in *Paragraph 1* of this Introduction Chapter, the spontaneous or resting-state fluctuations of the BOLD signal in the fMRI analysis represents an effective tool to analyse and delineate human neural functional architecture.

In this Chapter is represented a focus on the resting-state fMRI, considering spatio-temporal and spectral characteristic of resting state network activity and the acquisition and processing step of this kind of fMRI data.

The majority of the resting-state fMRI study *use model-driven methods* to analyse this spontaneous neural activity. This model drive-methods, described in particular in *Paragraph 3*, is based on a priori hypothesis that consider the function connectivity of a

small number of regions of interest (ROIs). Other approaches analyse multiple number of ROIs using both *model-driven* and *data-drive method*.

When the subject is in a resting-state condition the spontaneous neural activity recreate architectures of dynamics and complex networks that result active at the brain level. These networks are called ***Resting State Networks RSNs***. The neuronal activity patterns that data-driven and model-driven method want to analysed are created by these RSNs, active at different brain regions. The main signal processing technique used for resting-state fMRI are seed-based correlation analysis (SCA) and independent component analysis (ICA). ICA approaches of Single-Subject ICA and Group-ICA ensure the reproducibility and reliability of RSNs.

2.1 Spatio-temporal characteristics

The estimation of spatio-temporal characteristics of these low-frequency fluctuations from fMRI data is still present as a challenge for analytical technique in literature.

The most important spatio-temporal characteristic assessed by various researches is the location of ***RSNs in grey matter regions***. Furthermore, this finding demonstrates that these networks reflect functional systems supporting core perceptual and cognitive processes.

Many studies in literature analysed ***spatio-temporal structure*** of the RSNs, also called intrinsic connectivity networks (ICNs).

The first study that apply ICA on resting-state fMRI data to analyse low-frequency patterns and their spatial characteristics was *Kiviniemi et al. (2003)*. Subsequently, to optimize the analysis on fMRI data was introduced by *Beckmann et al. (2004)* pICA technique.

Beckmann et al. (2005) study applies pICA to resting-state fMRI data in order to extract ***spatio-temporal structure of these data***, to identify low-frequency resting-state patterns from the data. This study identifies spatial characteristics of resting state fluctuations. The analysis demonstrates that the low-frequency resting fluctuations appear within the ***grey matter*** and the functional relevance of these low-frequency patterns depends on the spatial locality in grey matter. pICA shows that significant voxels, associated to low-frequency patterns, are generally located within grey matter and include a little or no white matter.

Then in the study of *Beckmann et al. (2005)* was performed a group data analysis of 10 subjects to demonstrate the *consistency of resting-state fluctuations across subjects* predominantly contained in grey matter. Also appear that these low-frequency resting patterns appear to be localized within discrete areas of functional significance as visual, sensory and motor cortex area [32]. *Beckmann et al. (2005)* has demonstrated that these patterns of intrinsic functional connectivity of RSNs are consistent with stimulus evoked co-activation patterns in sensory and motor cortices. Other studies reveal the consistency of low-frequency resting state patterns with either language and memory system and higher cognitive control networks.

These findings lead to the idea that RSNs appear to be either *up-regulated and down regulated during specific cognitive tasks*. In fact, RSNs can be described as “task-positive” or, if consider “default mode networks”, “task-negative” in terms of the direction of correlation between the mean network activity and the event timing during the task.

Other researches also demonstrate that RSNs display *consistent functional connectivity patterns with specific thalamic and cerebellar nuclei*. These studies have been focused the attention on the *cortical contribution* to these intrinsic connectivity networks (ICNs, equivalent to RSNs), followed then by the contribution obtained by *sub-cortical areas*, with at first a limited attention on cerebellar contribution. Subsequently, new studies explore resting-state cerebellar connectivity. This investigation enables to underline cortico-cerebellar and sub-cortical connectivity associations.

To summarize, studies on ICNs (equivalent to RSNs) allow to attribute various functions and spatio-temporal characteristics on these networks, analysing at the same time the association with different discrete functional areas. In particular, they help to quantify and characterized neural substrates of system-level function and dysfunction [33].

2.2 Spectral characteristics

RSNs are characterized, as introduced in *Paragraph 1*, by low-frequency contribution, in terms of spectral characteristic. One of the first study to characterize the spectral characteristic of RSNs was *Cordes et al (2000)* that demonstrate that the synchronous, spontaneous BOLD signal oscillations can be identified as a low-frequency fluctuation (0.01 Hz-0.08 Hz). *Cordes et al (2000)* display that other low-frequency fluctuations, that

could be associated to cardiac or respiratory cycle artefacts, are separable from spontaneous fluctuations of interest related to RSNs. Cardiac fluctuations are related to 0.6Hz-1.2 Hz frequencies, and respiratory fluctuations present between 0.1-0.5Hz.

Other recent fMRI analysis, suggest that low-frequency BOLD signals from RSNs is more “broadband” than was previously thought. *Smith et al.2008* and *Niazy et al.2008* show that the main spectral power of RSNs is visualized in practise at low-frequency band (0.01 Hz), but the signal contribution of these networks can be extended to higher frequency of 0.15 Hz. It has been shown that filtering RSN signals, to account for the frequency content of their HRF, “flattens” the power distribution from 0.01 Hz up to 0.15 Hz [34].

This suggests that the low peak power characteristics of BOLD fMRI-derived RSNs are largely induced by the haemodynamic and this finding underlies the idea that the neural dynamics of RSNs may be more “broadband” than previously thought.

Taking into account all the spectral characteristics of RSNs described before, is important to note that many artefacts can still be present in the frequency ranges of RSNs signal.

Many artefactual signals have spectral peaks that can be either within similar low frequency ranges seen with RSNs, or could be aliased by the fMRI temporal sampling into these ranges.

The main solution to this artefacts’ issue is related to the introduction of a clean-up strategy, such as *ICA technique* introduce in the *Paragraphs* before, to reduce confounding factors in that frequency range to separate *signal* and *noise pattern*.

2.3 Acquisition and pre-processing of resting state BOLD fMRI data

The *acquisition time* used for resting-state fMRI session is typically *5-10 min*, but the optimal duration of a resting experiments is still an open issue. The trade-off to be found is between the acquisition time and how much detailed parcellation of functional connectivity pattern is required. In order to obtain a more detailed parcellation (acquire more measure of the volume of the brain) is used an higher- dimensional ICA decomposition that consequently increase the degree of partial temporal correlation between sub-systems, decreasing the ability of interpretation and delineation of these networks [35]. In addition

to the acquisition time issue, does not exist any kind of consensus the *experimental settings* to be used to obtain the most significant impact on the results and interpretation. Different studies analysed many kinds of experimental settings to study resting-state condition, these can consider subjects that are awake or asleep, with eyes closed or open. To analyse stable RSNs patterns when the patient is asleep, require to acquire data in various sleep states, excluded deep sleep.

Successively to the data acquisition, to obtain a better data quality and extract in the following steps meaningful information is applied on Resting state BOLD data the *standard pre-processing steps* of BOLD fMRI data, used also for task-related data. For each subject, the pre-processing includes the spatial realignment of the fMRI volumes, structural-functional coregistration, tissue segmentation (on the T_1 – *weighted image*), then spatial normalization to the standard MNI space and spatial smoothing using a Gaussian window of a fixed FWHM.

As has been said, the *removal of confounding factors* can improve the quality of neural activity to be analysed. These confounding signals can be eliminated, *in the pre-processing* step before applying the RSNs pattern analysis, by using external recordings of physiology or data-based method that use only resting-state fMRI data. The first method models the influence of each physiological process on the BOLD signal as a time series, then is fit to the data using a linear regression procedure. This fit is then subtracted to the data to remove the related physiological variance. The second method, in case of a lack of physiological recordings is present, simply is necessary to band-pass filter the data to eliminate noisy fluctuations outside the frequency range of interest.

An alternative clean up strategy to denoise the data, after pre-processing step, is applying *ICA technique*, as described in *Paragraph 1.2.6*. In this case, after the decomposition of the data in spatial components ICA is able to isolate the IC associated to signal from the noise IC.

2.4 Methods for RSN identification

Methods used to identify and analyse RSNs in the different brain region and analyse the connectivity pattern between these spatially distributed networks are divided in *model-based method*, for example seed based correlation analysis (SCA), or *model-free method*

as ICA technique. These two possible approaches to study functional connectivity between RSNs will be described in *Paragraph 3* related to functional connectivity study in fMRI (fcMRI).

3. Methods for functional connectivity study

As has been said before, fMRI can be discriminated between two type of studies with different target of the analysis. One type is task-based fMRI, in which is perform a task by the subject and the aim is to find spatial activation pattern in human brain created by performing a specific cognitive or sensorial task. The other type of fMRI is performed during a period in which the subject is resting and is called *functional connectivity fcMRI*. Studies related to fcMRI have the goal to find temporal correlations of spatially remote neuro-physiological events and examine the regional interactions in the brain at a macro level. fcMRI is generally obtained analysing data from resting state fMRI.

The main aim is to study the connectivity patterns of multiple, functional, distributed, large scale *networks* of the brain dynamics to obtain a useful tool for studying the domain of systems and neuroscience.

Methods used for functional connectivity analysis via fMRI are distinguished into two categories: *model-based method* and *data driven-method* [14].

3.1 Model based method

The model-based approach is used to detect functional connectivity in fMRI studies. These methods select *region of interest (ROIs)* called “seed” that represent the nodes of the dynamic brain network, and define whether other regions are connected to these seeds using a definition of a certain metrics, and as result generate connectivity map that represents functional network present in the human brain.

These *model-based or hypothesis-driven* approach are based on an a priori selection of a seed region and require strong prior knowledge of neuroscience or expert contribution.

These kinds of techniques explore the statistical dependence of a lower frequency fluctuation of BOLD signals between regions. The approach is based on test the statistical dependence of low-frequency fluctuations of BOLD signals between a pair of ROIs. The

voxel-based functional connectivity method, also called seed-based methods, can be used as functional connectivity analysis based on a priori ROI, defined as the seed region, and then test the statistical dependence of low-frequency fluctuations between the seed and all the other voxels in the brain. This analysis explores all the voxels in the whole brain that have a significant statistical dependence with the seed region, obtaining a functional connectivity map. This technique of voxel-based method, also called seed-based method, requires an a priori selection of the seed-region, ROI, which also represents the node of the dynamic brain network.

Depending on which metric is choose for the functional connectivity analysis to analyse the statistical dependence of low-frequency fluctuations of BOLD signals between a pair of ROIs, the model-based method can be distinguished for example in *Cross Correlation Analysis, Coherence Analysis, Statistical Parametric mapping or Mutual Information analysis*.

Cross Correlation analysis is used to detect regions of functional connectivity defined as region with a high correlation between fMRI measures of brain activity. A simple measure of correlation is the correlation coefficient calculate at each voxel to produce an image of correlation coefficients. If the brain's region related to a correlation coefficient, of each voxel composing that region, is over a fixed high threshold value means that these regions are functional areas of high correlation [36]. First is necessary to select the seed (ROI) that represents the region of interest, then is used the Cross Correlation to highlights connections between different brain regions.

The main assumption in Cross Correlation analysis is that: if one region of the brain is functionally connected to a certain seed, there should be a correlation in terms of their BOLD time courses. Defining $F_x(k)$ as the recorded fMRI BOLD time course and a seed $F_y(k)$, defined also as time course, the Cross-Correlation Analysis CCA estimates the correlation at time lag μ as:

$$Corr_{x,y}(\mu) = \frac{Cov_{xy}(\mu)}{\sqrt{Var(x) \times Var(y)}} \quad (1.19)$$

In which $Var(x)$ and $Var(y)$ define the variances of the two time courses $F_x(k)$ and $F_y(k)$, $Cov_{xy}(\mu)$ defines the cross variance of $F_x(k)$ and $F_y(k)$ at a time lag μ . This cross

variance can be expressed as the expected value of the product, respectively, of the difference between the mean of $F_x(k)$ with $F_x(k)$ and the mean of $F_y(k)$ and $F_y(k)$:

$$Cov_{xy}(\mu) = E\{(F_x(k) - E(F_x(k))) \times (F_y(k) - E(F_y(k)))\} \quad (1.20)$$

If the Cross variance $Cov_{xy}(\mu)$ is over than a fixed high threshold means that also the Cross Correlation $Corr_{x,y}(\mu)$ has an high value: in this case we consider the two time courses, of the BOLD signal $F_x(k)$ and of the seed $F_y(k)$, are functionally connected.

The main limitation of the application of CCA is related to the fact that the calculation of the Cross-correlation evaluated considering the full-lag-space is heavy and expensive.

Fortunately, for the hemodynamic response of the blood is not necessary to consider the full-lag-space: the duration of the Hemodynamic response function HRF is limited, even if exist a variability of this function between subjects and between regions in the same subject. Considering the HRF of the blood, the correlation can be calculated in a time windows equal to the duration of this function (about 10 sec). This kind of time window focus on a limited number of time points permits to calculate in CCA a correlation characterized by zero lag.

The *drawbacks* of this technique are based on the sensitivity of the correlation to the shape of HRF: the HRF has limited duration but the duration can vary between subjects and between regions of the same subject. This interregional variability of HRF shape and duration leads to a decreasing in the interregional correlation measure, independent on the underlying neural activity. Other *drawbacks*, are related to the confounding and artefacts created by cardiac activity and blood vessel activity in the brain: these confounding processes can create the false representation of a high correlation between region created by BOLD signal.

Another kind of model-based method is the *Coherence Analysis* use to measuring the interregional functional connectivity in the fMRI data. Coherence represents the spectral representation of the Correlation in frequency domain [37].

Defining the same two times courses $F_x(k)$ and $F_y(k)$ of Eq. (1.19) Coherence can be expressed as:

$$Coh_{xy}(\lambda) = \frac{|F_{x,y}(\lambda)|^2}{F_{x,x}(\lambda)F_{y,y}(\lambda)} \quad (1.21)$$

Where $F_{x,y}(\lambda)$ represents the cross-spectrum and $F_{x,x}(\lambda)$ and $F_{y,y}(\lambda)$ represent the power spectrum. The cross-spectrum can be defined using the Fourier transform as the FT of the Cross Variance $Cov_{xy}(\mu)$:

$$F_{x,y}(\lambda) = \sum_{\mu} Cov_{xy}(\mu) \times e^{-j\lambda\mu} \quad (1.22)$$

The power spectrum of $F_{x,x}(\lambda)$ and $F_{y,y}(\lambda)$ and define as the same way as the cross-spectrum in Eq. (1.22) considering the Auto-covariances $Cov_{x,x}(\mu)$ and $Cov_{y,y}(\mu)$.

The *benefit* of Coherence analysis is related to the invariance to interregional differences in the HRF. The coherence can estimate the time-invariant relationship between time series and is used to study functional connectivity, based on fMRI data, across regions with variable hemodynamic properties.

Studies demonstrate that brain region that recreate signals characterized by high value of coherence at low frequency range (<0.1Hz) are subjected to functional connectivity between each other [10]. The *drawbacks* of this method are that is sensitive to fluctuation of cardiac activity. The cardiac activity is present at a frequency of 1.25 Hz, so can be create a false coherence value around this frequency because it could rise due to a higher cardiac activity and not for a higher functional connectivity.

The last model-based method presented is the *Statistical Parametric Mapping (SPM)*. This method used at the same time a general linear model (GLM) and a gaussian random field (GRF) theory to apply statistical inferences to obtain statistical parametric maps. In connectivity studies, the GLM technique is divided in two level analysis. First is necessary a scaling and filtering process for all brain voxels and applying an average over voxels in certain seed region. Then each brain voxel is characterized by a time series, if the time series of the voxel can be related to the time series of the seed region (ROI) this voxel time series is introduced as covariate, regressor in first level analysis.

In the *first level analysis* is obtained the contrast image corresponding to this regressor for each subject and it is used to feed the second level random effect analysis. *This second*

level apply a classical statistical inference to obtain statistical parametric maps: these maps are related to the brain area that shows a significant functional connectivity across subjects. The main aim in resting state fMRI that use SPM method, since it is based on spontaneous fluctuation and there is not a designed cognitive activity, is to mimic the stimulus based on the selected region of interest (seed) and this one is used as the real stimulus in cognitive task.

Another approach used to establish the statistical dependence of low-frequency fluctuations of BOLD signals between a pair of ROIs, is the calculation of the functional connectivity based on ***Mutual Information*** between sets of seed and target voxels. The Mutual information and interaction shared between two time series of different ROIs, indicates a measure of functional connectivity between ROIs sensitive to non-linear interaction between two different brain regions.

Model-based methods are widely used to detect interregional functional connectivity within fMRI data in resting state and task-based condition. ***The main issues*** associated to this method are, for example, the *sensitivity of the initial location of the seed* within the ROIs: different definition of the seed achieve different interregional functional connectivity. Then, another concern is associated to the *necessity of prior neuroscience knowledge and experience*: if we focus only on prior knowledges related to certain region of the brain, is possible to avoid useful information about a region that shows a high functional connectivity. This method is based on a *dependence* related to the definition of the initial seed in the ROIs and to focusing only on brain regions relative to prior knowledge [14].

3.2 Data Driven method

The other category of methods to analyse functional connectivity between regions in the brain is called ***data-driven method***. These methods are independent of a priori information and knowledge assumed and can overcome the limitation imposed by model-based methods. The types of data-drive methods are grouped in ***two principal types*** [14].

The *first type* has the aim of *decompose the original fMRI dataset* in a linear combination of basis vectors (Principal Component analysis PCA and Singular Value Decomposition SVM) or in statistically independent components (Independent Component Analysis).

The *second type* of methods are related to apply *traditional clustering technique* to fMRI dataset such as: Fuzzy Clustering Analysis (FCA), Hierarchical Clustering Analysis (HCA). In accordance to the aim of this work, it will be described in detail Independent Component Analysis ICA.

3.2.1 Independent Component Analysis

Independent Component Analysis, as has been described in *Paragraph 1.2.4*, is a data analysis technique accounting for higher order statistics. ICA represents a generalization of PCA, furthermore PCA can be used as pre-processing step in some ICA algorithm.

ICA technique has the aim of recovering unobserved signals or “sources” from observed linear mixtures of this sources, consider only the assumption of mutual independence between signals. The mixture is supposed to be linear and not Gaussian; the hypothesis of sources statistically mutually independent is possible to solve this problem called “*Blind source separation*”. The mixture of sources is characterized by this lack of a priori information, that is compensated by the statistically strong hypothesis of linearity and independence of the sources [38].

The main analytical steps of ICA technique are described in *Paragraph 1.2.4*.

All these methods of PCA, SVD and ICA are used to obtain a linear combination of the component of the signal. The difference is that ICA would find the component such that are as much independent as possible. PCA and SVD would find orthogonal components.

ICA is characterized by *two main difference with respect to PCA*: the frame of reference directions is not orthogonal and also use second and higher order statistics. The reason is that the distribution of the data (Fig. 1.19) is more representative of real data distribution using non orthogonal axes.

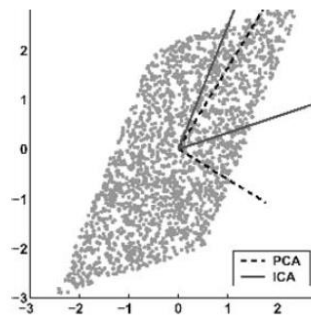


Figure 1.19 Differences in PCA and ICA reference directions.

In addition, differently for PCA, the ICA first define the number of sources to be computed. Then, changing the dimension of the unmixing matrix to be estimated we can change the number of independent components to be extracted [38].

3.3 Dynamics and Graph-analysis of Brain's Networks

The studies on connectivity pattern between networks in the brain want to analyse *how functionally specialised areas interact with each other*. These methods of fMRI are connected to the architecture of the networks that are active in the brain, organized in nodes, and also to the relationship between nodes in the dynamic processing stream.

Based on the measure of functional connectivity, using the methods described before, is possible to derive *different functional networks in the brain during the resting-state condition (RSNs)*, differing between each other for specific networks characteristics and properties. The definition of these connectivity networks could be useful to visualize the particular architecture of these connectivity between nodes in a network, as well as the *dynamic relationships* and *topological characteristics* related to the network itself.

The functional architecture of the brain can be described as a dynamical system where components interact in flexible ways, constrained by physical connections between regions. Recent advances in the science of these complex networks have utilized tools from topological data analysis to investigate the connections between constituent parts of networks using powerful and flexible algorithm.

The *topological data analysis TDA* combines algebraic topology and other tools from pure and applied mathematics to support the study of the architecture of the dynamic and complex network. An example of simple type of topological data analysis is the *graph-*

theoretic connectivity, that has found a wide application in functional neuroimaging. This graph-theoretic connectivity analysis allows to represent the functional brain connectivity networks as a graph, in which the connection between each node indicates the functional connectivity between brain regions. Moreover, more advances use of topological data analysis is emerging to provide new insights related to brain networks functionalities of the subject.

As has been already said, the whole brain can be modelled as a network, the so-called *human connectome*, where nodes represent cortical and sub-cortical grey matter areas. Functional brain networks derive from measures of functional connectivity, in particular correlated activity between regions over time, assessed using rs-fMRI, task-based fMRI or other imaging modalities as EEG or MEG. Networks nodes are associated with distinct grey-matter regions, while white-matter fibers relate to the interconnecting network links. However, the lack of a gold standard for *regional parcellation* in brain MRI makes the definition of nodes arbitrary, meaning that network nodes are defined using templates employing either random or anatomical parcellation criteria. We used the parcellation method to reconstruct the brain network using the AAL template which decomposed the brain in 116 regions. Subsequently, are selected the first 90 ROIs that represent the region of interest for this study.

After the parcellation of the brain in distinct ROIs, is performed the *extraction of the BOLD signal time course*, used to obtain the matrix of correlation between pair of regions called *functional connectivity matrix*. The functional connectivity matrix represents the connectivity between every pair of nodes in a network and is defined as a two-dimensional matrix, where each row/column is a *node* and each element of the matrix, called *edge*, represents the connection between two regions. The connectivity matrix is also known with the name of *adjacency matrix*, due to the fact that in graph theory two nodes that are directly connected by an edge are said to be *adjacent*. With this definition we can consider that the *adjacency matrix* R defines the pattern of pairwise adjacencies between nodes (ROIs).

The functional connectivity matrix is used to obtain the graph-based representation of the brain network. The most important characteristic to be defined in a network is the *directionality* and the *connectivity weights*. In this work we start to consider the functional connectivity matrix as a *weighted and undirected network*.

The variation between brain regions' connections can be described defining connectivity weight for graph-based representation. It is possible to identify a *weight of connectivity* between node *ith* and *jth* equal to the element of the matrix in position *ith* and *jth*, $C_{ij}=w_{ij}$. The other characteristic of functional connectivity matrix is that it represents an *undirected graph or network*. If we consider the matrix representing an undirected graph, the matrix is considered to be symmetric $C_{ij}=C_{ji}$. Such networks allow us to identify the connection between pairs of nodes, but without obtain any conclusion about the directions of those connections.

Another kind network that is generally consider for the for graph-based representation is the ***binary network***, used for network analysis and extraction some kind of topology metrics. To obtain a binary network is applied a thresholding procedure reduced the weighted connectivity matrix to a set of binary graphs.

The topological properties of the brain can be mathematically analyse based on the *graph-based theory* and considering the brain as an *undirect graph*. Coupled with this graph-representation of the brain, is used the *functional connectivity matrix* to represent the brain as a *weighted and undirected network or a binary network*. Graphically the functional brain networks are described by a series of topological properties.

In this work we defined ***two types of Functional Connectivity matrix***. First the ***Cross-correlation matrix*** which defines the connectivity between brain regions using the measure of cross-correlation between ROIs and is obtained using a linear metrics of Pearson's correlation coefficient. Then, we defined a ***Functional Connectivity matrix based on a non-linear metrics***, estimated using the measure of Mutual Information between ROIs. This matrix is named ***Mutual Information matrix*** and defined the functional connectivity between brain regions estimating the non-linear metrics of Mutual Information between ROIs.

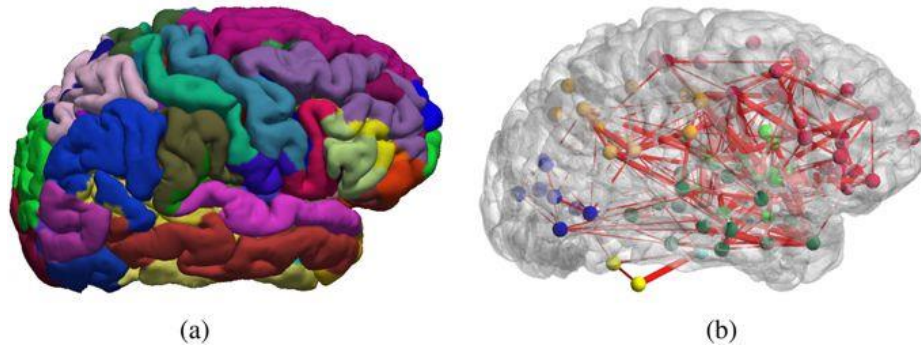


Figure 1.20, a) Example of cortical parcellation of the brain used to extract the BOLD signals in each ROIs and obtain, after computing the correlation matrix, the b) functional brain network to be analysed with graph-analysis

The **main topological and graph-theoretic metrics** that can be extracted and characterize a certain network can be divided into node-level (calculated for each node), network measures (related to the brain network) and link-level parameters (calculated for each link between a couple of nodes).

As last, the **two link-level parameters** that are extracted in this work are:

- The *Cross-Correlation matrix*, containing the relationships of cross-correlation between BOLD signal obtained from two separate regions of the brain. This parameter indicates the functional connectivity between pairs of nodes in the network, estimated using a linear metric.
- The *Mutual information matrix*, indicating the non-linearity of functional connectivity among time-series from different ROIs. This parameter indicates the functional connectivity between pairs of nodes in the network, estimated using a non-linear metric. It represents a measure of connectivity sensitive to non-linear variation.

In this work of thesis are extracted **seven node-level measures, from the Functional Connectivity Matrix of Cross-Correlation**. The node-level parameters extracted are:

- *Node degree*, number of links connected to the node indicating how many connections a node has to other nodes.
- *Node strength*, average weight of connections each node has with other nodes. Calculated as the sum of the nodes associated to positive and negative weights.
- *Local efficiency*, describing the regional efficiency indicating the integration of each node. It represents the global efficiency computed on the neighbourhood of the node.

- *Clustering coefficient*, describing the ability for functional segregation and efficiency of local information transfer.
- *Node betweenness centrality*, indicates the fraction of all shortest paths in the network that contain a given node, if a node has a highest fraction of shortest paths, more communication across the network will pass through this node.
- *Nodal Strength of positive weights*, calculated based on a weighted undirected signed network. This parameter is obtained as the sum of the nodes with positive weights, indicated by the sum of the links connected to the nodes associated to a positive correlation with the others. Represent the total positive strength of the node, and how much this node communicates in synchrony with the others.
- *Nodal Strength of negative weights*, calculated based on a weighted undirected signed network. This parameter is computed as the sum of the nodes with negative weights, indicated by the sum of the links connected to the nodes associated to a negative correlation with the others. Represent the total negative strength of the node, and how much this node communicates in asynchrony with the others.

On the other side, the *seven network-level measures* that are extracted *from the Functional Connectivity Matrix of Cross-Correlation*, are divided in:

- *Global efficiency*, obtained as the average inverse shortest path length in the network, representing the integration over the whole brain network.
- *Characteristic path length*, obtained as the average shortest path length in the network and representing how “efficiently” the brain is connected.
- *Network degree*, represents the average degree in the network.
- *Density of the graph*, is the fraction of present connections out of all possible connections, indicate how densely connected is a graph.
- *Louvain Modularity*, the modularity of a network quantifies the “strength” of partition of a network into modules (also called communities and clusters). Louvain method is a simple, efficient method to identify communities in large network. The method is a greedy optimization that attempts to optimize the modularity of a partition of a network by: firstly, looks for small communities optimizing modularity locally, then it aggregates nodes belonging to the same community and builds a new network whose nodes are the communities.

4. Twins study: Heritability of brain development

Sir Francis Galton was an English explorer and anthropologist during the Victorian era, best known for his research in eugenics, human intelligence and the first researcher to study the effects of *human hereditary on the environment*.

Galton uses Darwin's theory to introduce the theory of heredity in humans. In the "*Origin of species*" wrote by Darwin, it is shown that species become adapted to their environment through natural selection acting on heritable variations. Galton focused on this concept and his first paper "*Hereditary Talent and Character*", related to human's hereditary and published in 1865, introduced the concept of hereditary in humans. This concept was subsequently expanded in his work "*Hereditary Genius*". In this latter research, Galton analysed clerical ability, scholastic aptitude, athletic skill and other characteristic of father and son in different families. This was used to show that many *human characteristics are strongly influenced by heredity*. The role of the environment was not completely taken into account and analysed by Galton, but he considered the environmental factors to have less degree of influence with respect to hereditary.

Successively, many researchers continue to study the effects and interactions between heredity and environment as Thomson and Wilde (1973) that define the methods of study and the characteristics most important to be analysed in animal and human research. The major goal of these studies was the extraction of estimates of heritability. **Heritability** is defined by *Harrè and Lamb, 1983* as the variance in behaviour attributed to genetic factors when the environmental condition does not change. It is further noticed that the most common method used to determine these estimates is through the use of *twin studies* [39]. Similarly, in the work of Sir Galton named "*The History of Twins*" is suggested that twins might be used to determine the relative importance of nature and nurture.

The *development of the brain structure and function* shows large inter-individual variation. The idea that this variation is due to genetic and environmental influences has been investigated in the last decade using *twin studies*, whose analyse structural and functional brain differences in MRI and fMRI studies. In addition, cross sectional studies demonstrate that heritability estimates moderately increase from childhood to adulthood [40].

The *brain development* starts in the utero, through the interaction of various of complex synchronized processes, and continues into young adulthood. In the early years of childhood, this brain development displays a rapid growth, reaching the 95% of the adult brain size approximately at age of 6. The consequent development is associated to dynamics changes in cortical and subcortical regions of the brain, and remodelling of the grey and white matter. MRI studies allow us to analyse the development of the brain structure and function ‘in vivo’, providing knowledge to distinguish normal and abnormal brain morphology and function. Furthermore, MRI is used as non-invasive technique to analyse the heritability of the brain morphology and functions across different developmental phases. *Heritability* is defined as the proportion of variation that arises from genetic influences. *Environmental influences* explain the other part of the variation, and these influences are divided in shared environmental influences, and in non-shared environmental influences. The majority of *heritability studies analyse twins*, as the twin design allows the most optimal estimation of the effects of genes and environment on development.

4.1 Monozygotic and Dizygotic Twins

The twin study makes possible the control of both genetic and shared environmental background without specifying all the particular mechanism, and thus make it possible to isolate and test for the presence of the environmental effects of interest. In other word, the importance of twin studies is based not only on their ability to estimate those genetic influences but rather because they can be used as quasi-experimental tests of environmental explanations.

Twins are classified in two categories: *Monozygotic twins* (MZ) and *Dizygotic twins* (DZ).

Monozygotic twins

Monozygotic twins are genetically identical and share all additive and non-additive (i.e. interactions of alleles within and across genes) genetic effects. Monozygotic, or identical twins, develop when a single egg cell (reproductive cell) is fertilized to form one zygote (hence, *monozygotic*) which successively divide into two separate embryos. These twins are usually of the same sex, genetically identical and very similar in physical aspect.

Differences in physical aspect in MZ twins can be due to environmental factors. For example, 60-70% of MZ twins share the same placenta but are characterized by separate amniotic sac, only a small number (1-2%) share the same placenta and amniotic sac.

Dizygotic twins

Dizygotic twins, differently from MZ twins, refers to non-identical twins and are also called *fraternal twins*. This kind of twins share on average 50% of their additive and 25% of their non additive genetic effects. Since they result from two egg cells that are independently fertilized by two different sperm cell, DZ twins develop from two zygotes (hence the term of *dizygotic*) and may be of the same sex or different sex. DZ twins may be similar, but not identical, due to the fact that each zygote has a separate placenta and a separate amniotic sac.

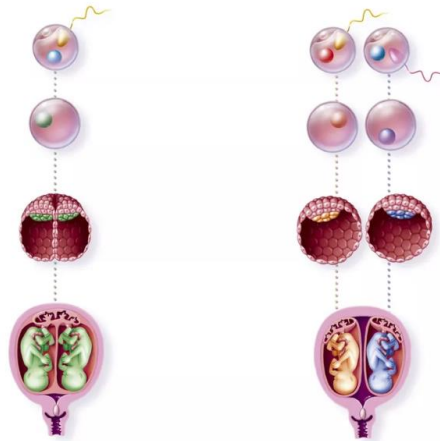


Figure 1.21 Development Monozygotic and Dizygotic twins

Heritability estimates extract from a classic “twin design” are based on the ***comparison of within MZ and DZ twin pair resemblance***, where the genetic influences are indicated when the average within MZ pair resemblance is larger than the average within DZ pair resemblance, generally quantifies as *twin correlation* (r_{MZ} or r_{DZ}).

4.2 The Twin Method

The twin method consists in a formal comparison between the resemblance between identical twins (MZ) and the resemblance between fraternal twins (DZ) for some traits of interest. The difference in resemblance between two members of MZ twins and the

difference for the pair of DZ twins can then be compared, and functions of this difference give a measure of the degree to which genetics contributes to the variation in the trait.

Considering that MZ twins have 100% similar genes and DZ twin shared 50% of similar genes, if a trait is characterized by a genetic influence the within-pair resemblance of that trait should be higher in MZ twins than in DZ twins. If is made the assumption of a common environment of a pair of twins, differences between MZ twins would be an indicator of the amount of environmental variability. On the other side, differences between DZ twins are connected to a genetic component.

Studying the differences between these resemblances, is possible to extract qualitative (e.g. whether both members of a twin pair suffer from the same disease) or quantitative (e.g. differences in statute between a pair of twins) measures.

The *similarity and dissimilarity between twins* can be studied also considering pair of twins of the same sex or different sex. DZ-SS represent dizygotic twins of the same sex, that indicate a more appropriate measure to compare DZ twins with MZ twins.

Based on the pattern of *twin correlations (or concordance)*, a *twin model* can be characterized generally with the total variance decomposed in additive genetic (A), non-additive genetic (D) or common environmental effects (C). Non-shared environmental effects (E) contain potential measurement error and could be include or not into the model [40]. It can be also included age as a potential modifier of heritability and total variance.

Considering that the influences related to the phenotype of an individual are genetic and environmental influences. **Additive genetic effect** occurs when two or more genes contribute to the final phenotype of an individual, or when alleles of a single gene (in heterozygotes) combine so that their combined effects equal the sum of their individual effects. In summary, they describe the effects of multiple genes that exert influence in a linear or additive fashion. **Non-additive genetic factors**, by contrast describe interactive effects of different alleles and include genetic dominance (of alleles at a single locus) and epistasis (across locus interaction of alleles). In most of the studies non-additive genetic factors are represented by genetic dominance. **The common environmental factors** represent environmental effects that tend to make members of the same family more similar whereas unique environmental factors influence siblings in the same family to be

different from each other. On the other side, *non-shared environmental effects* represent the environmental effect that tend to make the same family member less similar from each other. Another effect that can also be studied is the *Epistatic Effect*, is also part of the Dominant genetic factors. The Epistatic effect indicates the high genetic influence created by genes associated to different loci.

Different models based on equations, that consider the different kinds of influences described before, are applied in twin studies to analyse the genetic and environmental effects on a phenotype. One of the generic models which consider all the influences (*A, D, C and E*) described before is *ADCE model*. Related to this work of thesis, the two models that derive from *ADCE model* and applied in the twin design of this study are the *ACE model* and *ADE model*.

Classical twin studies are used to reach inferences on genetic and environmental influences on a specific phenotype (e.g. volume of the brain region). This analysis is called “*cross-twin within-traits*” in which is compared the *intrapair variable correlation* (or concordance) between MZ and DZ.

Other twin studies are also used to analyse the *etiology* of associations between two variables of interest and this type of research are called “*cross twin-cross trait*” *correlation*. This analysis also allows to genetics and environmental effects on any relationship. The main goal is to estimate the correlation between measure A of twin 1 (e.g. hippocampus volume) and measure B of twin 2 (e.g. thalamus volume). If cross twin-cross trait correlations are higher in MZ twins compared to DZ twin pairs, this means that share genetic factors (partly) explain the association between these measures. Similarly, one can examine whether particular brain areas are influenced by the same genetic factors [40].

4.2.1 Assumptions of Twin Method

The classical twin method compares resemblance of reared-together identical (monozygotic MZ) twins and same-sex fraternal twins (dizygotic DZ) on a trait. *The main assumptions of the method* are divided in:

1. Identical twins share 100% of the same segregating genes, Fraternal twins share, on average, 50% of their genes.
2. Findings related to twins are generalizable to the entire population.

3. MZ and DZ pairs are assumed to share equal environment.

These three primary assumptions are necessary in order to claim that the method is measuring the genetic influence. The third assumption is called “*equal environment assumption*” *EEA* and indicates that identical and fraternal twins experience equivalent trait-relevant environmental exposure. The *EEA* assumption is what differentiates ordinary siblings and DZ twins, that instead are equal from a genetic point of view. If the three assumptions are valid, and if identical twins are found to be significantly more similar than fraternal twins, this represents an evidence for a genetic component for a particular condition.

The *third assumption* is used to claim that MZ-DZ concordance/correlation rate difference proves the existence of the influence of the genetic factors. The *EEA* is considered to be a *critical assumption* for the twin method (*Scarr & Carter-Saltzman, 1979*): the basis of twin studies, that look at genetic components of human behaviour and psychiatric condition, can stand or fall based on the truthfulness of this assumption. Based on this assumption (*EEA*) the greater MZ similarity is attributed to genetic influence; but if MZ twins have lived in a more similar environment than DZ twins, the greater similarity may be due to environmental factors and not only genetics. According to *EEA*, the environments of identical and same-sex fraternal twin pairs are so similar that the observed variance in behavioural phenotypes must derive overwhelmingly from genetic variance.

Many studies tested the *EEA* and although there is an evidence that suggests that MZ twins are treated more similarly than DZ twins (*Scarr, 1968*). It is demonstrated that this different treatment does not significantly affect twin similarity for behaviours such as personality or cognitive functions (*Morris-Yates, Andrews, Howie, & Henderson, 1990*). These studies represent the evidence for genetic effects driving environmental influences (*Plomin & Bergman, 1991*): showing that presumed measures of the environment have shown them to have a substantial genetic component. So, the thesis that “*the environment is genetically influenced*”, in addition to the overview published in 1983 by *Kendler* regarding the validity of *EEA*, represents the *proof* that the *EEA is valid* because the difference between MZ and DZ twins have not been originally caused by environmental effect [41].

What remains a concern is the extent to which findings relating to twins are generalizable to the entire population of singletons (e.g. *Petersen et al., 2011*). Many existing studies

demonstrate that outcomes such as parental attachment and peer affiliation (Beaver, 2008), personality traits (Johnson et al., 2002), cognitive ability (Christensen et al., 2006) are similar across twins and singletons. Less researches, has considered whether twins differ on behavioural outcomes such as involvement in delinquency, drug use and victimization likelihood (Levy et al. 2006; Robbers et al 2010). Moreover, *Rutter and Redshaw (1991)* and other studies conclude that socio-emotional levels adjustments and behavioural problems were similar in twins and non-twins. In the review of *Barnes and Boutwell (2013)* is explored the compatibility of twins and non-twins on development, cognitive, and behavioural phenotypes that are interesting variable for a wide range of studies. The result was that twins did not differ from non-twins on most variables/scales.

Based on these assumptions, the *Twin Method* can be used to examine the different sources of variation in human phenotype and allow the researchers to estimate for a particular population the relative influences of nature and development at a specific time, on a specific population.

4.3 Statistical tools and measures of Twin Model

The common model used to analyse how genetics and environmental influence produce a mixture of similar and diversified characteristics of the human brain is *ADCE model*. The common equations of the model considering two individuals, with two traits X_1 and X_2 are:

$$X_1 = f(G_1) + C + E_1 \quad (1.23)$$

and

$$X_2 = f(G_2) + C + E_2 \quad (1.24)$$

These equations display the influences of two environmental factors (common environmental factors C and unshared environmental factors E_1 and E_2) that are independent and act additively. The genetic factor $f(G_i)$ can be decomposed in $f(G_i)=A_i + D_i$ that represents respectively additive genetic effect and dominance effect (non-additive genetic effect), and are assumed to be independent (or uncorrelated).

When the dominance factor D is absent the model is known as *ACE model*, as introduced in *Paragraph 4.2*. Otherwise, when the C factors representing the common environmental factors is removed is used the model called *ADE model*. In the ADE model the genetics

effects are expected to be more important than common environmental effects, so D factors are included in the model.

The main goal in this model of twin method is to *estimate similarity between twins' phenotypes in the pair* (“cross-twin within-traits”). To obtain this estimate are used different statistical tools as the measure of *concordance*, used widely to analyse qualitative factors (e.g. susceptibility of the twin pair to suffer from different or same disease), or measure of *correlation*, used to analyse quantitative factors (e.g. difference in stature of members of a twin pair). In the “cross-twin within-traits” is possible to extract a measure of a *trait heritability*. Heritability is defined as the proportion of phenotypic variance due to genetic factors and it measures the contribution of the genes in the inter-subject variability observed.

Most complex estimation of heritability, with respect to the one calculates with correlation or concordance, are introduced using *structural equation modeling (SEM)*. SEM can model the contributions of different variables to phenotypic difference in a twin pair by analysing univariate data from MZ and DZ twins or also multivariate data.

Is important to study the heritability of the brain function during the neurodevelopment in twin studies, taking into account that heritability estimates strongly depend on the reliability of the measured phenotype and should be interpreted accordingly [42].

According to test-retest studies, it is shown a good reliability for local and regional measures of cortical morphology. Differently, meta-reliability studies on fMRI show an important impact of processing parameters on functional networks metrics [43].

Nevertheless, to maintain the consistency to the topic of this thesis, we are going to present the *methods of correlation and concordance*, we introduced before, used to obtain a measure of heritability.

4.3.1 Concordance measure

For twin similarity in dichotomous traits, concordance represents the probability of disease in one (or both twins), conditional on the disease status of the other (or at least one) twin.

The concordance measures differ depending on the information available to condition on: there are *casewise P_c and pairwise P_p concordance measures*. P_c is related to individuals within a set of twins, differently P_p the is related to twin pairs. For example, P_c is used

when we're interested in estimate the probability of a disease in an individual given his or her twin's disease. Considering a sample of n twin pairs, as random sample of the population, where n_{ij} represents the number of twin pairs where the disease status of one is i the other twin's disease status is $j, j, i = 0,1; j = 0,1$, such that $n_d = n_{01} + n_{10}$ is the number of pairs discordant. If the sampling is random is used the maximization of log likelihood to estimate the outcome in terms of P_c and P_p :

$$P_c = \frac{2n_{11}}{2n_{11}+n_d} \text{ and } P_p = \frac{n_{11}}{n_{11}+n_d} \quad (1.24)$$

Where n_{11} indicate the number of concordant sick-couples and n_d the number of discordant sick couples [44].

4.3.2 Correlation measure

As has been said, in case of quantitative traits, the similarity between twins' phenotypes in the pair can be estimate using the Pearson correlation coefficient or intraclass correlation coefficient. **Pearson correlation coefficient PCC** is a measure of correlation and represents the measure of the linear correlation between two variables. The PCC can assume the value of 1 indicating total positive linear correlation, 0 represents the situation in which no linear correlation is present and -1 represents a situation related to total negative linear correlation.

PCC is defined as the covariance of the two variables (of the twins in a pair in twin method's case), divided by the product of the respective standard deviation. If we consider the twin as random sample of the population, PCC is defined as:

$$\rho_{X,Y} = \frac{cov(X,Y)}{\sigma_X\sigma_Y} \quad (1.25)$$

Where X and Y are the two variables that characterized each member of the twin pair.

The **intraclass correlation coefficient ICC** is a descriptive statistic that can be used when quantitative measurements from different entities are organized into groups (or pairs). This correlation coefficient describes how strongly these entities resemble each other. In the Twin Method, ICC is used to determine the degree to which twins in a pair resemble each other in terms of quantitative trait. The difference between *ICC* and *PCC* is that the ICC

consider the true variance and the pooled variance within the pairs, the reason is that when we estimate intraclass correlation the pairs are considered to be unordered. These unordered pairs hypothesis of ICC is not consistent with resemblance of twins' study, where there is no possibility to order the values for the two individuals within a twin pair.

In both cases, *ICC* or *PCC*, high value of correlation for MZ than DZ twins indicate that there is a genetic effect on the trait, character consider. The correlation is mostly used to obtain an estimation of heritability.

4.3.3 ACE, ADE Twin model and Epistatic Effect

ACE twin model

As introduced before, ACE model is a statistical twin model used to evaluate the genetic and environmental influences based on specific latent variables which represents the variable that cannot be directly observed. As consequence we have to use the model to estimate the contribution of these variables. The three latent variables are:

- **Additive genetic factor (A):** MZ twins share 100% of genetic factors, DZ twins on average 50% of their genetic information.
- **Shared environmental factor (C):** MZ or DZ twins can be more similar to each other if they shared a common environment; Due to this factors DZ twins can be more similar than MZ twins independently of the genetic effect of zygosity.
- **Unique environmental factor (E):** MZ or DZ twins can be less similar to each other if they do not share the same environmental factors.

The total variance V of a certain phenotype is determined by the variance created by A, C and E factors on each phenotypic value of the twins in the couple.

We consider A, C and E as latent variables and P as the observed phenotype.

The univariate twin analysis is illustrated in Figure. 1.22 in which P1 and P2 represent the phenotypic values observed in each twin of the couple composed by Twin 1 (P1) and Twin 2 (P2). The path coefficients a , c and e quantify the influence of each latent factors on the value of the phenotype. The unidirectional arrows indicate the causal influence, the bidirectional arrows indicate covariances between variables. Based on the assumption that MZ twins share 100% of their genetic information and DZ twins on average share 50% of

their genetic information, we have a correlation between genetic-latent factors (α) equal to 1 for MZ twins and 0.5 for DZ twins. For the equal environment assumption, the correlation between shared environmental factors (β) equals 1 for MZs and DZs. By definition, E factors are uncorrelated in both MZ and DZ twins because they are unique for each individual [45].

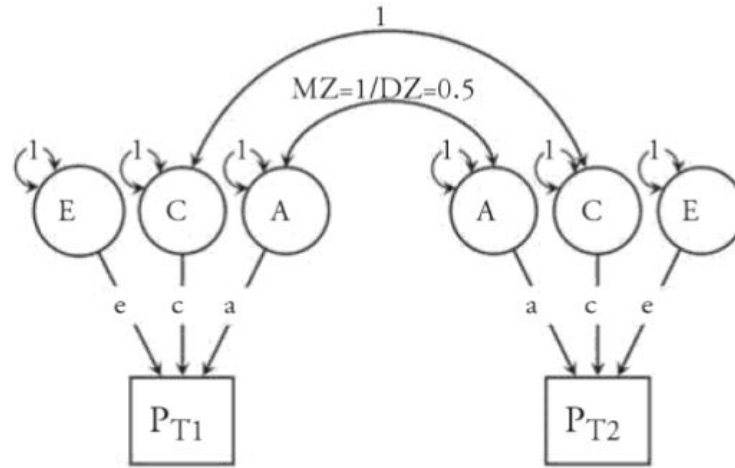


Figure 1.22, Univariate twin analysis using on ACE model.

If the correlation values in MZs and DZs indicates the similarity between twins, A and C factors are used to estimate this similarity in twins couples. On the other side E factors represents the differences between Twin 1 and Twin 2 in the couple.

Based on the previous considerations, is possible to obtain estimates of the three latent factors based on the value of the correlation coefficient r_{MZ} in MZ twins and r_{DZ} DZ twins [46]:

$$A = 2(r_{MZ} - r_{DZ}), C = 2r_{DZ} - r_{MZ} \text{ and } E = 1 - r_{MZ} \quad (1.26)$$

ADE twin model

ADE model differently from ACE model, consider the influence of two genetic factors and the influence of non-shared environment.

The difference between these two factors, A and D, is related to the fact that the *additive genetic variation* refers to the variance of the mean phenotype due to inheritance of a particular allele and this allele's relative (to the mean phenotype of the population) effect

on phenotype. In contrast, the *dominant genetic variation* involved deviation due to interactions between alternative alleles at a specific locus.

In this ADE model representation, illustrated in Fig. 1.23, the correlation between additive genetic factors (A) is fixed to 1 for MZ pairs and 0.5 for DZ pairs, as for the ACE model. Differently, the correlation between dominant genetic factors (D) is fixed to 1 for MZ twins and 0.25 for DZ twins.

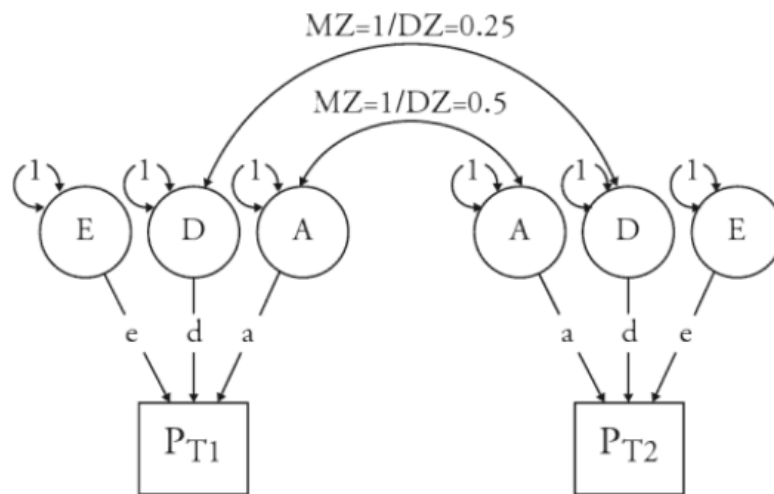


Figure 1.23, Univariate analysis on twins using ADE model.

ADE model to study the variation of a certain phenotype if is valid the condition on correlation values $0 < 2r_{DZ} < r_{MZ} < 4r_{DZ}$. In this case are estimate the coefficient of the ADE model as:

$$A = 4r_{DZ} - r_{MZ}, D = 2r_{MZ} - 4r_{DZ} \text{ and } E = 1 - r_{MZ} \quad (1.27)$$

Epistatic Effect

In addition to the study of genetic and environmental influences implemented by ACE and ADE model, is possible to analyse the *genetic influence* created by the Epistatic Effect. This *Epistatic Effect* indicates the genetic influence on a specific phenotype created by genes at different loci. Unfortunately, is not possible to quantify the Epistatic Effect based on the correlation values estimate for MZ and DZ couple for a certain phenotype.

4.3.4 ACE and ADE Twin model Heritability estimation

The *formula of heritability* that is extracted depends on which model, *ADE or ACE model*, is applied. If ACE model is applied is estimated a measure of “*narrow-sense heritability*” that coincides with the estimate of the coefficient A (Additive Genetic Influence) of the model:

$$h^2 = A = 2(r_{MZ} - r_{DZ}) \quad (1.28)$$

When an ADE model is applied, a measure of “*broad-sense heritability*” is extracted and coincides with the sum of the coefficient A (Additive Genetic Factor) and D (dominant Genetic factor):

$$h^2 = A + D = 2(r_{MZ} - r_{DZ}) \quad (1.29)$$

Chapter 2: Experimental Data

Aim of the research

The present thesis has been carried out in the department of Electronics, Informatic and Bioengineering, B^3 Lab (Biosignals-Bioimaging-Bioinformatics) at Politecnico di Milano in collaboration with the MiBrain (Milan Brain Research on Affective and Integrative Neuroscience) Lab coordinated by Prof. Paolo Brambilla in the Fondazione IRCCS Ca' Granda Ospedale Maggiore Policlinico and the University of Milan. The experimental data used for the present research has been acquired at the Scientific Institute IRCCS E. Medea of Bosisio Parini during the SPES (GR-2010-2316745) and *Why Me?* (RF-2011-02352308) projects granted by the Italian Minister of Health to Prof. Brambilla.

The experimental thesis work deals with the analysis of resting-state fMRI datasets from a unique Italian sample of 50 young twin pairs, used to examine the functional brain connectivity similarity between twins and estimate the level of heritability of local and global topological characteristics of the brain functional networks. The fMRI technique enables us to study the development of brain function “in vivo” and provides insights into the extent of genetic and environmental effects on brain functional characteristics.

The main objective of this study is the analysis of genetic and environmental influences on the functional brain network's patterns, with extraction of heritability measures, taking into account linear and nonlinear metrics of functional connectivity as well as local and global topological parameters of the functional brain networks.

To this end, each connectivity measure is compared in each couple of twins and across MZ and DZ twin pairs and the most appropriate twin model - if any - is selected and applied.

In this *Chapter of Experimental Data*, the methods used for the ***pre-processing*** and ***processing of resting-state fMRI data will be described step-by-step***. In particular, the biggest pre-processing section is dedicated to the introduction of a novel spatiotemporal tool for automatic classification of fMRI noise based on ICA, which was developed, validated on a training dataset and applied to the entire dataset. The fast, easy-to-use tool for subject-level identification and removal of fMRI artefacts relies on both temporal and spatial features.

After pre-processing, the cleaned fMRI dataset was parcelled into regions of interest (ROIs), representing the nodes of the functional brain network. A functional connectivity analysis was conducted using the approach of ***Seed-based functional connectivity (SCA)***, which allows to study the instantaneous functional interactions between the regions of the brain. SCA was assessed at a link of the functional brain network using both Cross-Correlation (CC) and mutual information (MI) metrics, which measure the statistical dependencies between brain regions, being sensitive to linear (CC) and linear and non-linear (MI). Then, from the FC matrix based on Cross-Correlation (CC) we extracted a set of Node-level and Network level-topological parameters.

Topological parameters, which include ***network-level, node-level and link-level measures***, are compared within each twin pair, and then between MZ and DZ couples of twins to demonstrate and rate the higher phenotypic similarity between MZs with respect to DZs, obtaining a ***cross-twin within-trait analysis***. This similarity analysis is based on the extraction of the intra-pair correlation of the values of the topological parameter in MZ and DZ twins, at net of Age and Sex of the twin couples.

Based on the intra-pair correlation values extracted for MZ and DZ couples, we selected - if any - the most appropriate twin model. We checked for the presence of Epistatic Effect, which indicates a genetic influence created by genes at different loci. When appropriate, we analysed the ***genetic and environmental influences*** on the topological parameter using twin models ACE or ADE, including also measures of heritability for each functional brain network pattern. Then, for the topological parameters that resulted suitable for ACE or ADE model or resulted associated to an Epistatic Effect, we applied a quantitative analysis of the intra-pair difference of correlation values between MZ and DZ couples. In all cases (ADE, ACE model or Epistatic Effect) we extracted the number of ***significant intra-pair correlation differences between MZ and DZ couples***.

As last, we evaluated the ***effects of sex and age*** of the twin couples on the value of ***intra-pair difference of each topological parameter***, at net of zygosity effect. This last analysis wants to capture how the age and sex of the twin couple influence the intra-pair phenotypic difference of the specific parameter associated to the couple.

1. Subjects and Data Acquisition

The present work of thesis was developed in the Department of Electronics, Bioinformatics and Bioengineering, *B³ Lab* (Bioengineering-Bioimaging-Bioinformatics) at Politecnico di Milano in collaboration with the Scientific Institute IRCSS E. Medea of Bosisio Parini (Lecco) and the Fondazione IRCSS Ca' Granda Ospedale Maggiore Policlinico of Milan.

Resting-state fMRI data were acquired from 100 subjects representing 50 pairs of twins, at the Scientific Institute "IRCSS Eugenio Medea" in Bosisio Parini.

The dataset consists of 50 *pairs of twins and* includes both sexually concordant and sexually discordant twins. In the present work of thesis, we excluded the latter twins, considering that the brain similarity might be altered in the twin couples that are discordant for the parameter of sex. Considering only the *twins' pairs sexually-concordant* the dataset results in **46 couples of twins**, characterized by 19 pairs of MZ twins (10 males, 9 females, mean age 16,7) and 27 pairs of DZ twins (9 males, 18 females, mean age 19,3). The data acquired from the subjects were obtained considering the research of *Why Me? Project* financed by the Italian Minister of Health. *Why Me? Project* is aimed to investigate white matter connectivity in schizophrenia at imaging, cellular and transposone levels in monozygotic discordant twins.

MRI acquisitions were performed using 3 Tesla MR scanner (Philips Achieva, Best, The Netherlands) equipped with a 32-channel head coil.

The *resting-state fMRI (rs-fMRI) data* were obtained asking the subjects to keep their eyes closed, not to think anything in particular and not to fall asleep. In the same MRI session, T_1 -weighted 3D Turbo Field Echo (TFE) sequence was run for morphological referencing of MRI data. The relevant parameters of the standard echo planar imaging (EPI) sequence used to capture the BOLD contrast for rs-fMRI and the ones related to anatomical T_1 -weighted 3D Turbo Field Echo (TFE) sequences are reported below:

EPI sequence parameters for rs-fMRI data

- The Repetition Time (TR) = 2500 [msec]
- Echo Time (TE) = 35 [msec]
- Flip Angle = 8 [deg]

- Voxel Size = $1.8 \times 1.8 \times 3$ [mm^3]
- Plane Matrix size = 128×128
- Number of axial slices = 30
- Number of Volumes = 200

T₁- weighted 3D structural sequence parameters

- The Repetition Time (TR) = 8.3 [$msec$]
- Echo Time (TE) = 3.8 [$msec$]
- Flip Angle = 8 [deg]
- Voxel Size = $1 \times 1 \times 1$ [mm^3]
- Plane Matrix size = 240×240
- Number of axial slices = 190

In addition, the ***Task-based fMRI data*** were obtained during an *Emotional Continuous Performance (eCPT) test* [47] and used in this work of thesis to test and validate the tool for subject-level ICA-based identification of fMRI artefacts that will be presented in this Chapter. The relevant parameters of the standard echo planar imaging (EPI) sequence used to capture the BOLD contrast for task-based fMRI using eCPT test are reported below:

EPI sequence parameters for task-based fMRI data

- The Repetition Time (TR) = 2000 [$msec$]
- Echo Time (TE) = 35 [$msec$]
- Flip Angle = 8 [deg]
- Voxel Size = $3.75 \times 3.75 \times 3.8$ [mm^3]
- Plane Matrix size = 128×128
- Number of axial slices = 30
- Number of Volumes = 200

2. MRI Data Pre-processing

MRI data pre-processing begins with the ***DICOM to NIFTI conversion*** of the fMRI images of each subject. It is necessary to apply a conversion of these images into an image format called NIFTI that is a used in many software for scientific analysis of the brain and

also is required for SPM (Statistical Parametric Mapping) software that will be used in the next step of pre-processing of the data. To achieve this conversion is used or the application “*dicom2nifti*” that is included in the MRICron package or is used directly the MRICron package that contains in the GUI the possibility to import images and convert it from DICOM into NIFTI format. After the conversion, the output results the 4D image of each subject. Then, for the SPM pre-processing of the images is necessary the 4D NIFTI image containing the fMRI scans of each subject and the T_1 - weighted NIFTI image associated with each subject.

Starting from the 4D NIFTI image of the fMRI scans is possible to obtain, using the 4D to 3D conversion, 200 scans of fMRI images in the NIFTI format, representing the set of 3D fMRI volumes obtained in consecutive repetition time. Next, on this 3D data, are applied all the steps of pre-processing from SPM software described in the following *Paragraph 2.1*.

2.1 Pre-processing with SPM

After the conversion from DICOM to NIFTI, we obtain all the subjects’ images in a NIFTI format. Then, after applying the 4D to 3D conversion each subject is associated to 200 scans of fMRI volumes. In this work the data are *pre-processed using the Statistical Parametric Mapping SPM software* (<https://www.fil.ion.ucl.ac.uk/spm/software/spm12/>). We used *SPM12* version running on *Matlab 2019b*. For each subject, we applied the spatial pre-processing using *SPM12*. The different steps of fMRI data pre-processing are illustrated in Fig 2.1 and described below:

1. ***Spatial Realignment of the fMRI volumes:*** the main goal of this step is the correction of the subject motion between volumes, by minimizing the mean-squared difference. Satisfactory corrections are achieved only if the subject did very small movement during the acquisition, comparable to the voxels size. This effect of spatial realignment can be obtained by applying a rigid-body transformation to the images. To apply this transformation is necessary to estimate the 6 parameters (3 of translation and 3 of rotation) that describe the transformation. Then, each image is resampled, according to the transformation parameters estimated before, using different interpolation function as “Nearest Neighbour”, “B-spline” or “Linear Interpolation”.

During spatial realignment is checked for each subject if the translational movements of the head is higher than 5 mm and the rotational movement is higher than 3° . The subjects with head movements over these thresholds are marked inside an Excel file.

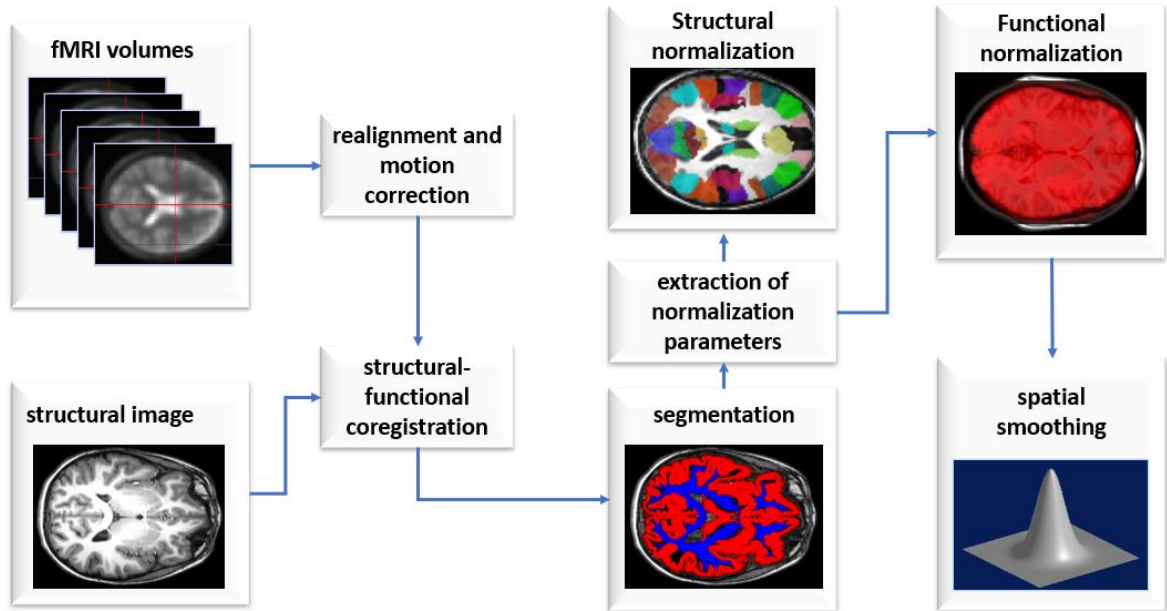


Figure 2.1, fMRI data pre-processing scheme

1. **Structural-Functional Coregistration:** This step represents an intermodality, intrasubject registration. This step allows to match the geometry of functional and structural images from the same subject, to obtain a spatial correspondence and derive specific functional information about well-defined cerebral structures. To do this, the coregistration has to find an *affine transformation* between both images to define the spatial correspondence. In the SPM12 software is necessary to specify the “Reference Image”, in this work represented by the mean of the functional images as reference, and a “Source” image, here represented by T_1 - weighted structural image.
2. **Tissue Segmentation, on the T_1 - weighted image:** This step is used to obtain the classification of the brain tissue into the three main cerebral tissue, grey matter GM, white matter WM and cerebrospinal fluid CSF; using the high resolution T_1 - weighted structural images. The prior probability that any voxel contains grey or white matter can be defined using a *probabilistic atlas/map of tissue types*; this

prior probability is then combined with the data from the image determine the tissue class. The probabilistic image of each tissue that are created are called “c1”, “c2”, “c3”. Then from each segmented area is created a normalized version, called “c4”, and a normalized with modulation version, called “c5”. Lastly, is calculated also the deformation field that contain the normalization parameters called y_{T1} . This deformation field is the non-linear transformation that makes tissue class distribution in structural image most plausible.

3. ***Spatial Normalization on the standard MNI Space:*** This allows to write out structural and functional image in the standard space for multi-subject statistical analysis. If we consider subjects characterized by distinct brain, each one is related to a different shape and size. The goal is to deform human brain scans so one location in one subject's brain scan corresponds to the same location in another subject's brain scan. The normalization can be used to report findings between subjects, in common anatomical space (*MNI space*). This step applies the deformation field, that is a 3D non rigid transformation, to all structural and functional images. The deformation field is described as a displacement field for each image voxel that tells where it should be moved to the standard MNI space. In this research, the normalization is applied to the functional images previously realigned, and to the structural T_1 - weighted image, to obtain normalized images indicated by the prefix “w”.
4. ***Spatial Smoothing with a 6 mm FWHM Gaussian window:*** This step is performed with a spatially stationary Gaussian filter where the user has to specify the kernel width in mm, also called “full width half max” FWHM. The smoothing is implemented as a convolution of the imaging data with a Gaussian smoothing kernel. The main goal of spatial smoothing is to manage the inter-subject variability that is not compensated by spatial normalization (“warping”) and to increase the signal to noise ratio, the sensitivity. The optimal smoothing kernel used to recover a signal, an activation, need to have the same size as our activation. After all, is not possible to know the exact signal/activation size before the experiment, so the level of smoothing that is optimal for real can only be determined empirically. For this reason, the choice of the parameter of FWHM of the Gaussian filter need to be very accurate. In this work we use a *FWHM of 6mm*, which corresponds to three times

the size of the voxel. The output of this step are the smoothed images indicated with prefix “sw”.

3. ICA analysis and Denoising tool

3.1 Melodic Toolbox: Extraction of ICs

After the SPM pre-processing of the fMRI images, is performed the spatial ICA to estimate the spatially independent and temporally coherent sources contributing to BOLD signal.

The ICA analysis was performed using *Multivariate Exploratory Linear Optimized Decomposition into Independent Components (MELODIC) toolbox* by the FSL software (<https://fsl.fmrib.ox.ac.uk/fsl/fslwiki/MELODIC>). This toolbox is used to decompose a single or multiple 4D fMRI dataset into spatial and temporal components. Traditional ICA models are based on deterministic methods which ignore process uncertainties caused by contamination of random noise [48]. A more natural expression for the process data can be obtained using a probabilistic model structure. This is the model of pICA, described in *Paragraph 1.2.6*, implemented in Melodic. In this work of thesis MELODIC toolbox is used to perform individually single subject sICA.

In our application, the pre-processed fMRI volumes from each subject were prepared as a unique 4D NIFTI volume. Before running ICA analysis with the MELODIC toolbox, is applied a *temporal high pass filter* to the resting-state temporal series using the function of FSL *fslmath*. In this function is specified the parameter sigma that is related to the Repetition time T_R and the cut off frequency f_{cut_off} . In our case $T_R = 2,5 \text{ sec}$, we want to apply a high pass filter with *cut off 100 sec* that is equivalent to an $f_{cut_off} = \frac{1}{t_{cut_off}} = \frac{1}{100 \text{ sec}} = 0.1 \text{ Hz}$. Sigma parameter can be calculated using the formula:

$$\sigma = \frac{1}{2 * T_R * t_{cut_off}} = 20 \quad (2.1)$$

In this case the sigma parameter to be applied with *fslmath* to apply the correct high pass filtering results 20. Next to the filtering of the data, a single session probabilistic ICA is ran on the dataset using the *melodic* command of FSL.

The main options to be specified in the *melodic* command, in addition to the 4D NIFTI *input volumes*, to which we apply also the high pass filtering, are related to the *repetition time* $T_R = 2,5 \text{ sec}$ of the data and the *number of ICs* to be extracted. MELODIC toolbox allows to compute a number of extracted ICs using automatic dimensionality estimation based on a criterion of model order selection or set a fixed the number of ICs to be extracted by the user. The latter option has been chosen in this work and from all 4D fMRI data of each subject were extracted the same number of ICs.

In this work we set arbitrary the *number of ICs to be extracted to 33*. We chose a fixed number of ICs across subjects to facilitate the test of the method performances at the group level. The selection of this number of extracted ICs is achieved by running MELODIC automatic dimensionality estimation on fMRI datasets on five subjects of example. This choice of ICs was found to guarantee a good ICA fitting to our fMRI datasets, with an amount of explained data variance sufficient to obtain good estimates of the fMRI signals, while reducing the risk of signal and noise overfitting.

Optimal fitting means that the amount of explained data variance is sufficient to obtain good estimates of the signals and at the same preventing the appearance in the result of spurious component. If the number of estimated ICA components are higher than 33 means that is reached overfitting, including too many components to recognize the signal of interest. Otherwise, if the number of estimated ICA components are lower than 33, means is reached underfitting, considering an amount of variance that is not enough to recognize the signal of interest. The practical justification of the choice to fix the number of ICs extracted to 33 will be explained in the next *Paragraph 3.2.1*.

The *outputs of melodic* command are composed by a *directory containing ICs time courses and spectral power*, a *report* to visually analysed the ICs of each subject and the key output that is the *melodic_IC.nii.gz file* that is a 4D image where each volume is a component generated in the single-subject ICA.

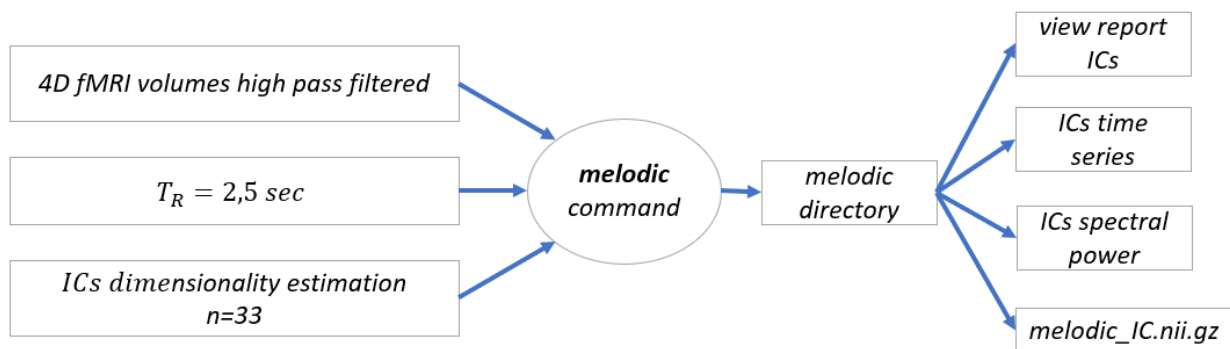


Figure 2.2 Single-subject ICA via MELODIC: inputs and outputs of melodic command from FSL.

The complete diagram which describes the inputs and outputs of *melodic* command is illustrated in Fig.2.2.

After the application of *melodic* command, that indicates the application of *pICA technique*, the subject's fMRI data were thus decomposed in Independent Components (ICs) characterized by a series of spatially independent maps and the related temporal series.

The Figure 2.3 gives an overall view about the procedure applied: from the step in which are received as input the patient's 4D fMRI data affected by noise, to the clean-fMRI data of the patient obtained as output of the general process.

The ICs extracted using MELODIC toolbox were subjected to the following analysis and used to discriminate the ICs related to noise from the ones related to the sources of brain activity, whose indicate the RSNs' activation. Lastly, noise-related ICs will be removed from the subject pre-processed data.

The process of classification between signal and noise related ICs and the removal of noise components will be described in the next *Paragraph*.

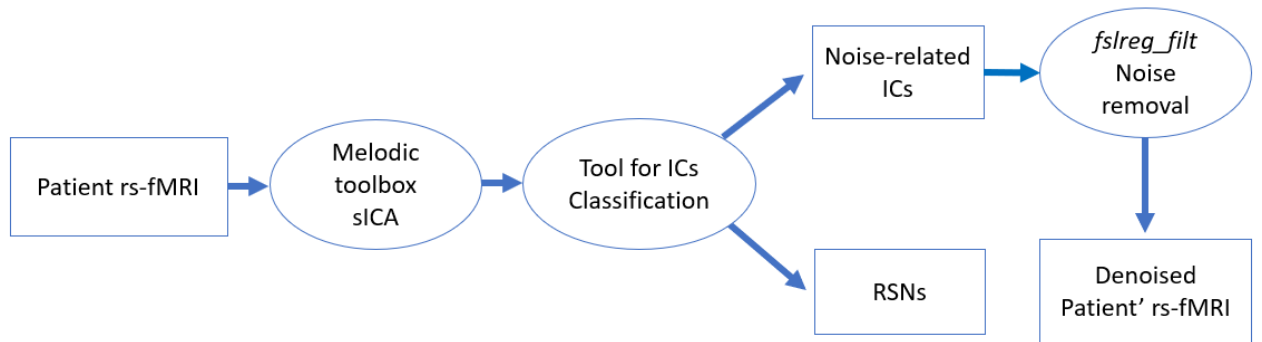


Figure 2.3, Spatial ICA performed by MELODIC toolbox and the consequent ICs classification and Denoising of the rs-fMRI data.

3.2 Automatic Tool for ICs' Classification

The main objective of this spatio-temporal tool for the automatic classification of ICs is to identify the *noise/signal label* to be assigned to unknown ICs, obtained from each subject in analysis. Thus, in this work of thesis is developed an easy-to-use method that performs an *automatic selection of the artefactual ICs* based on their temporal and spatial features with respect to a reference set of manually labelled ICs. The classification procedure is illustrated in Fig. 2.5 and detailed in *Paragraph 3.2.1 and Paragraph 3.2.2*.

3.2.1 Tool development, test and validation using eCPT-based reference sets

The newly developed method was adjusted and tested on different fMRI datasets, as shown in the schematic diagram in Fig. 2.5. The tool was first developed, tested and validated using as reference an eCPT fMRI dataset. Subsequently, in this work of thesis the tool is applied using as reference set the resting-state fMRI dataset of twins set.

The tool is based on a *number of 33 ICs components* extracted from 4D pre-processed fMRI data. As has been said, this fixed number of ICs extracted was used to guarantee a good ICA fitting to our fMRI datasets and obtain good estimates of fMRI signals characterized by a sufficient amount of explained data variance.

As has been introduced before, we practically justify the choice of 33 ICs extracted by applying the *MELODIC automatic dimensionality estimation* to fMRI datasets of five exemplar subjects. This automatic dimensionality estimation of ICs provided a number of ICs extracted between 30 and 40.

For all the applications used to test the tool, the reference ICs were obtained from eCPT fMRI datasets. The choice of an *eCPT fMRI dataset as reference set* has facilitated the identification of the ICs representing brain activity and in turn the hand-labeling of the *noise*-related ICs using this dataset.

The *method parameters* of *Spatial Correlation (SC)* and *Relative Power Spectra (SP)* were set in the *first method's application* using the eCPT fMRI datasets from one reference subject (*reference set #1*) and five test subjects (*test set #1*). Both *reference* and *test* ICs were manually marked as *signal/noise* in order to measure the method performance. The comparison between the real labels and those assigned by the tool at varying thresholds in the temporal and spatial analyses allowed the identification of the optimal thresholds for the *test set #1*, which were used in the subsequent analyses. The parameter setting procedure is described later in detail. To verify the quality of fMRI cleaning, we removed the ICs marked as *noise* and performed the inverse spatial ICA on the *test set #1*. Then, we visually compared the brain regions that resulted activated by the eCPT task in the original and cleaned fMRI datasets from one exemplar subject.

The method performances were measured in *three additional applications*. First, we checked whether the capability of marking *noise*-related ICs increased using as reference the eCPT fMRI datasets from two subjects (*reference set #2*). We purposely considered subjects with different fMRI data quality, one characterized by a high number of labelled *noise*-related ICs and one with more *signal*-related ICs. In the first application, the *reference set #2* was used to mark *noise*-related ICs on the eCPT-based *test set #1*. Then, the method versatility was further assessed by using the eCPT-based *reference sets (#1 and #2)* to classify artefactual ICs from an unknown dataset characterized by different acquisition parameters, the resting-state fMRI dataset (5 subjects, *test set #2*). In all these analyses, both *reference* and *test* ICs were manually labelled to measure the method performances.

Identification of noise-related ICs

In this paragraph are described all the *steps used in the automatic phase* of noise-related ICs identification, based on ICs of the test set and ICs of the reference set.

For each *test* subject, the extracted ICs ($n=33$) are analysed and compared to the *reference* ICs ($n=33$) as follows. After extraction of IC maps and time courses from the MELODIC output directory, all spatial maps were masked using a brain tissue template mask and reshaped in the form of vectors for an easier computation of the 3D correlation. The spatial correlation (SC) coefficients among the *test* and *reference* IC spatial maps are computed, resulting in a 33×33 matrix with the rows representing the 33 *reference* ICs and the columns representing the 33 *test* ICs extracted from the analysed subject. The (i,j) value in the SC matrix represents the correlation between the i^{th} *reference* IC and the j^{th} *test* IC.

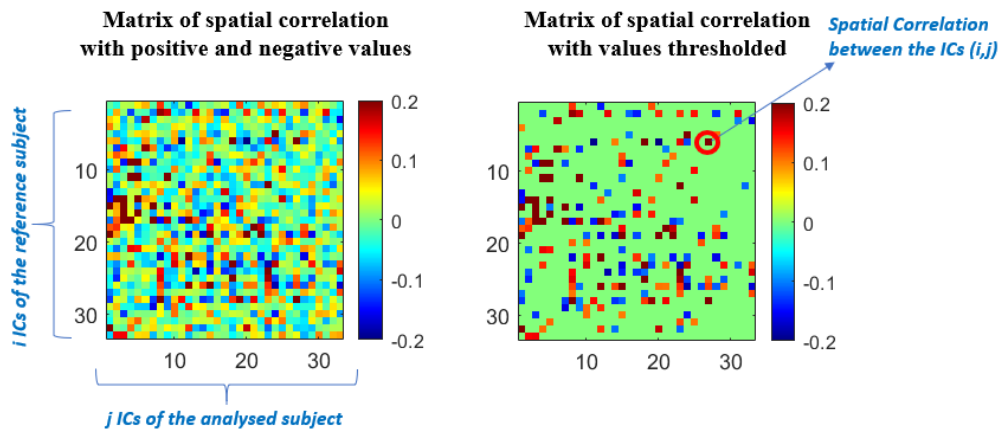


Figure 2.4, on the left, the matrix of spatial correlation with positive and negative values; on the right the matrix of spatial correlation thresholded by for example 0.1.

The higher is the SC value, the higher is the spatial similarity between the two ICs. **In this step of the analysis, a *test* IC is marked as artefactual if its SC with at least one *noise-related reference* ICs is above a certain threshold.** In parallel, an analysis regarding the spectral characteristics is introduced: the *test* IC time series are analysed to extract the relative percentage of spectral power (SP) in the high frequency band (above 0.1 Hz) with respect to the total SP, calculated by summing all the SP values in the signal frequency range. Based on the fMRI sampling frequency ($fs=1/TR$) and the number N of fMRI volumes, the SP estimation was computed in the $[0-fs/2]$ Hz frequency range with fs/N frequency resolution. Since the physiological BOLD signal is characterized by low frequency

fluctuations in the 0.01-0.1 Hz band, the frequency cut-off for artifact detection was set to 0.1 Hz. For each *test* subject, we obtained a vector of 33 elements with the high frequency SP for each *test* IC. **In this analysis, the ICs having high frequency SP above a certain threshold are labelled as noise.** To summarize, once the SP and SC thresholds are defined, a novel, unknown IC (*test* IC) is labelled as *noise* if at least one of the next two conditions is verified: 1) the SC between the *test* IC and at least one *reference* IC manually labelled as *noise* is higher than the SC threshold, 2) the percentage of SP in the higher frequency band with respect to the total SP is over the SP threshold.

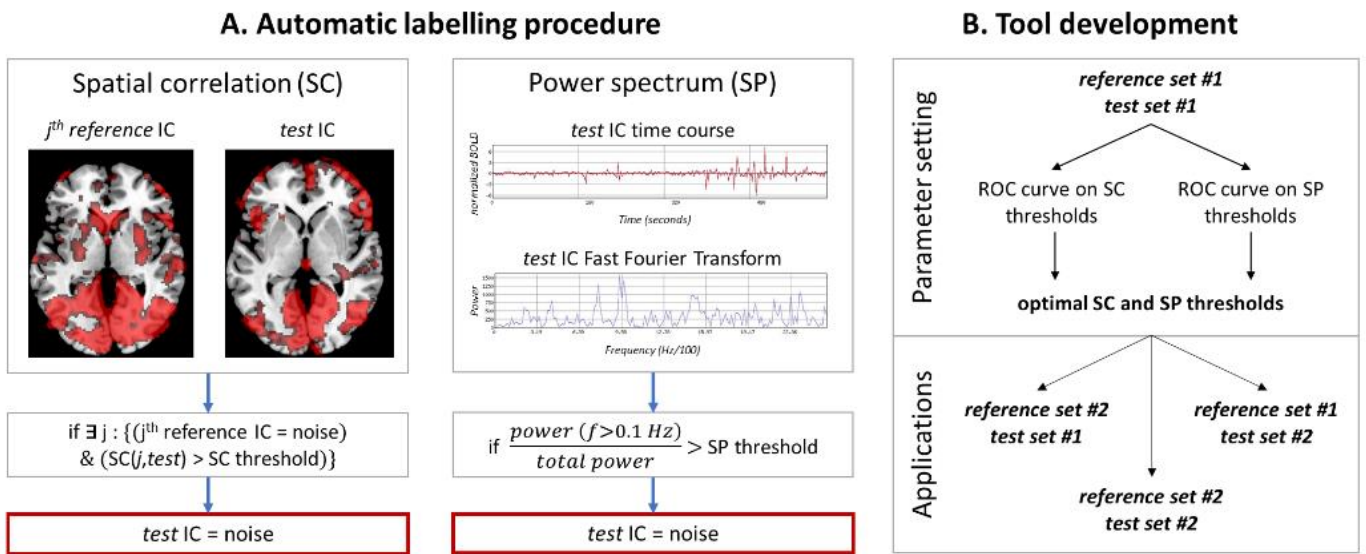


Figure 2.5. A. Pipeline for identification of artefactual independent components. B. Schematic diagram of tool development and testing

A key point of this ICs classification is the choice of the proper threshold values to be used in the SC and SP analyses for marking artefactual ICs were extracted using the procedure described subsequently.

Selection of SC and SP threshold

The spatial and temporal IC analyses of the *test set #1* using the *reference set #1* were followed by the selection of the optimal thresholds for the discrimination of *noise*-related ICs.

The selection of the SC/SP thresholds was performed by varying the parameter of interest while keeping the other threshold constant. Specifically, the SC thresholds were

progressively increased from 0.2 to 0.4 with 1 step in between, while considering the SP threshold equal to the average SP of the *reference set #1* in the high frequency band; then, the SP threshold was varied from 23 to 41 with 1 step in between while maintaining the SC threshold selected as optimal in the previous condition.

We use the results from two ROC curves, obtained by considering the matches between real and predicted IC labels, to extract the optimal thresholds. The two ROC curves are presented in the Chapter of Results.

Tool's performance on eCPT fMRI dataset

As, has been said, the tool is developed, tested and validated using the previous four applications, that consider respectively:

- **Application #1:** one eCPT based reference sets and five eCPT based test set (*Reference set #1, test set #1*)
- **Application #2:** two eCPT based reference sets and five eCPT based test set (*Reference set #2, test set #1*)
- **Application #3:** one eCPT-based reference sets and five rs-fMRI based test set (*Reference sets #1, test set #2*)
- **Application #4:** two eCPT-based reference sets and five rs-fMRI based test set (*Reference sets #2, test set #2*).

The detailed method performances as function of method parameters and dataset types are discussed in the section related to the Results.

To apply this Tool on the resting state fMRI data of Twin Dataset is important to underline that the automatic tool obtained in terms of accuracy, specificity and sensitivity good results. These preliminary results suggest that the method is versatile and accurate in the classification of unknown ICs resulting from different fMRI protocols.

3.2.2 Application of the Tool on rs-fMRI data of Twins Dataset

Considering the results of the tool from the previous four applications, used to validate it, in this work of thesis is introduced the application of the automatic tool for noise-related ICs classification considering as reference set the resting-state fMRI datasets from one

subject and as test set resting-state fMRI dataset from 50 young twin pairs. For the reference subject are extracted a number of ICs equal to 33, as for the test subjects.

The reference ICs were manually labelled, according to the hand classification of fMRI ICA noise components [49], and the Automatic Classification Tool described before is applied to the ICs of the test set, using the optimal threshold of *Spatial Correlation Coefficient (SC=0.3)* and *Relative Percentage of Spectral Power (SP=31)*.

As reference set is chosen a single subject that is characterized by 33 ICs, composed by noise-related ICs and signal-related ICs in approximately equal proportion. We choose as reference set the ICs obtained from the rs-fMRI data of a subject characterized by a *balance of hand-labelled noise and signal-related ICs*. Noise- and signal-related components in the *reference set of ICs* are necessary since we want to obtain a good classification of noise and signal components in the test ICs.

Subsequently to the application of the automatic tool, as output of this step is created a binary excel file for each subject containing the labelling obtained for each ICs: *noise-related ICs are associated to 1* and *signal-related ICs are associated to 0* in this output file.

3.3 FSL cleaning tool: *fslregfilt*

The primary purpose, after identified the Independent Components related to noise, is to clean the single-subject data by removing the noise-related ICs from the pre-processed 4D resting-state fMRI data to produce a *“clean” version of the pre-processed data*.

In this work of thesis, the process of “clean up” the EPI data is achieved using the *FSL command* called *fsl_regfilt* which will regress the time courses of the noise components from the data of each subject. This command receives as input the *4D NIFTI volumes*, to which we apply the high pass filtering, that represents the same input as the *melodic* command. The other inputs to be specified are the *ICA time series of each ICs*, created after applying MELODIC with the name of *“melodic_mix”* and lastly the *list of noise component numbers* for the specific subject to be eliminated from the original data.

The output of *fsl_regfilt* is the clean pre-processed 4D resting state data, in which are removed the noise-related ICs remaining only the classified signal-related ICs.

In Fig.2.6 are briefly illustrated the inputs and outputs of the *fsl_regfilt* function used to clean the fMRI data of the subjects.

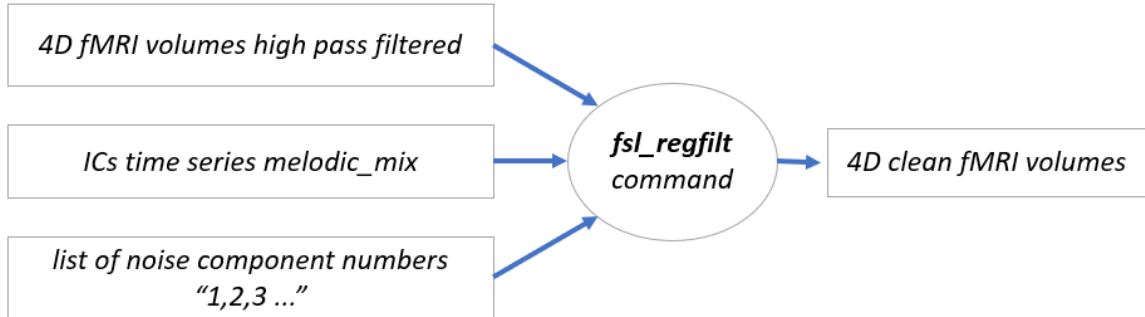


Figure 2.6, FSL command *fsl_regfilt*: inputs and outputs.

In this step for each processed subject is taking trace, in the Excel file of the database, of the ***total number of components removed*** from each subject's 4D fMRI volume. We decide to consider for the next step of the analysis the subjects in which are *fsl_regfilt* removed no more than 75% of the 33 initial ICs. The subjects characterized by a ***removal of more than 25 ICs*** during the cleaning procedure are not consider in the following steps of the SCA and topological parameter analysis.

Considering the ***removal in this step*** of the ***subjects***, and corresponding twins, that are characterized by a ***number of removed ICs higher than 25*** (75% of total ICs removed), we consider for the following analysis a number of ***25 DZ couples*** and a number of ***18 MZ couples***.

4. SCA: Seed-based functional connectivity analysis

The analysis of Seed-based functional connectivity analysis was performed on 43 subjects, 25 DZ couples and 18 MZ couples.

As was introduced in *Paragraph 3 of Chapter 1*, the ***functional connectivity*** is typically defined as the observed temporal correlation between neuro-physiological measurements from different parts of the brain. If we consider rs-fMRI this kind of definition indicates

that the functional connectivity shows the relationship between BOLD signal obtained from two separate regions of the brain: the hypothesis behind the functional connectivity for rs-fMRI is that if two regions shows similarities in their BOLD signals over time, they are functionally connected. *Seed-based functional connectivity analysis (SCA)* is the most common way to explore the functional connectivity within the brain in the context of rs-fMRI data. This method is based on the time series of a seed voxel, called ROI, and calculates the connectivity, using for example the linear metrics of correlation of time series for all other voxels in the brain. As result, a significantly **high correlation between time series of ROIs** indicates a significantly **high level of functional connectivity** between these regions. This method is characterized by several steps described below and represented in Figure 2.7:

1. **Definition of the nodes**, that means grouping the voxels together into areas that could be considered functionally homogeneous regions.
2. **Extraction of each node time series**.
3. **Calculation of the connectivity** between **all pairs of nodes** using the extracted time series of the step before.
4. **Estimating the functional connectivity matrix** in which each element (i, j) describes the strength of functional connectivity between node i and node j .

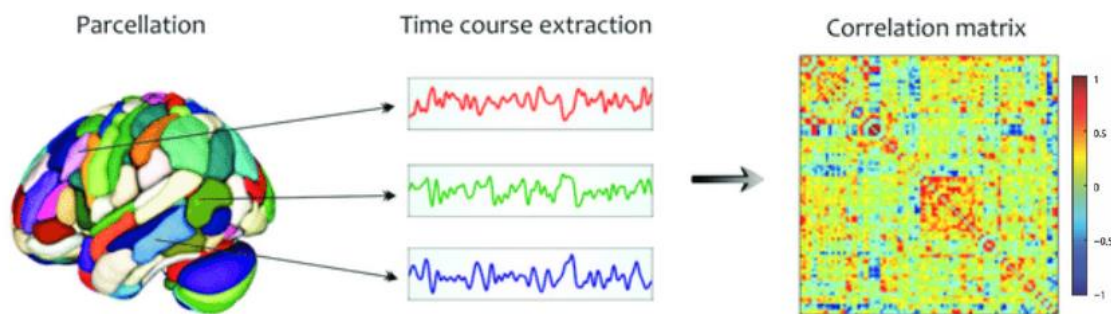


Figure 2.7, Steps of Seed-based correlation analysis SCA.

In this work of thesis this method of **SCA** is used to analyse the specific *connections between couples of ROIs* and verify if the *functional interaction between brain regions* can be attributed to genetic factors. If we consider two ROIs and we evaluate the functional connectivity between this pair in couple of MZ twins and DZ twins, a significantly higher

functional connectivity in MZ twins with respect to DZ twin indicate that the genetic factors influence the level of functional connectivity between these regions. To quantify this influence of *genetic factor on functional connectivity* between regions will be necessary to use Twin Models. In this research, we analyse the interaction between each couple of ROIs in the whole fMRI volume of the brain.

4.1 Anatomical parcellation of the Brain

Regarding the *first step of the SCA*, the identification of the nodes is generally obtained through the anatomical parcellation of the brain. In this step, the whole brain is divided into a set of anatomical regions of the AAL atlas, characterized by 116 ROIs. Each region of interest was required to serve as a distinct node (vertex) in a graphical brain model, and each node was constrained to lie within the periphery of one and only one AAL region of interest.

In this work to obtain the *parcellation of the brain* are used the toolboxes of *MarsBar v0.44*. MarsBar is an open source software toolbox for SPM which provides routines for region of interest analysis. This toolbox is implemented for SPM and developed in Matlab environments.

Firstly, is used the option “Import” from MarsBar that allows the user to obtain the parcelled ROIs from the nifti image of the atlas. This option receives as input the atlas nifti image and creates a set of 116 regions in MarsBar ROI file format. Each ROI of the atlas is defined by a number label as ROI_1, ROI_2, ... ROI_116.

Subsequently, after the atlas parcellation, is applied the second step of the Seed-Based correlation analysis that is represented by the extraction of the summary time series of the voxels within each ROI using the option of MarsBar “Extract ROI data (full options)”, for each subject. The output of this options is the summary time course that has one value per scan, per ROI and by default is made up of the means of all the voxels value in the specific ROI. At the end of this step we obtain a matrix of dimension 200×116 . The rows indicate the number of scans (200 for each subject), the columns represent the number of ROIs of the atlas from which are extracted the data for the specific subject.

Analysing the signals and the fMRI volumes, we notice that in most of the subject the field of view *did not cover the Cerebellum and the Vermis*, therefore there was no fMRI signal

in these corresponding regions. We decide to exclude them from our analysis and consider only the first 90 ROIs of the AAL atlas.

The average fMRI time series of the voxels within each 90 selected ROI, described by the AAL atlas, for each subject is used for the third step of the Seed-based correlation analysis related to the connectivity analysis.

4.2 Functional connectivity adjacency matrix

The third step of the Seed-based correlation analysis SCA is the *extraction of the functional connectivity matrix* estimated for each subject. The functional connectivity can be defined as the temporal dependency of neural activation patterns of anatomically separated brain regions. In case of resting state functional connectivity, we focus on the connectivity assessed across individuals BOLD time points during the rest condition. Studies on functional connectivity have revealed new findings about the functional connection of the specific brain region and about the overall organization of functional communication in the brain network.

In this work the *Functional connectivity matrix* is calculated using *linear metrics of Pearson's correlation coefficient*, estimating *Cross-Correlation (CC)* matrix which underlines the linear dependence between time series, or using statistical measure that additionally considers the *non-linear dependence* between BOLD time series, obtaining *Mutual Information (MI) matrix*. Both CC and MI matrices represent a Functional Connectivity matrix, the difference between the two is based on the linear/non-linear metrics used to obtain the functional connectivity between couple of ROIs.

Each point of the Functional connectivity matrices of CC and MI represents a *link-level* parameter of the brain network, since these matrices indicate a parameter extracted at the level of the link between ROI couples.

Firstly, is obtained the Functional connectivity matrix by calculating the temporal correlation between BOLD time series of different ROIs at single subject level using a linear correlation measure that represents the most used measure of interaction between two time series related to two different ROIs (node of the network).

Starting from the 200x90 matrix obtained in the step before, is applied the most commonly used linear correlation represented by the *Pearson's linear correlation coefficient*. The function *corrcoef* in Matlab can correlate each pair of ROIs' time series, through Pearson correlation coefficient, to investigate the similarity between these two nodes. Correlation ranges from -1, that indicates perfect negative correlation between nodes, to +1, that indicates perfect positive correlation between nodes. The value of 0 indicates no correlation between the pair of nodes. The outputs of this function are a cross-correlation matrix R of dimension 90x90 and p value matrix P that is used to test the hypothesis of no correlation. Each p-value represents the probability of getting a significant correlation, when the null hypothesis is no correlation between observed phenomena. If P is smaller than the significance level 0.05, then the corresponding correlation in R matrix is considered significant. R matrix is a *functional connectivity matrix*, is calculated for each subject and represents the *cross-correlation between BOLD time series of the nodes*.

This *functional connectivity matrix* evaluated using linear metric of Pearson's linear correlation coefficient is named *Cross-Correlation (CC) matrix*. This CC matrix is extracted for each Twin 1 and Twin 2 in the couple, for all MZ and DZ couples.

The *CC matrix*, also indicated by R , is defined in *Paragraph 3.3 of Dynamics and Graph-analysis of Brain's Networks* of Chapter 1. This matrix indicates the connectivity between every pair of nodes in a network. Connectivity matrix can be used to generate the graph-based representation of the network. In this matrix each row and column represent a different node of the graph, and the corresponding element in the matrix, related to the functional connections between brain regions, represents an **edge**. The off-diagonal element of the matrix C_{ij} , in the position *ith* of the row and *jth* of the column, encodes the information about the connection between region (ROI) i and j . In this work we start from the parcellation of the brain in 90 ROIs (nodes), the connectivity matrix that we obtain is a square matrix 90 x 90.

The *Cross-Correlation matrix* that we extract at this single subject level has also the characteristic to represent a **weighted and undirected network**, it also called *undirected weighted cross-correlation matrix*.

After defining the *CC matrix* is necessary to quantify the useful connections between nodes of the network. For this purpose, is used a **thresholding** procedure of the *CC matrix*

R by applying a cut-off threshold on the p-value of the nodes, in order to determine which connections should be retained in the *CC matrix*. R matrix is thresholded considering only the significant cross-correlation between nodes (with p-value < 0.05) and setting to 0 the non-significant ones.

After applying a threshold to the *CC matrix*, the remaining elements can be binarized such that the elements of the matrix that have a value C_{ij} over the threshold are set to 1, the elements with a value below the threshold are set to 0. Using this binarization, we obtained a **binary network**.

As has been introduced, in this work is estimated another Functional Connectivity matrix using a *non-linear metric*, used to obtain a measure of functional connectivity between couple of ROIs based on non-linear interaction.

Starting from the BOLD time series of different ROIs, the brain area (ROI) connectivity can be evaluate using also non linearity measure. The Pearson's correlation coefficient described before, measures the linear dependence between two time series, whereas *Mutual Information* is a statistical measure that extract information about also the non-linear dependence [50]. The Mutual information quantifies the shared information between two time series. If two time series are independent, there is no shared information and the MI is zero. In this work of thesis MI is used to investigate the non-linearity of functional connectivity among time-series from different ROIs (i.e. node of the graph). As in many research studies, in this work we consider the non-linearity an inherent feature of the brain dynamic and we use also a non-linear approach to study the functional connectivity between the nodes if the subject's network.

In this work Mutual Information is evaluated between BOLD time series to obtain the *Mutual Information (MI) matrix*, representing a Functional Connectivity matrix estimated using non-linear metrics.

Intra-pair difference of the CC and MI matrix, for MZ and DZ couples

Once computed the *CC matrix* for all the subjects, we estimate an intra-pair connectivity similarity between the two twins of each couple, separately for MZ and DZ twins. We calculate the *intra-pair CC difference*, called *delta*, as the distance between the two cross-correlation matrices of the twins in the couple, using the absolute value of the difference

due to the irrelevant order of Twin 1 and Twin 2 in the couples. ***This first step*** of intra-pair similarity analysis is based on the estimation of *intra-pair CC difference*.

The matrix that we obtain is also called *intra-pair CC difference matrix*. For a visual inspection of the results, we averaged the intra-pair difference matrices across MZ and DZ twins, obtaining two averaged matrices and in the end, we compared them. We also compute the difference between these two averaged matrices to compare better the averaged intra-pair difference matrices in MZ and DZ twins. Based on the twin study literature, we expected to find higher whole-brain connectivity similarity in MZ twins compared to DZ.

Regarding the ***MI matrix estimation***, this matrix is obtained for each Twin 1 and Twin 2 in a couple, for all MZ and DZ couples. Then we apply the same ***first step*** of CC matrix, used to analyse the ***functional connectivity similarity, based on MI measures***, of each connection.

Firstly, is applied the ***intra-pair similarity analysis*** based on the calculation of the ***intra-pair MI difference*** in MZ and DZ twins. This *intra-pair MI difference (delta)* is calculated between the 2D-MI matrices of the two twins of each couple, separately for MZ and DZ twins. This difference is used to analyse the MI similarity between twins in a couple.

For a visual inspection of the result, we *average the intra-pair MI difference* matrices in MZ and DZ and compared the results. We achieve in the end two average intra-pair MI difference matrices, one averaged between all MZ couples and one averaged between all DZ couples. If the average matrix of intrapair difference of MI has lower values, means that the twin couples have similar Mutual Information, representing the shared information (MI) between two BOLD time series. The Mutual Information indicates a functional connectivity measure between regions. We expected to appreciate a higher MI similarity in MZ compared to DZ. We also compute the difference between the two averaged matrices associated to MZ and DZ couples, to compare better the averaged intra-pair difference matrices in MZ and DZ twins.

In the end is calculate a matrix to evaluate the difference between MZ and DZ twin in terms of Mutual Information. This matrix is obtained as difference between the two averaged matrices of intra-pair difference between MZ and DZ twins.

Intra-pair correlation coefficient of CC and MI matrix, for MZ and DZ couples

The *next step* used to analyse, *in the CC matrix, the intra-pair functional connectivity similarity* of each connection using an *intra-pair correlation analysis*. We applied *partialcorr function* on each element (i, j) of the Cross-Correlation matrices estimated for Twin 1 and Twin 2 in a couple, in MZ and DZ twins. The *partialcorr function* is used to evaluate the effect of Zygoty on the functional connectivity, at net of the effects of Age and Sex. The outputs of the *partialcorr function* are represented by two *correlation matrices* for MZ and DZ twins.

As was already introduced, *partialcorr function* is applied on each element of Cross-Correlation matrices of MZs and DZs. Each matrix contains the correlation values obtained considering the connectivity (Cross-Correlation value of the matrix R) within every pairs of nodes between Twin 1 and Twin 2 in the couple, for all MZ couples and for all DZ couples. The results will be two *intra-pair correlation matrices of nodes' connectivity, one for MZ couples and one for DZ couples*.

For each twin in the couple are created two vectors, one containing the matrix elements (i,j) for all Twin 1 in the couple, and the other containing the matrix elements (i,j) for all Twin 2 in the couple. Then is calculated the correlation between the two vectors using *partialcorr* receiving in input the two vectors and other two vectors containing the age and sex of the couple of twins. This function, differently from *corrcoef*, estimate the intra-couple correlation of connectivity within each pairs of nodes, removing the eventual effect of Age and Gender.

This approach, illustrate in Figure 2.8, is repeated for all MZ couples and all DZ couples. In the end, considering the element (i, j) for the previous calculation, we obtain one value of intra-pair correlation between all MZ couples and one value of intra-pair correlation between all DZ couples. These two values of correlation will be respectively the element (i, j) of the correlation matrix for MZ twins and the element (i, j) of the correlation matrix for DZ twins. To fill the two correlation matrices, this estimation of MZ and DZ value of correlation is repeated for all element in the MZ and DZ functional connectivity matrix.

We decide to apply these following analysis for the value of functional connectivity between the couples of nodes (i,j) only if this connectivity is associated to a value of ***intra-pair correlation (i,j) between MZ and DZ twins that is positive.***

This condition to be respected $r_{MZ}(i,j) > 0$ AND $r_{DZ}(i,j) > 0$, imposes on the correlation values is used to select only a cluster of correlation values (i,j) between nodes in the matrix of correlations for the analysis of ***Epistatic Effect, Twin's Model, Heritability*** and ***Quantitative analysis*** on the difference of correlation ($r_{MZ} - r_{DZ}$).

In this step is also taken note of the correlation values that ***result positive and significant*** between MZs and DZs. A correlation value is considered ***significant*** if the associated probability value is lower than a ***probability threshold*** based on ***Bonferroni Correction***:

$$p_{threshold} = \frac{0.05}{\frac{n_{nodes} \times (n_{nodes} - 1)}{2}} \quad (2.2)$$

Regarding the ***MI matrix***, we apply the same step of ***intra-pair correlation analysis*** that we applied on CC matrix used to analyse the intra-pair similarity of the Mutual Information between couple of ROIs across MZs and DZs twins, representing a measure of intra-pair functional connectivity similarity. As before, for this ***intra-pair correlation analysis*** is applied the ***partialcorr function*** on each element (i,j) of the Mutual Information matrices estimated for Twin 1 and Twin 2 in a couple, in MZ and DZ twins. The main aim is to evaluate the effect of Zygosity on functional connectivity, measures using Mutual Information, at net of the effects of Age and Sex.

The approach starts with the estimation of the ***correlation matrices***, one for MZ couples and one for DZ couples, each one containing the correlation values obtained considering the Mutual Information evaluated within every pairs of nodes (i,j) between Twin 1 and Twin 2 in the couple, for all MZ couples and for all DZ couples. The approach used to calculate these matrices is the same explained for the functional connectivity matrix and illustrated in Figure 2.8.

These *two intra-pair correlation matrices for MZ and DZ twins* are necessary for the analysis of Epistatic Effect, Twin's Model, Heritability and Quantitative analysis on the difference of correlation ($r_{MZ} - r_{DZ}$) of the parameter MI in each couple of ROIs.

In this step is also taken note of the correlation values that result *positive* and *significant* across MZs and DZs; considering a significant correlation values the ones associated to probability value lower than a *probability threshold* (Eq.2.2).

Also in this case, it will be applied analysis of Epistatic Effect, Twin's Model, Heritability Twin's Model and Quantitative analysis on the difference of correlation ($r_{MZ} - r_{DZ}$) only for the functional connectivity value between a couple of ROIs that shows a value of *intra-pair correlation values (i,j) between MZ and DZ twins that result both positive*.

5. Topological parameters estimation and Intra-pair Similarity analysis

In this study, the topological parameters of network-level and node-level are extracted from the *Cross-Correlation matrix*, obtained by applying the linear correlation coefficient of Pearson. The topological parameters extraction is applied considering brain as an undirected graph where each of the 90 ROIs represent a node of the network, so we are able to extract the topological properties.

In general, many topological parameters are achieved by analysing both binary and weighted networks, corresponding to binary and weighted adjacency matrices. Knowledge about topological properties could advance a comprehensive understanding of how brain networks are organized and how they can generate complex dynamics. In this study are analysed the intra-pair correlation values of r_{MZ} and r_{DZ} estimated for each topological parameter, separately for MZ and DZ twin pairs.

The topological parameters estimated in this work of thesis are already mentioned in *Paragraph 3.3 about Dynamics and Graph-analysis of Brain's Networks of Chapter 1*.

5.1 Node-level Topological parameters estimation and Intra-pair similarity analysis

We use the functional connectivity matrix of Cross-Correlation to estimate the node-level parameters of *Node strength and the Nodal strength of positive/negative weights*. To obtain the remaining parameters we use the binarization of the CC matrix by using the threshold set to 0.5; all the value of the CC matrix higher than the threshold are associated to 1, the value below the threshold are associated to 0. This binary matrix is used to estimate node-level parameters of *Node degree, Local efficiency, Clustering coefficient, Node betweenness centrality and Optimal community structure*.

Intra-pair difference Node-level parameter, for MZ and DZ couples

Subsequently, is applied *to each node-level parameter the same intra-pair similarity analysis* applied on CC and MI matrix that consists in the extraction of the intra-pair difference of the measure of the selected parameter, called *delta*, separately for MZ and DZ twins. The value of intra-pair difference is estimated for each node-level topological parameter and using the absolute value of the difference, because the order of Twin1 and Twin2 in the couples has no influence on the intra-pair difference.

Intra-pair correlation coefficient of Node-level parameter, for MZ and DZ couples

Thereafter, is applied to each network-level and node-level parameter the *same intra-pair correlation analysis* applied *on CC and MI matrices*. This approach is aimed to estimate the intra-pair correlation values associated to each node of node-level parameters, separately for MZ and DZ twins.

For *node-level parameter* of the network we achieve one value of intra-pair correlation associated to each of the 90 nodes of each parameter, separately for MZ and DZ twins.

In all cases node-level parameters are taken note also of the correlation values that result *positive and significant* across MZs and DZs. For node-level parameter, significant correlation values are associated to probability values lower than 0.05.

In case of *node-level parameters*, the parameter is characterized by 90 values, each one associated to one node (ROI).

The *intra-pair correlation approach* for node-level parameter is performed at single node level. This process is illustrated in Figure 2.9.

In this case are created two vectors for each of the 90 nodal values of the node-level parameter, for each twin in the couple. One vector contains the measures of that parameter associated to a certain node (one of 90 nodes) for all Twin 1 of the couple and the other vector contains the measures of this node for all Twin 2 in the couple. Next, the intra-pair correlation coefficient of Spearman is calculated between the two vectors using *partialcorr*, use to estimate the *intra-pair correlation* associated to each node-level parameter, removing the possible effect of Age and Gender.

This process is done for all MZ and DZ couples. The intra-pair correlation values between MZs and DZs are obtained for each node. We computed 90 values of intra-pair correlation, for MZs and for DZs, for each node-level parameter.

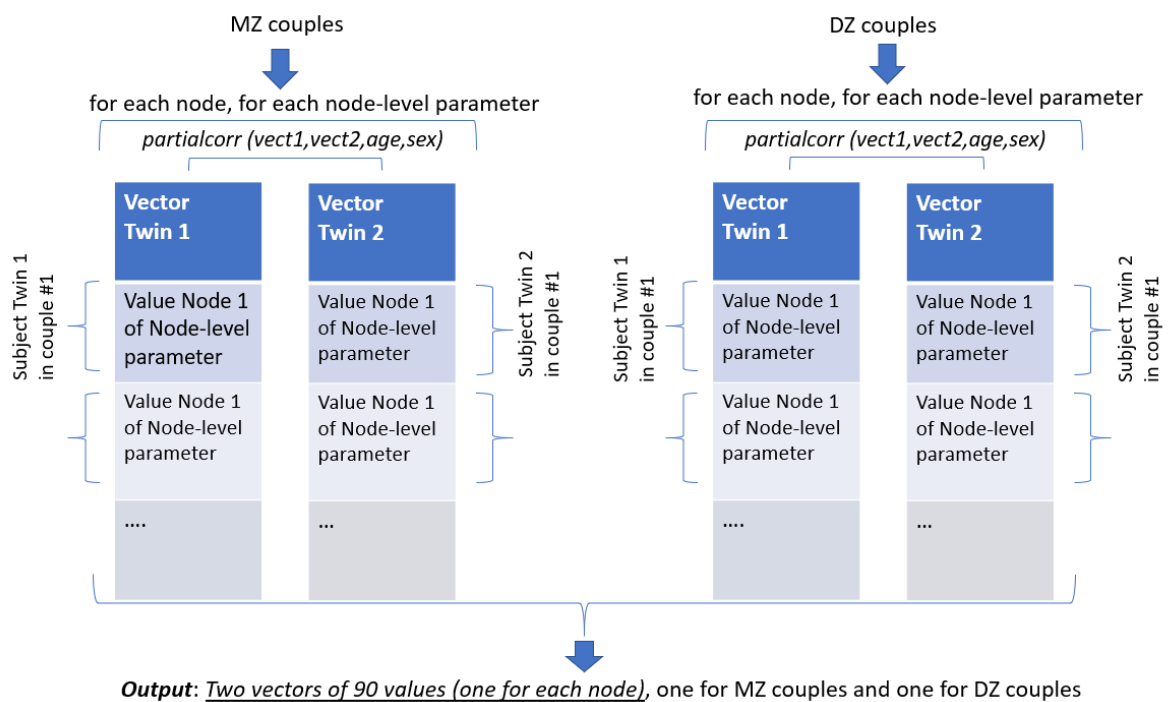


Figure 2.9, Correlation between node-level parameter of all Twin 1 and Twin 2, for each node, in MZ and DZ couples.

We decide to apply the analysis of Epistatic Effect, Twin's Model, Heritability and Quantitative analysis on the difference of correlation ($r_{MZ} - r_{DZ}$) only for the nodes of

node-level parameters that result associated to *positive correlation values* r_{MZ} and r_{DZ} such that: $r_{MZ} > 0$ AND $r_{DZ} > 0$.

5.2 Network-level parameter estimation and Intra-pair similarity analysis

We use the functional connectivity matrix of Cross-Correlation to estimate the network-level of *Total strength of positive and negative Weight*. As before, to obtain the remaining parameters we use the binarization of the CC matrix by using the threshold set to 0.5. This binary matrix is used to estimate network-level parameters of *Global efficiency, Density of the graph, Characteristic Path Length, Network Degree and Maximized modularity*.

Intra-pair difference of Network-level parameter, for MZ and DZ couples

Subsequently, is applied *to each network-level parameter the same intra-pair similarity analysis* applied on CC, MI matrix and node-level parameters that consists in the extraction of the intra-pair difference of the measure of the selected parameter, called *delta*, separately for MZ and DZ twins. The value of intra-pair difference is estimated for each network-level parameter and by calculating the absolute value of the difference, because, as introduced before, the order of Twin 1 and Twin 2 in the couples has no influence on the intra-pair difference.

Intra-pair correlation coefficient of Network-level parameter, for MZ and DZ couples

Subsequently, is applied to each network-level the *same intra-pair correlation analysis* applied *on CC, MI matrices and node-level parameters*. This approach calculates the intra-pair correlation values associated to each network-level parameter, separately for MZ and DZ twins.

In the case of *network-level parameter* we obtain one value of intra-pair correlation associated to each network-level parameter estimated between MZs and one value of intra-pair correlation for DZs. For all network-level parameters are taken note also of the correlation values that result *positive* and *significant* across MZs and DZs. For network-

level parameter, significant correlation values are associated to probability values lower than 0.05.

To each network-level parameter is applied the following approach, illustrated in Fig. 2.10, to calculate *the intra-pair correlation values associated to the specific network parameter*, for either MZ and DZ couples.

For each twin in the couple are created two vectors, one contains the measures of that network-level parameter for all twin 1 of the couple and another vector contains the measures of the network-level parameter for all twin 2 of the couple. Then is calculated the Spearman's correlation coefficient between the two vectors, containing respectively the network parameters for all Twins1 and Twins 2 in the couple, using *partialcorr*.

In the end is obtained one value of correlation for the specific network-level parameters. This is done for all MZ couples and then for all DZ couples, obtaining two values of intra-pair correlation for the specific network-level parameter one estimated between MZ twins and one between DZ twins. This approach is repeated for each network-level parameter that we estimated.

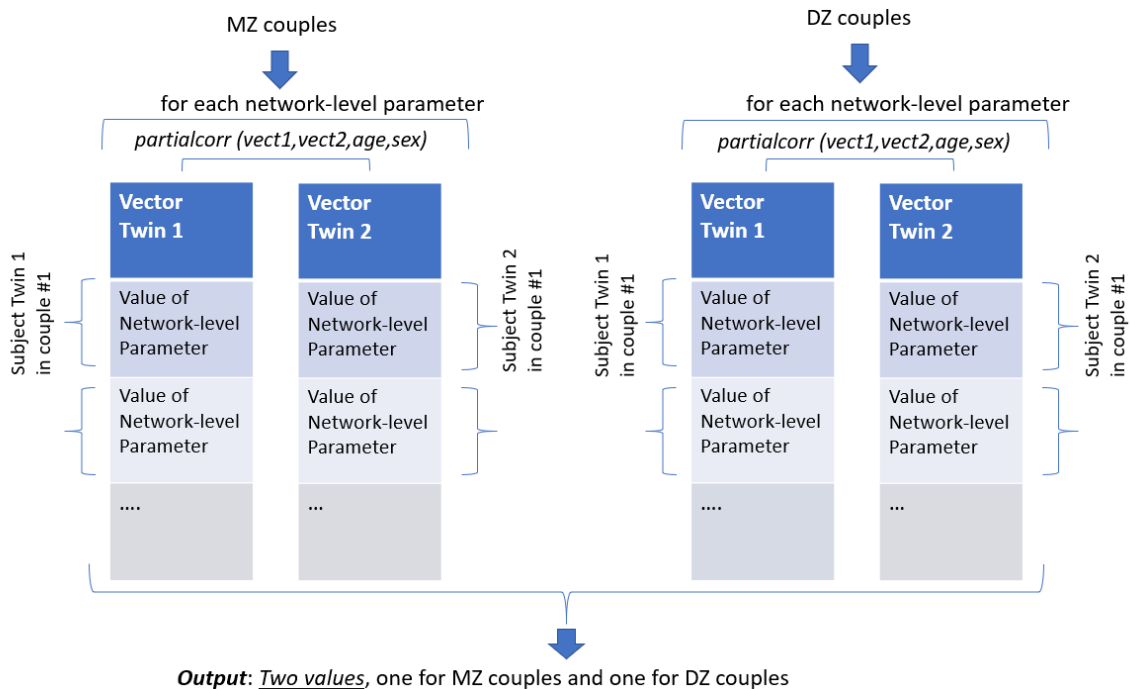


Figure 2.10, Correlation between the network-level parameters of all Twin 1 and Twin 2 in MZ couples and DZ couples.

We decide to apply the analysis of Epistatic Effect, Twin’s Model, Heritability and Quantitative analysis on the difference of correlation ($r_{MZ} - r_{DZ}$) only in the case that **both correlation values r_{MZ} and r_{DZ} associated to the specific network-level parameter result positive**.

6. Analysis of Genetic and Environmental Influences of Topological Parameters

This section is related to the evaluation of the genetic and environmental influence of the topological parameters that we extract (*network-level, node-level and link-level*), using the intra-pair correlation coefficients of each parameter, one extracted between MZ couples, indicated by r_{MZ} , and the one estimated between DZ couples indicated by r_{DZ} .

We distinguish **four main cases** of analysis based on the intra-pair correlation values, obtained between MZ (r_{MZ}) and DZ couples (r_{DZ}), calculated for each topological parameter:

- If $r_{MZ} > 4r_{DZ} > 0$, there might be **genetic effects at different loci, called Epistatic Effect**. In this case, there is not a precise formula to estimate these specific effects based on the intra-pair correlation values calculated between MZs and DZs.
- If $0 < 2r_{DZ} < r_{MZ} < 4r_{DZ}$, **Genetic effects** can be partitioned into **additive** (i.e. the effect of one allele is added to the effect of the other allele) and **dominant** (i.e. the deviation from purely additive effects) effects or a combination of the two effects. These effects on the phenotype can be modelled using an ADE model which estimates the contributions of **additive (A), dominant (D) genetic effect** and an **unshared environmental influence (E)** on the value of the selected parameter and. In the ADE model Genetic effects (additive and dominant) are considered to create high influence on the phenotype, while the *common environmental effects (C factors)* are not taken into consideration due to their less importance with respect to the Genetic Effects.

In the case of ADE model, explained in Paragraph 6.2 a “broad sense” estimate of **heritability** is obtained considering the coefficients $A + D$.

- If $0 < r_{DZ} < r_{MZ} < 2r_{DZ}$, there exists a contribution of *additive genetic effects* (A) and also a contribution of the *shared (C) and non-shared (E) environment* on the value of the selected parameter. The contribution of the non-additive (*dominant, D*) genetic effects is removed because it is less important than the shared environmental effect. In this case is necessary to quantify the genetic and environmental influence using the *ACE model*, explained in Paragraph 6.1. In the case of ACE model can be obtained a “narrow sense” estimate of heritability considering the coefficient A.
- If $r_{MZ} < r_{DZ}$ means that it *does not exist a genetic contribution* on the value of the selected parameter.

The application of the suitable model (ADE or ACE) on the value of each topological parameter is followed by *the “narrow-sense” or “broad-sense” heritability estimation*, depending on the model applied on the topological parameter.

6.1 ACE Twin model and Heritability Estimation

The classic ACE model is used in univariate twin analysis for assessing the genetic and environmental influences on individual topological parameters of the functional network. The observed parameters in the model are associated with the phenotypic values observed across twins’ pairs. In our case we consider as phenotypic values the link-, node- and network-level FC parameters estimated before.

The ACE model analysed the effects created by the *Additive genetic factor* (A), *Shared environmental factor* (C), *Unique environmental factor* (E).

As has been introduced, in the Paragraph related to the introduction of the twins’ model in Chapter 1, is possible to obtain estimates of these three factors of influence:

$$A = 2(r_{MZ} - r_{DZ}), C = 2r_{DZ} - r_{MZ} \text{ and } E = 1 - r_{MZ} \quad (2.3)$$

The case in which is applied an ACE model is when is respect the condition $0 < r_{DZ} < r_{MZ} < 2r_{DZ}$. In this case exist a contribution of genetic effect and also a contribution of common environment to the variance of the phenotype, in our case represented by the topological parameter, to quantify these contributions is developed an ACE model.

If the condition of ACE model introduced before is valid, is calculated the coefficients A, C and E of the model using the Eq. 2.3.

We analysed the case of ACE suitable model, verify under the correlation coefficients' condition $0 < r_{DZ} < r_{MZ} < 2r_{DZ}$, in the case of network-level, node-level or link-level parameters. ***ACE model analysis is applied only if both correlation values r_{MZ} and r_{DZ} of the topological parameter result positives.***

If the ACE model is suitable, and is valid the condition $0 < r_{DZ} < r_{MZ} < 2r_{DZ}$, we can achieve a ***“narrow sense” heritability based on the estimation of coefficient A:***

$$h^2 = 2(r_{MZ} - r_{DZ}) \quad (2.4)$$

The calculation of h^2 is implemented using Eq. (2.4) for each *network-level, node-level* and *link level* topological parameters. If the selected parameter is ***network-level parameter***, means characterized by a single value of r_{MZ} and r_{DZ} , we obtain a ***single value of heritability of this parameter***. Otherwise, if the selected parameter is a ***node-level parameter***, it means that we have correlation values of r_{MZ} and r_{DZ} for each node, ROI. As result we achieved a heritability estimates for each ROI, so a number of ***90 heritability measures, one for each node*** of the node-level parameter.

The estimate of ***heritability h^2*** was obtained also in the case of a ***link-level parameter***, that is evaluated between each couple of ROIs. This is the case of heritability estimation of the functional connectivity between ROIs, represented by each point in the matrix of ***MI and CC***.

The result in this case is ***a matrix of heritability measures*** obtained considering the values r_{MZ} and r_{DZ} ***for each pair of nodes (i, j)*** in the MZ and DZ intra-pair correlation matrices.

6.2 ADE Twin model Heritability Estimation

The other model used in this work of thesis for univariate analysis on twins is ADE model. In this model the three latent factors that can influence a certain phenotype are: additive genetic influences (A), non-additive genetic influences (D) and non-shared environmental influences (E). The factor *D* ***indicate the dominant genetic variance*** that contributes,

including also the other factors, to influence the total variance of the selected phenotype. Together, the factors ***D (non-additive genetic influence) and A (additive genetic influence)*** yield the total amount of ***genetic variation*** responsible of a particular phenotypic trait.

ADE model is used to study the variation of a certain phenotype if is valid the condition $0 < 2r_{DZ} < r_{MZ} < 4r_{DZ}$. If the condition is valid, are estimated the coefficients of the ADE model as:

$$A = 4r_{DZ} - r_{MZ}, D = 2r_{MZ} - 4r_{DZ} \text{ and } E = 1 - r_{MZ} \quad (2.5)$$

If the correlation coefficients' condition of $0 < 2r_{DZ} < r_{MZ} < 4r_{DZ}$, is verify for the topological parameter, ADE model is applied only if both ***correlation values r_{MZ} and r_{DZ} associated to the topological parameter result positives.***

In the case of ADE-suitable model, when is valid the condition $0 < 2r_{DZ} < r_{MZ} < 4r_{DZ}$, is possible to estimate a ***“broad sense” heritability using the coefficient A+D:***

$$h^2 = A + D = (4r_{DZ} - r_{MZ}) + (2r_{MZ} - 4r_{DZ}) \quad (2.6)$$

7. Quantitative analysis on the difference

$r_{MZ} - r_{DZ}$ based on the Fisher test

We decide to perform a ***quantitative analysis on the difference of correlation values*** obtained in MZ and DZ couples, for each topological parameter. This analysis is completely independent of the Heritability analysis and is irrelevant to the model that results suitable (ACE/ADE) for the value of the parameter.

This quantitative analysis is applied only in the case of a ***topological parameter associated to positive intra-pair correlation values of r_{MZ} and r_{DZ} .***

We analyse in a ***quantitative way the difference between the correlation values obtained in MZ and DZ couples***, indicated by $r_{MZ} - r_{DZ}$, ***using the Z Fisher test.*** The Fisher test indicates the existence of a statistically significant difference between the correlation

values in MZ and DZ couples. The Z Fisher transformed value is proportional to the difference of correlation values in MZ and DZ couples, so it can be used to obtain a quantitative analysis of the difference ($r_{MZ} - r_{DZ}$). If the Z fisher transformed value result significant, it means that the difference between correlation values of MZ and DZ couples is significant.

The Z transformed value, associated to the correlation difference $r_{MZ} - r_{DZ}$, and the related probability value are calculated using the following steps:

- Obtain the intra-pair correlation of the selected topological parameter, in the couples of MZ and DZ twin separately.
- Calculation of the distance, called *delta of correlation values*, between MZ and DZ correlation values of the selected topological parameter.
- Application of Z-fisher transformation to the delta $r_{MZ} - r_{DZ}$ estimated before, to obtain a normal distribution.
- Estimation of the p-value by assessing the variance of the Z-Fisher transformation value of the *delta*, to obtain the significant correlation differences ($r_{MZ} - r_{DZ}$) between MZ and DZ couples.

As described in the steps listed above, we applied the Z-Fisher transformation to the delta ($r_{MZ} - r_{DZ}$). The z transformed value associated to each correlation values of r_{MZ} and r_{DZ} are defined as:

$$z_1 = 0,5 \times \ln\left(\frac{1 + r_{MZ}}{1 - r_{MZ}}\right) \quad (2.7)$$

$$z_2 = 0,5 \times \ln\left(\frac{1 + r_{DZ}}{1 - r_{DZ}}\right) \quad (2.8)$$

The Z-fisher transformation representing the normal distribution and based on these two coefficients is defined as:

$$Z = \frac{z_1 - z_2}{\sigma_{z_1 - z_2}} \sim (r_{MZ} - r_{DZ}) \quad (2.9)$$

Where Z represents the normal cumulative distribution, z_1 and the z_2 are the z transformed value of the MZ correlation and DZ correlation for a certain parameter and $\sigma_{z_1-z_2}$ is the standard error of the difference between the z values of the correlations, depending on the number MZ couples and DZ couples. In Matlab is used the command `normcdf(Z,0,1)` to obtain the cumulative distribution of the z values in the Z normal distribution with 0 mean and standard deviation equal to 1. At the end, is assessed the significance of each delta ($r_{MZ} - r_{DZ}$) of the selected parameter by estimating the p-value looking at the variance from the normal cumulative distribution function. P-values are obtained using the function `1 - normcdf(Z,0,1)`.

Values of probability lower than 0.05 were assumed to be indicative of a **significant correlation difference**, indicated by ($r_{MZ} - r_{DZ}$), associated to the selected topological parameter, between MZ and DZ. We estimate the Z-fisher transformed values that result significant for network-level, node-level and link-level parameters.

8. Effect of Sex and Age on Intra-pair phenotypic difference

The analysis described in this Paragraph wants to study the effects of sex and age of the twin pairs on the intra-pair difference of the topological parameter, at net of the Zygosity.

For this aim is used the Matlab function `partialcorr` to evaluate Spearman's correlation coefficient between the variable Age and Sex and the intra-pair difference of the selected parameter (**delta**) in twins' couples, at the net of zygosity associated to the couples. The application of `partialcorr` function to calculate the effect of age and sex on the intra-pair phenotypic difference is equivalent to apply multiple linear regression model, using as **independent variable** age and sex and as **dependent variable** the intra-pair phenotypic difference.

This analysis is based on intra-pair phenotypic difference (**delta**) calculated for each topological parameter. This **delta** is estimated separately for MZs and DZs to obtain a comparison. In this Paragraph, the intra-pair difference of the parameters is calculated considering all the 43 couples of twins, MZs and DZs at the same time.

Firstly, is calculated the intra-pair difference (*delta*) related to each topological parameter. In the case of ***network-level parameter***, *delta* is calculated as the absolute value of the difference between the value of the selected network-level parameter in Twin 1 and Twin 2, considering all MZ and DZ twins. Each network-level parameter is associated to one value of *delta* for each twins' couples. We obtain a *delta vector of size 43x1* for each network-level parameter, in which 43 represents the total number of twins' couples, MZs and DZs.

On the other side, if we consider ***node-level parameters***, *delta* value is calculated for each of the 90 nodes associated to each node-level parameter. For the *node i*, *delta* is the absolute value of the difference between the value of the *node i*, of the selected node-level parameter, in Twin 1 and Twin 2, repeated for all twins' pairs of MZs and DZs. Each node-level parameter is associated to 90 values of *delta* for each twins' couples. In this case, each node of the selected node-level parameter is characterized by a *delta* vector of size 43x1 and each node-level parameter is characterized by 43x90 values of *delta*, in which we consider to have 43 twins' couples and 90 nodes.

Lastly, if we consider a ***link-level parameter*** we have to calculate a *delta* value for each couple of ROIs in the matrix. For the couple of ROIs (*i, j*) in the link-level parameters matrix, *delta* is calculated as the absolute value of the difference between the value (*i, j*) of Twin 1 and value (*i, j*) of Twin 2 of the link-level parameters matrix, repeated for all twins' pairs of MZs and DZs. Each couple of ROIs (*i, j*) in the link-level parameters matrix is associated to the vector of *delta* values 43x1, that means one value of *delta* for that ROI couple (*i, j*) and for each twins' couple.

To evaluate the effect of age and sex on this ***delta, intra-pair phenotypic difference***, using the Matlab function ***partialcorr***, is necessary to organize the input matrix, such that each column represent a variable. This matrix is created by organizing as first column the variable of intra-pair difference of the phenotype, represented by the vector 43x1 of *delta* values containing the intra-pair difference of the parameter for each couple of twins. As second column the variable age, represented by an age-vector with the same dimension 43x1 containing the age of each twins' couple. As third column the variable sex, represented by the vector containing the sex of each couple, taking into account that all couples consider at this step are sex-concordant. Lastly as fourth column of the variable of

zygosity, associated to the logical vector containing the zygosity information indicated by 0 if DZs and 1 if MZs. All the vectors used to create the matrix have the same dimension of 43x1 (that means one value for each couple) and create an *input matrix* of dimension 43x4. Each case of *partialcorr* application is illustrated in Fig. 2.11.

We apply *partialcorr* for each *network-level parameter*, considering as first column of the input matrix the *delta* vector of dimension 43x1 associated to the specific network-level parameter. The *kth* network-level parameter is associated to the Δ_{vector_k} . For *node-level parameters*, *partialcorr* is applied for each node, by using as first column of the input matrix the *delta* vector 43x1 created for each *node i*, repeated for each node-level parameter. The *ith node* of the *qth* node-level parameter is associated to the $\Delta_{vector_{i,q}}$ with size 43x1.

For *link-level parameters*, *partialcorr* is applied for each ROI couple by using as first column of the input matrix the *delta* vector 43x1 associated to each ROI couple in the matrix of link-level parameter and repeated for each link-level parameter. The *couple (i, j)* of the *pth* link-level parameter is associated to the $\Delta_{vector_{(i,j),p}}$ of dimension 43x1.

The function *partialcorr* computes the partial correlation coefficients between pairs of variables (columns) in the input matrix, while controlling for the effects of the remaining variables in the matrix. The function estimates also the probability value, associated to these partial correlation coefficients.

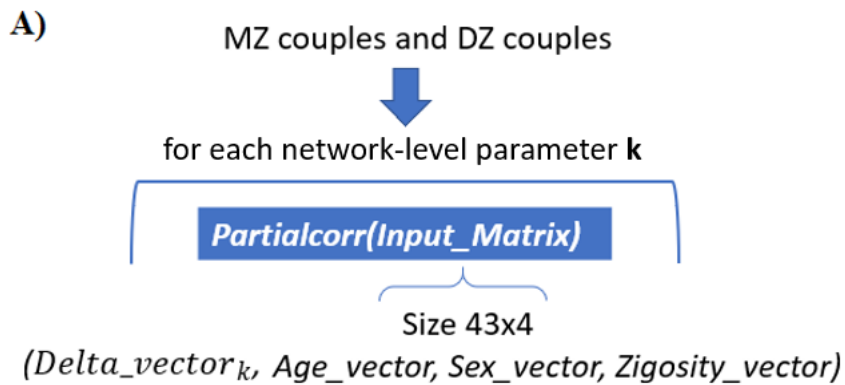
We obtain as *outputs* of *partialcorr* one *matrix of partial correlation values, named r_delta*. This matrix is symmetric, has dimension 4x4 and contains the partial correlation coefficients between pairs of variables (columns) in the input matrix, while controlling for the effects of the remaining variables in the matrix. The other output is the *matrix of probability values, named p_delta*, which is symmetric and with dimension 4x4. Each probability value is associated to each partial correlation coefficients.

We are interested in the network, node-level or link-level parameters that show a *significant partial correlation coefficient* between either *delta value and variable of age* and *delta value and variable of sex*. For this aim, we proceed based on the following steps:

- Extract the probability values associated to the partial correlation coefficients between *delta* value (column 1 of the input matrix) and *variable of age* (column 2 of the input matrix), which correspond to the $p_delta(1,2)$ in the probability matrix.
- Extract the probability values associated to the partial correlation coefficients between *delta* value (column 1 of the input matrix) and *variable of sex* (column 3 of the input matrix), which correspond to the $p_delta(1,3)$ in the probability matrix.
- We assess the significant partial correlation coefficients, $r_delta(1,2)$ and $r_delta(1,3)$, by evaluating if these $p_delta(1,2)$ and $p_delta(1,3)$ are lower than a 0.05 if are considered *network-level and node-level parameters*. In the case of *link-level parameters* is considered a threshold of probability value based on Bonferroni correction:

$$p_{threshold} = \frac{0.05}{\frac{n_{nodes} \times (n_{nodes} - 1)}{2}} \quad (2.10)$$

This analysis based on *partialcorr* function will lead us to investigate if the intra-pair phenotypic difference is influenced by the variable of sex or the variable of age.



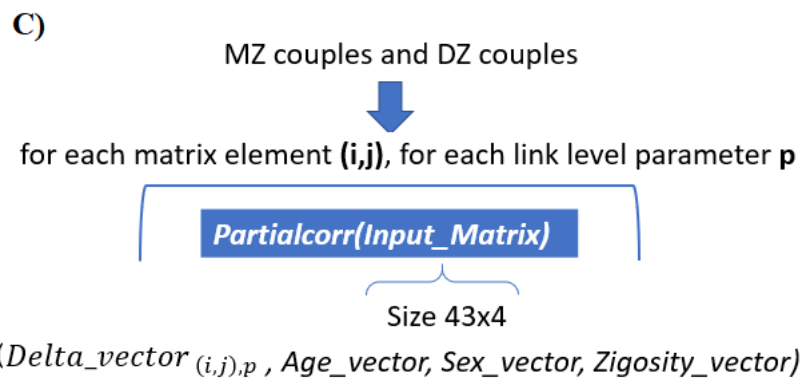
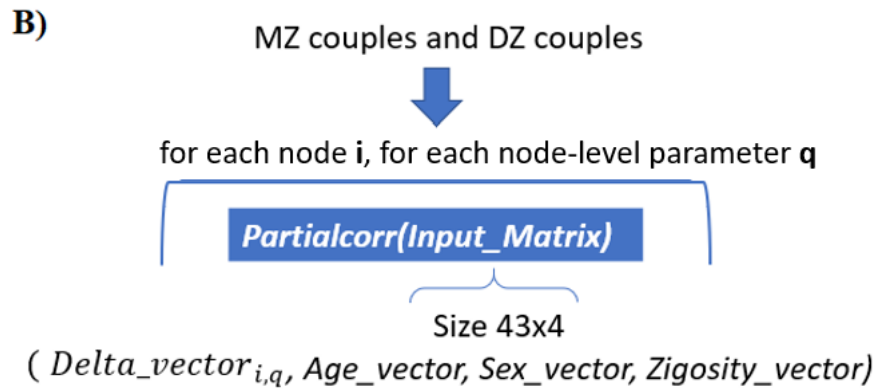


Figure 2.11, Application of partialcorr function to network-level, node-level and link-level parameter to estimate if exist an effect of Age and Sex on intra-pair difference of the parameter.

Chapter 3: Results and Discussion

This Chapter is dedicated to the description and interpretation of the results obtained using the processing pipeline described in *Chapter 2*, starting from the outcomes of the application of the new automatic tool for the classification and removal of noise-related ICs from fMRI data to the results of the seed-based connectivity analysis applied to estimate the functional connectivity between brain regions, including 3) the rating of genetic and environmental influences on local and global parameters of the brain network, 4) the results of the quantitative comparison of MZs and DZs correlation values and the effects of age and sex on the intra-pair difference of the parameter, at the net of zygosity of the twins couple.

The MELODIC decomposition of 4D fMRI data in spatio-temporal ICs, and later the classification of ICs, are applied to the initial database composed by **46 couples of twins** (19 MZ couples and 27 DZ couples). After the clean-process with FSL are excluded from the analysis the subject, and the corresponding twin, in which are removed more than 75% of ICs. Subsequently, the Seed-based connectivity analysis is applied to the remaining **43 couples of twins** (18 MZ couples and 25 DZ couples).

As has been said, the **first part** is dedicated to the results obtained from **application of the automatic spatio-temporal tool** for ICs classification. As first step, are described the results related to the test and validation of the Tool applied on a reference set of an eCPT subject and test set of eCPT and then rs-fMRI subjects. This first part is useful to fix the optimal thresholds for subsequent practical application and show the good accuracy obtained from this first test of the tool that allow us to apply it on the twin's dataset used for this thesis.

The **second part** is focused on the results of the **application of this Tool on the rs-fMRI twin's dataset** using the optimal thresholds obtained in the first application of test and validation step of the tool.

The **third part** shows the results associated to the **intra-pair similarity analysis** across MZ and DZ couples, for each topological parameter extracted at the level of network, node or link between nodes. The intra-pair similarity between twin pairs is evaluated using first an **analysis based on the estimation the intra-pair difference** of each topological parameter

in MZs and DZs. Then, the intra-pair similarity between MZ couples and DZ couples is analysed by considering an *intra-pair correlation analysis of each parameter*, across MZ and DZ twins. The *fourth part* of the results is related to the result of the Genetic and Environmental influences estimated on each topological parameter. Based on the value of the intra-pair correlation across MZ and DZ twins, for each parameter, is analysed if exist an *Epistatic Effect* associated to the topological parameter or is suitable *ACE or ADE* model to study the relative influence of genetic and environmental effects. For the topological parameters for which is suitable ACE or ADE model, is also estimated the “narrow-sense” or “broad-sense” heritability associated to these topological parameters.

The next part of the results, reports the *significant quantitative difference between correlation values* of MZ and DZ couples, indicated by $r_{MZ} - r_{DZ}$, using the Z Fisher statistical test. As result, are reported also the significant Z fisher transformed value associated to each topological parameter.

In the last part of this Chapter, are reported the *results* associated to the *correlation analysis* used to study if exist an *influence*, created *by the variable of age and sex*, on intra-pair phenotypic difference (*delta*) of each topological parameter, at the net of zygosity of the twins' couple.

Considering that the twin's dataset is composed by rs-fMRI data that lead to a not easy interpretations, the present work of thesis represents a preliminary step for the optimization of the classification methods of ICs from rs-fMRI data, using the automatic spatio-temporal tool, and also this work is useful to obtain an improvement of the functional connectivity methods and topological parameter analysis of the functional network for the twin studies. The application of these methods on a twin's dataset of MZ and DZ twins couples could provide important insights also on the heritability of the brain network patterns at local and global levels.

1. Automatic tool for classification of noise-related ICs

1.1 Test and validation on a training fMRI dataset

In this Paragraph we report the results associated to the test and validation of the automatic tool for ICs classification. We discuss the method performances as function of method parameters and dataset types. The following paragraphs are dedicated to the different applications.

The method parameters were set using the *reference set #1*, composed by eCPT fMRI data from one subject and the *test set #1*, composed by eCPT fMRI datasets from five subjects. Both *reference* and *test* ICs were manually marked as *signal/noise* in order to measure the method performance. The comparison between the real labels and those assigned by the tool at varying thresholds in the temporal and spatial analyses allowed the identification of the **optimal thresholds** for the *test set #1*, which were used in all the subsequent analyses.

The optimal thresholds (SC and SP thresholds) were obtained by the inspection of the ROC curves representing the method performances in relation to spatial and power parameters. The ROC curve for SC analysis is obtained by progressively increasing SC thresholds from 0.2 to 0.4 with 1 step in between, while considering the SP threshold equal to the average SP of the *reference set #1* in the high frequency band. The ROC curve for SP analysis is obtained by varying the SP threshold from 23 to 41 with 1 step in between while maintaining the SC threshold selected as optimal in the previous condition. Based on the matches between real and predicted IC labels, we computed two ROC curves, for the SC and SP analyses, and selected the corresponding optimal thresholds.

In the **ROC curves** (Fig.3.1), each point represents the (1-specificity) and sensitivity corresponding to the selected thresholds of spatial and spectral analyses. The closest point

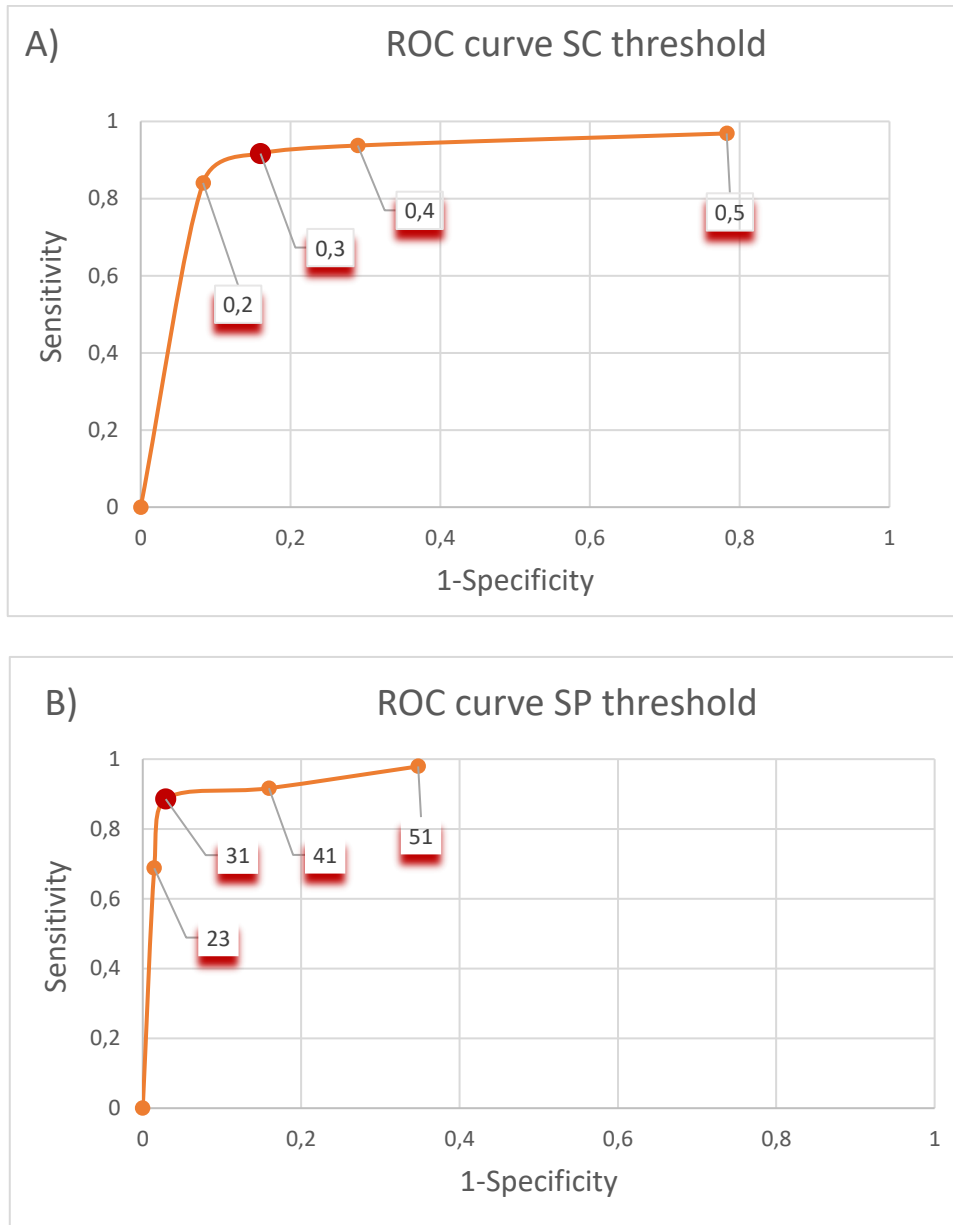


Figure 3.1, ROC curves: A) ROC curve used to evaluate the optimal SC threshold; B) ROC curve used to evaluate optimal SP threshold.

to the optimal situation with sensitivity equal to 1 (highest number of true positives identified) and (1-specificity) equal to 0 (highest number of true negatives identified) represents the optimal threshold.

We can analyse in Figure 3.1 the results of this first application of the method (*Reference set #1, test set #1*), used to establish the **thresholds** for the subsequent applications.

All the results are expressed in terms of accuracy, sensitivity and specificity. The accuracy indicates the probability to have a correct classification of *noise* and *signal* components.

The accuracy indicates the probability to have a correct classification of *noise* and *signal* components. The sensitivity estimates the rate of true positives, which in our case represents the correctly classified artefactual ICs. The specificity estimates the rate of true negatives, which in our study are the correctly classified *signal*-related ICs.

In this ***first application*** when varying the SC threshold in the comparison between *reference* and *test* ICs, the method accuracy ranged between 0.8424 and 0.8848. The sensitivity ranged between 0.9375 and 0.9167 and the specificity ranged between 0.7101 and 0.8406. The optimal SC threshold associated to the highest accuracy 0.8848 is the threshold 0.3. On the other side the optimal SP threshold associated to the highest accuracy of 0.8848 is the threshold 31. The results in terms of accuracy, sensitivity and specificity are reported in Table 3.1.

Is important to notice that the optimal SP threshold confirms our a-priori hypothesis; indeed, while testing different SC thresholds, the best SP threshold was assumed equal to 31%, which represents the average proportion, considering all ICs, of high frequency SP in the reference subject. Then, when different SP thresholds were tested by keeping the optimal SC threshold (0.3), the exact 31% threshold provided the highest accuracy.

The last check that is made on this first application of the tool on *reference set #1*, *test set #1* wants to verify that by applying the cleaning procedure we obtain a cleaned fMRI data without noise-related ICs labelled by the tool. The cleaning procedure consists in removing ICs marked as *noise*, identified by the tool with the use of optimal thresholds, from the original fMRI data and apply the inverse spatial ICA. After perform the inverse spatial ICA on *test set #1*, we visually compared the brain regions that result activated by the eCPT task in the original and cleaned fMRI datasets from one exemplar subject.

The result that we obtain is that fMRI cleaning using these thresholds led to an improved recognition of the brain regions involved in the eCPT task. Indeed, the General Linear Model analysis on the original fMRI dataset produced an artefactual “row-like” activation pattern, which did not emerge after the fMRI cleaning procedure. On the contrary, the same analysis on the cleaned dataset showed a reliable brain activity pattern associated with the processing of emotional stimuli (Figure 3.2).

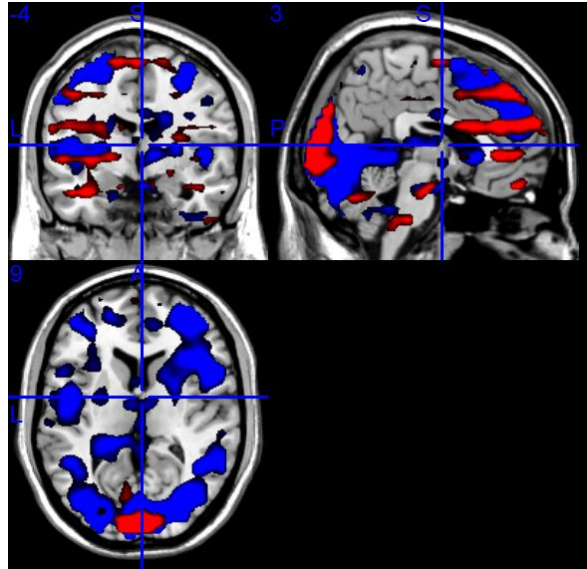


Figure 3.2, Results of the fMRI cleaning procedure: the red and blue clusters emerged from the activation analysis of the original and cleaned fMRI datasets, respectively.

After defined the optimal thresholds with this first application of the tool the method performance is measured in 3 additional applications.

Related to *the other three applications used to validate the method*, are defined the *reference set #2*, that consists in eCPT fMRI datasets from two subjects and *test set #2*, composed of resting-state fMRI dataset from five subjects.

In this *second application*, is used the *reference set #2* to mark *noise*-related ICs on the eCPT-based *test set #1*, then in the third and fourth application the method is tested using the eCPT-based *reference sets (#1 and #2)* to classify artefactual ICs from an unknown dataset characterized by different acquisition parameters, the resting-state fMRI dataset. The optimal thresholds of $SC=0.3$ and $SP=31$ are used for all these other applications.

The *third application* used *Reference set #2*, *test set #1*, and shows that the method performances slightly decreased in terms of accuracy and specificity, while maintaining the sensitivity obtained in the previous application. This result suggests that the automatic labeling of *noise*-related ICs can rely on a small set of representatives, artefactual ICs. The accuracy, sensitivity and specificity of this application are reported in Table 1.

The *fourth application* used *Reference sets #1 and #2*, *test set #2*, composed by eCPT-based reference sets and same pre-selected thresholds to mark the ICs on an independent rs-state

fMRI test dataset, indicate that the accuracy remained higher than 0.8, whereas the specificity slightly decreased compared to the previous applications. This important result suggests that 1) the selected thresholds provide acceptable accuracy, sensitivity and specificity of classification on different fMRI protocols, 2) the use of reference and test datasets with different fMRI acquisition parameters is feasible.

The Accuracy, specificity and sensibility results of each application of the tool are summarized in Table 3.1.

TABLE 3.1. METHOD PERFORMANCES.

	Accuracy	Sensibility	Specificity
<i>Reference set #1</i>	0.8848	0.9167	0.840
<i>Test set#1</i>			
<i>Reference set #1</i>	0.8303	0.8864	0.7662
<i>Test set#2</i>			
<i>Reference set #2</i>	0.8788	0.9167	0.8261
<i>Test set#1</i>			
<i>Reference set #2</i>	0.8303	0.8864	0.7662
<i>Test set#2</i>			

1.2 Tool application to the entire twin rs-fMRI dataset

The tool validated on the previously described four applications, based on the previously-selected SC and SP thresholds selected from the first application using as reference set an eCPT fMRI dataset from one subject and as test set eCPT fMRI datasets from five subjects, is then applied to the rs-fMRI dataset collected from the entire twin sample, in order to classify signal and noise related ICs and remove the latter.

To verify if the tool identifies correctly the noise-related ICs in the twins couples of the initial dataset, composed by 46 couples of twins, we use a *visual inspection* for the analysis of the BOLD signal, time course and power spectra associated to each ICs of

twenty exemplar subjects in this twins' dataset. The visual inspection has the aim to verify if the label associated by the tool to a certain IC corresponds to the IC's label determined by the visual inspection performed by a trained user.

The other investigation, used to verify the correctness of the tool's classification of ICs, regards the analysis of the number of noise-related ICs identified and removed to obtain a cleaned fMRI dataset.

After the application of the tool on the Twins' Dataset and the visual inspection we take *trace of the number of ICs*, for each subject, that are identified by noise and need to be removed from the original fMRI data. During the pre-processing steps, we also take *trace of the subjects* that present a *translational movement* higher than 5mm and a *rotational movement* higher than 3°, which represent the threshold values above which the subjects are considered associated to a translational and rotational movements over threshold. These subjects characterized by this over-threshold head-movement are definitely characterized by a higher number of ICs labelled as artefact, this means that we expect to find these subjects associated to a higher number of ICs removed in the cleaning procedure.

The total number of subjects is 92, given by the 46 twins' pairs. The subjects characterized by an over-threshold head movement in translation and rotation are 13 subjects of the total dataset of twins.

The *qualitative analysis* related to the extracted numbers of removed ICs, labelled as noise-related ICs by the tool, is based on *box-plots* showing the distribution of the number of ICs removed from 1) the 79 subjects (92 total subjects minus 13 over-threshold subjects) who were not associated to an over-threshold head movements, 2) the subjects characterized by high motion artefacts of translational and rotational movements (13 subjects). For the subjects characterized by higher motion artefacts we expected to see higher number of noise-related ICs removed with respect to the total number of subjects in the dataset. In Figure 3.3 we report the boxplots.

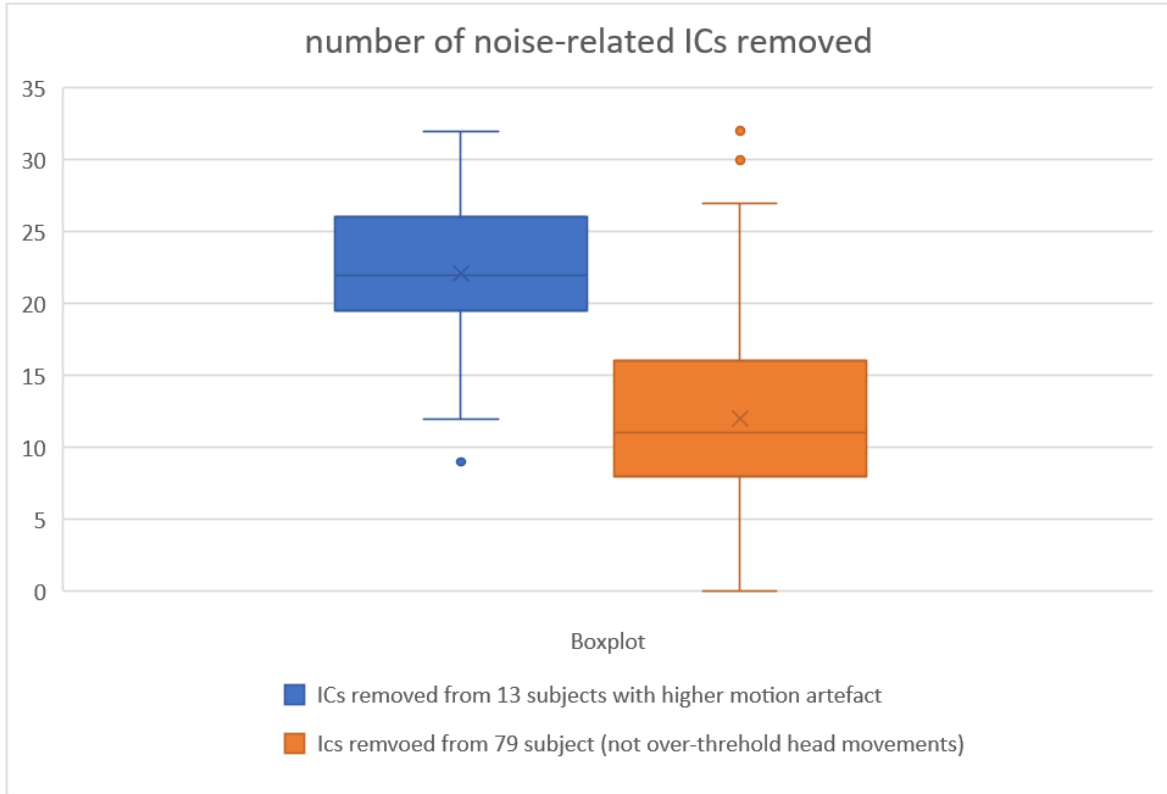


Figure 3.3, Boxplots of number of ICs removed from total dataset of 92 subjects and in 13 over-threshold head movement subjects

The visual inspection of the boxplots supports the expectations, that is, for the 13 subjects with higher motion artefact the number of noise-related ICs identified by the tool is higher compared to the rest of the subjects. The mean value of ICs removed from the subjects with over-threshold head movement is 22. The 79 subjects in the remaining dataset are characterized by a median value of 11 ICs removed.

Once extracted the statistics on the number of ICs removed per subject, we decided to keep the subjects, and the corresponding twins, in which the tool removed not more than 75% of the 33 initial ICs. This selection resulted in the removal of 3 pairs of twins, such that the *initial dataset of 46 pairs of twins ends up in 43 pairs of twins*. The following results consider a dataset of 43 pair of twins.

2. Intra-pair similarity analysis on FC matrix links

In this Paragraph we are going to show the results related to *intra-pair similarity analysis across MZ and DZ*, at the level of each topological parameter. In the first part, related to *Paragraph 2*, is analysed the *intra-pair similarity of each point of cross-correlation matrix and Mutual Information matrix* (link-level parameters of the network).

Subsequently, in *Paragraph 3* are evaluated the results of the *intra-pair similarity related to each specific network-level or node-level topological parameter* estimated from the brain network.

The intra-pair similarity analysis for all topological parameters (network, node or link level) is evaluated by the *calculation of the intra-pair difference and intra-pair correlation analysis* across all MZ and DZ twins' pair. We want to prove a higher phenotypic similarity in MZs with respect to DZs. If the intra-pair correlation between MZs is higher than those of DZs, it is possible to assume that there is an influence of the genetic component in determining the parameter under investigation. If, instead, the correlation values are similar for the two groups, the parameter is most likely connected to environmental factors.

2.1 Intra-pair Similarity analysis on Cross-Correlation matrix

In this section we present the result of the two analyses performed on the Functional Connectivity matrices of CC. The *first intra-pair similarity analysis* applied is based on the estimation of the intra-pair functional connectivity difference between MZs and DZs based on a visual inspection. *The second intra-pair similarity* used an intra-pair correlation-based approach. To obtain the Cross-correlation matrix based on linear metrics we extracted the BOLD signals in correspondence of the AAL region selected (90 regions), we checked the presence of the signal in the ROIs and in the end, we estimated the Cross-Correlation between each pair of ROIs by applying the Pearson's linear correlation coefficient.

Similarity analysis based on Intra-pair cross-correlation difference

Once computed the CC matrix estimated for each subject, we estimate the connectivity similarity between two twins of each couple but separately for MZ and DZ groups. For this purpose, we calculate the *matrix of intra-pair CC differences* for all MZ and DZ twins. The matrix of *intra-pair CC difference, representing the matrix of intra-pair functional connectivity difference* is calculated by making the difference between the CC matrix of Twin 1 in the couple and the CC matrix of Twin 2 in the couple.

For an immediate *visual inspection*, we *averaged the matrices intra-pair CC difference* across all MZ and all DZ twins, obtaining two averaged matrices of intra-pair CC difference for MZ (left panel) and DZ (right panel). Rows and columns represent the 90 AAL regions of brain taken into account for the analysis. Each point of the matrix represents the intra-pair difference of the functional connectivity between each couple of ROIs.

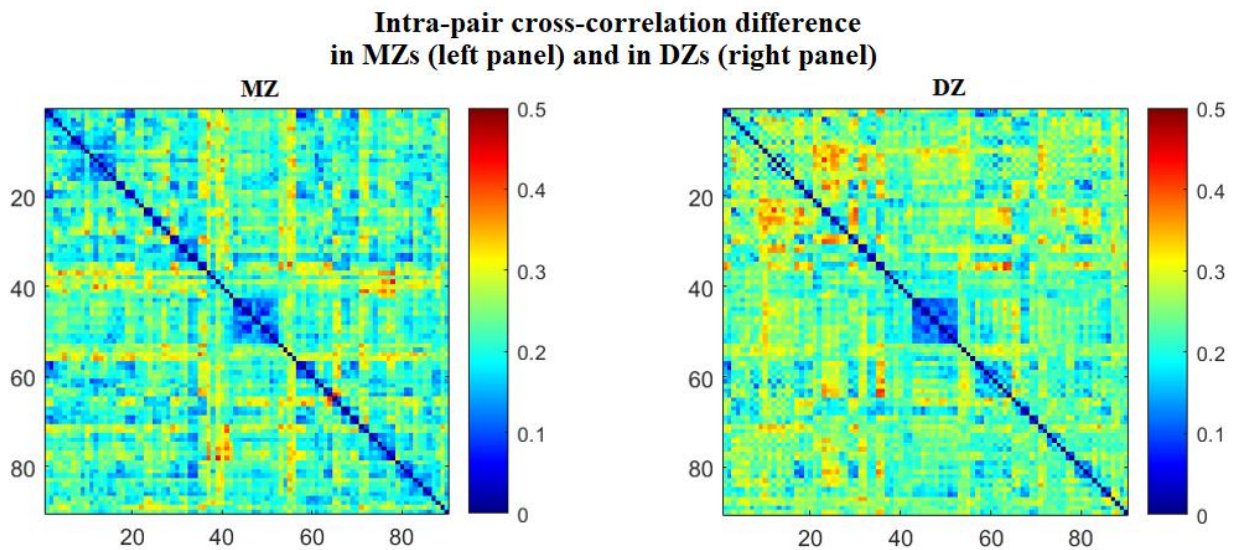


Figure 3.4, Intra-pair cross-correlation averaged difference across MZs and DZs

From the visual inspection of Figure 3.4, we can clearly observe a lower intra-pair difference of functional connectivity in MZ twins. This reflects a *higher similarity in MZ twins with respect to DZ twins*. Considering the colour bar placed beside the figures, we can see that MZ twins' panel is more blue colored and is characterized by lower number of red points, related to higher difference in functional connectivity. On the contrary, DZ twins' panel on the right presents a higher number of red points and is less blue colored with

respect to the right panel. This means that DZ twins have higher number of points related to higher difference in connectivity. These panels confirm our expectation of higher similarity in MZ twins with respect to DZ twins.

We also compute the *difference between these two averaged matrices obtained averaging between DZs and MZs*, illustrated in Figure 3.5. This is used to identify which couple of ROIs is associated to higher difference in functional connectivity *between DZs and MZs*.

Difference between intra-pair cross-correlation difference matrix evaluated in DZ couples and the one evaluated for MZ couples

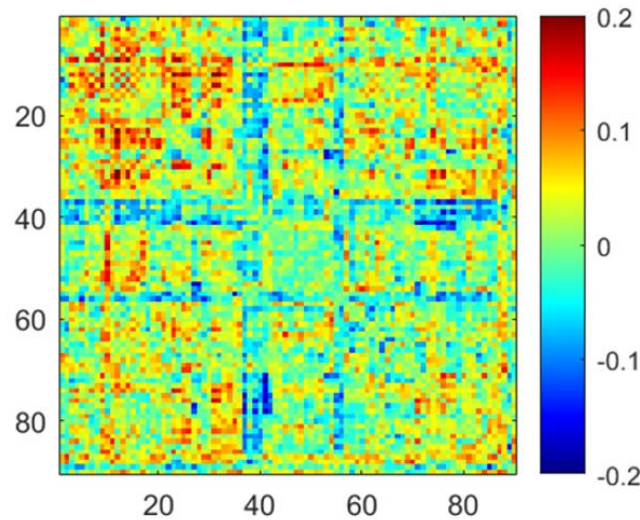


Figure 3.5, Difference between the two averaged intra-pair cross-correlation difference matrices of DZ and MZ twins

The positive points in the Figure 3.5 are associated to a higher intra-pair functional connectivity difference of DZ couples with respect to MZ couples. The red-points indicate the functional connectivity links for which DZ twins have a value of intra-pair functional connectivity more different.

Similarity analysis based on correlation values of r_{MZ} and r_{DZ} of CC matrix

Subsequently, we assess the *intra-pair functional connectivity similarity* of each connection using an intra-pair correlation analysis. The approach is based on applying *partialcorr function* on each element of Cross-Correlation matrices of all Twins 1 and

Twin 2 in a couple, in MZ and DZ twins. It is used to estimate the effect of Zygosity, at net effect of age and sex.

This *intra-pair correlation analysis* has the aim to research for higher similarity in MZs with respect to DZs. After the application of *partialcorr* on each element of the Cross-Correlation matrices, of all Twins 1 and Twin 2 in MZ and DZ couples, we can notice from Figure 3.6 that the correlation values of MZ couples are higher than the correlation values of DZ couples in most of the connections represented in the matrix. This indicates a *higher similarity of MZ couples in the link-level parameter of Cross-Correlation*. If Cross-Correlation indicates the functional connectivity between nodes, this result means that the *functional connectivity between pairs of nodes in MZ twins are more correlated*, with respect to DZs.

If the *intra-pair correlation values of MZs*, calculated for each functional connectivity value between pairs of ROIs, *is higher than those calculated for DZs* it is possible to assume that there is an influence of the genetic component in determining the functional connectivity under investigation. To quantify in a proper way the genetic and environmental influences on the functional connectivity established between ROIs has been applied specific twin models, and the results associated are presented in *Paragraph 4*.

Correlation values in MZs and DZs obtained after the application of *partialcorr*

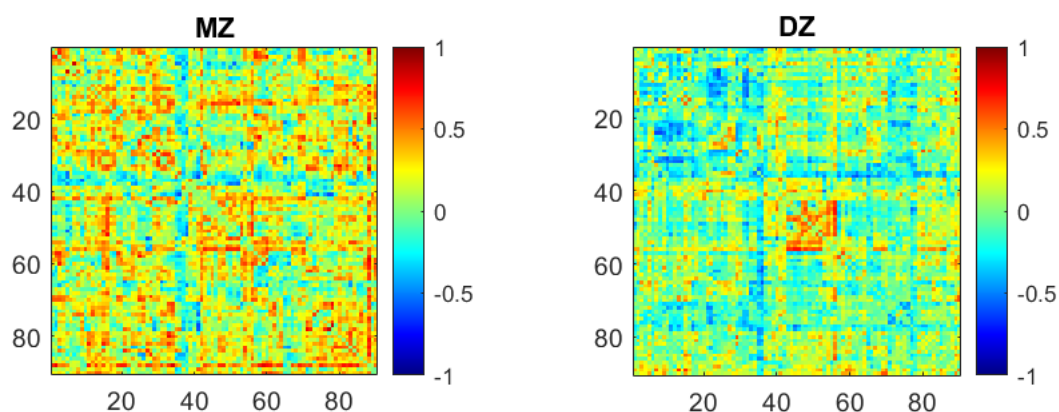


Figure 3.6, Two correlation matrices obtained after applying *partialcorr* on each element of the Cross-Correlation matrix to evaluate the similarity of this parameter between twins.

Unfortunately, for the link-level parameter of CC *none of the intra-pair correlation values of MZs and DZs associated to each link in the matrix*, obtained by applying *partialcorr*

on CC-matrices, *results positive and at the same time significant*. None of the r_{MZ} and r_{DZ} results associated to a probability value lower than the threshold based on Bonferroni correction (Eq.2.2), used for link-level parameters. The absence of significant correlation values of MZs and DZs can be explained by the lower number of subjects in the dataset. If the dataset has a restricted dimension is possible to find non-significant values of correlation.

2.2 Intra-pair Similarity analysis on Mutual Information matrix

As for the Cross-Correlation matrix, also for the Mutual Information matrix are performed two intra-pair similarity analyses. The former is based on the visual inspection of the *intra-pair MI difference between twins the couples*. The latter is an *intra-pair correlation analysis*.

The whole-brain mutual information is obtained starting from the BOLD time series of the 90 ROIs of the AAL atlas. The MI is calculated between each couple of brain regions to obtain a measure of shared information between the time series of each regions.

Considering that the Mutual Information represents a measure of Functional Connectivity between regions, estimated using non-linear metrics, we consider that analysing the similarity between Mutual Information values in MZs and DZs means obtaining a measure of functional connectivity similarity.

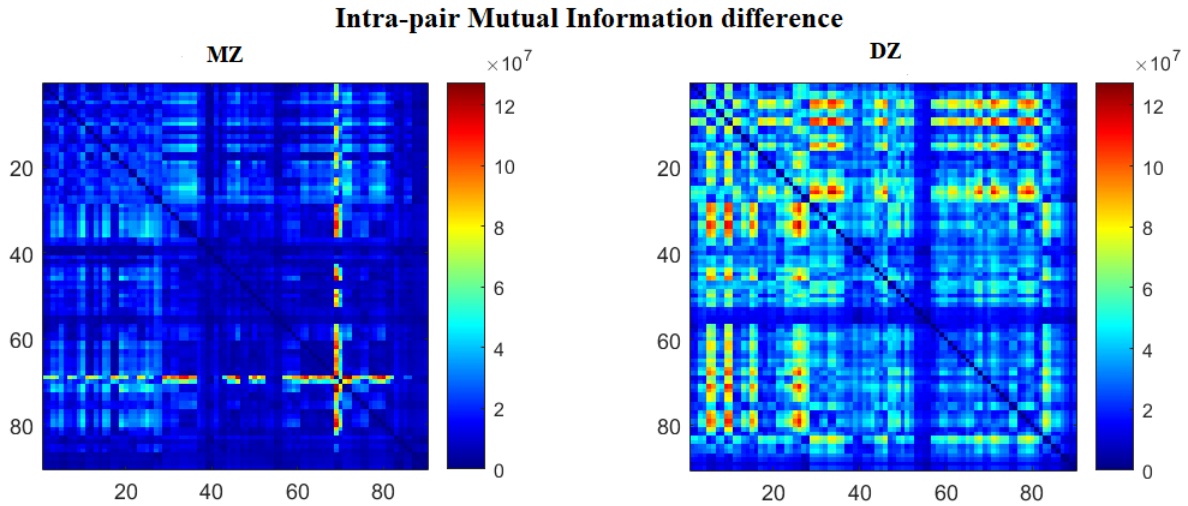
Similarity analysis based on Intra-pair MI difference

Once we obtain the MI matrix for each subject, we estimate the difference of MI between two twins of each couple, separately for MZ and DZ groups. This difference of MI is used to analyse the functional connectivity similarity based on Mutual Information measure between twins in the pair. For this purpose, we apply an analysis based on the calculation of the intra-pair mutual information difference in MZ and DZ twins.

As for Cross-Correlation analysis, we estimate the *two averaged matrices of intra-pair difference of MI across all MZs and all DZs*. In Figure 3.7 are represented the two averaged matrix of intra-pair difference of MI across MZ (left panel) and DZ (right panel) twins in which the rows and columns indicate the 90 ROIs that we consider from AAL

atlas and each element of matrix indicates the mutual information (shared information) between time series of a pair of ROIs.

The *visual investigation* of these panels leads us to observe a **higher similarity of MI in MZ twins with respect to DZ twins, which indicates a higher functional connectivity similarity in MZs with respect to DZs**. This can be deduced by the higher number of blues



colored points in the left panel related to MZ twins, represented a lower difference in mutual information.

Figure 3.7 Intra-pair Mutual Information averaged difference across MZs and DZs

For a visual identification of which couples of ROIs are associated to **higher difference in functional connectivity** between MZs and DZs, we compute the difference between the averaged matrix of DZs and the averaged matrix of MZs represented in Figure 3.7.

The difference between the two averaged intra-pair difference connectivity matrices of DZ and MZ twins is represented in Figure 3.8.

Difference between intra-pair MI difference matrix evaluated in DZ couples and the one evaluated in MZ couples

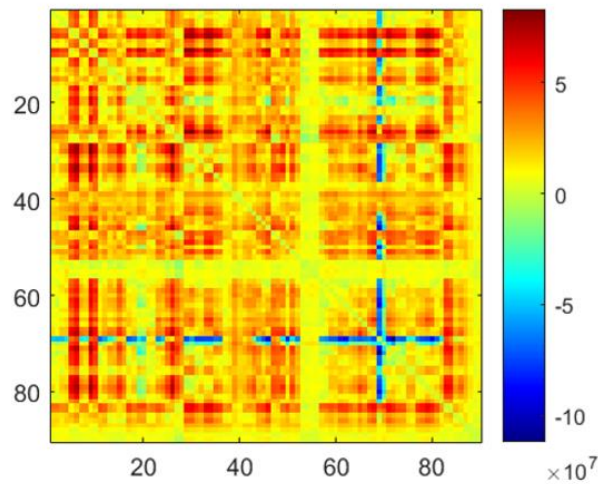


Figure 3.8, Difference between averaged matrices of intra-pair MI difference of DZs and MZs

As for Cross-Correlation matrix, we can observe that the positive points in the Figure 3.8 indicates a higher intra-pair functional connectivity difference of DZ couples with respect to MZ couples. The red-points indicate the functional connectivity links for which DZ twins have a value of intra-pair functional connectivity more different.

Similarity analysis based on correlation values of r_{MZ} and r_{DZ} of MI matrix

As introduced before, in this section are described the results associated to the *intra-pair correlation analysis* that has the aim to research for higher similarity in MZs with respect to DZs.

Considering Mutual Information, this analysis was performed by applying the *partialcorr function* on each element of Mutual Information matrices estimated for Twin 1 and Twin 2 in a couple, in MZ and DZ twins. The *partialcorr function* is used to evaluate the effect of Zygosity on functional connectivity, measures using Mutual Information, at net effect of Age and Sex.

From Figure 3.9 we can observe higher intra-pair correlation values between MZ couples with respect to the correlation values of DZ couples, for most of ROIs' couple represented in the matrix. Based on this visual inspection of the Figure, we can consider to obtain an higher similarity of MZ couples in the link-level parameter of Mutual Information. The MI

represents a measure of functional connectivity, obtained using non-linear metrics, and this result indicates a functional connectivity between pairs of nodes in MZ twins more similar with respect to DZs.

Correlation values in MZs and DZs obtained after the application of *partialcorr*

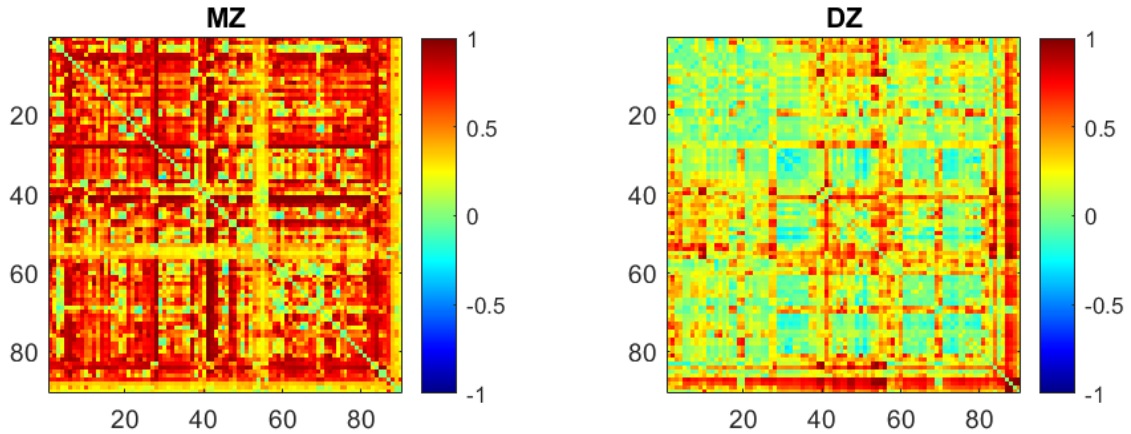


Figure 3.9, Two correlation matrices obtained after applying *partialcorr* on each element of the Mutual Information matrix to evaluate the similarity of this parameter between twins.

For the link-level parameter of MI we obtain **518 links of MI for MZs and 91 links for DZs** associated to a **significant correlation value of r_{MZ} and r_{DZ}** .

Despite the zero values of significant correlation coefficient of r_{MZ} and r_{DZ} that result for the Functional Connectivity matrix of CC, we can verify for the Functional Connectivity matrix of MI that the **functional connectivity created between couple of ROIs in MZ twins are more correlated** than the functional connectivity created between couple of ROIs in DZ twins. This means that **MZ twin pair are associated to a higher similarity** in functional connectivity created between pairs of brain regions.

As for the CC similarity analysis based on intra-pair correlation, if the **intra-pair correlation values of MZs**, calculated for each functional connectivity value of MI between pairs of ROI, is higher than the ones calculated for DZs it is possible to assume that there is an influence of the genetic component in determining the functional connectivity under investigation. This last consideration indicates only an assumption, that need to be verified by applying specific twin model to quantify genetic and environmental influences on the functional connectivity values. The specific results related to the

quantification of the genetic and environmental influences, using twin model, are presented in *Paragraph 4*.

3. Intra-pair Similarity analysis on network-level and node-level topological parameters

In this section we present the results of two intra-pair similarity analyses. As before, the first is an analysis on the *intra-pair difference of the selected parameter* between the twins of the couple. Then, is applied an intra-pair similarity analysis based on the estimation of the *intra-pair correlation values* of the node-level and network-level parameters between MZs and DZs.

3.1 Intra-pair similarity analysis based on Intra-pair difference of network-level and node-level parameters

We first estimate the *intra-pair difference of the selected parameter* (between Twin 1 and Twin 2 in the couple) across MZ and DZ twin couples. We explore the intra-pair distance of each parameter to verify, by using a visual inspection, a higher similarity, or less difference, in MZs with respect to DZs. These results are represented using boxplots.

In the case of *network-level parameters*, we extract the *boxplots* which indicate the distribution of the intra-pair difference of a specific network-level parameter in MZs and in DZs.

From the boxplots represented in Fig. 3.10, Fig.3.11, Fig. 3.12, Fig. 3.13 obtained for the different network-level parameters, we can observe that the *median value* of the distribution of the intrapair difference calculated across MZs, is always lower than the median value of the distribution related to the DZs.

Lower is the median value of the distribution of the intrapair difference, higher is the similarity across subjects for that network parameter.

From this *visual inspection the boxplots* of the different network-level parameters extracted, we can verify the expected *higher similarity of MZ twins with respect to DZ twins in the context of network parameters*.

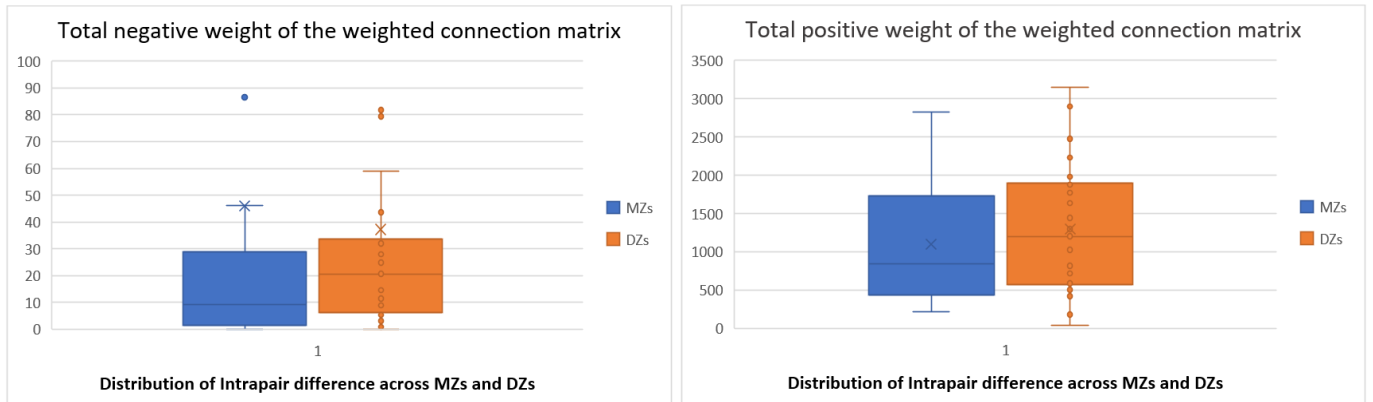


Figure 3.10, Boxplot of intra-pair difference in MZs and DZs, for the network-level parameters of Total negative and Total positive weight

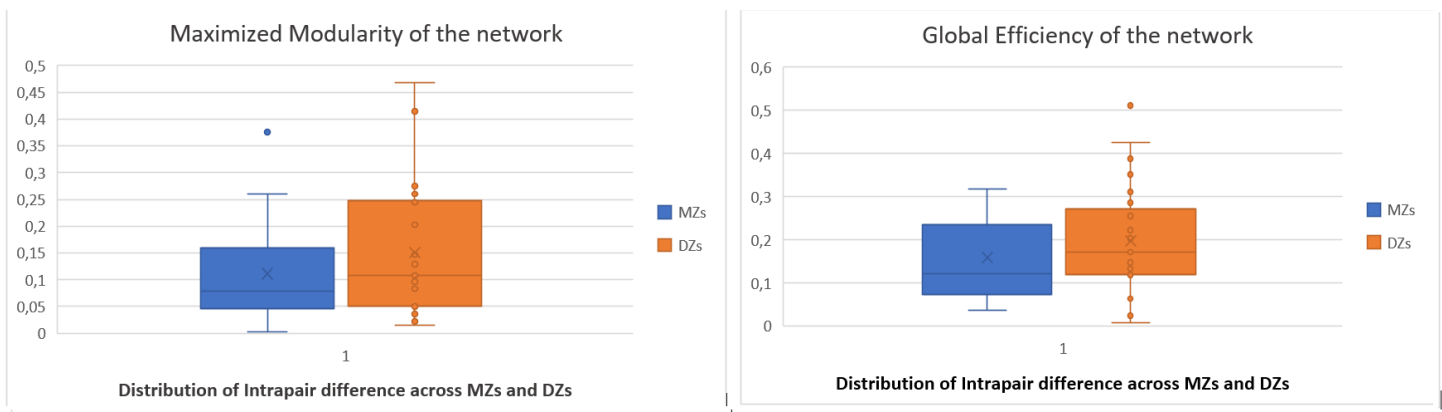


Figure 3.11, Boxplot of intra-pair difference in MZs and DZs, for the network-level parameters of Maximized Modularity and Global Efficiency of the network

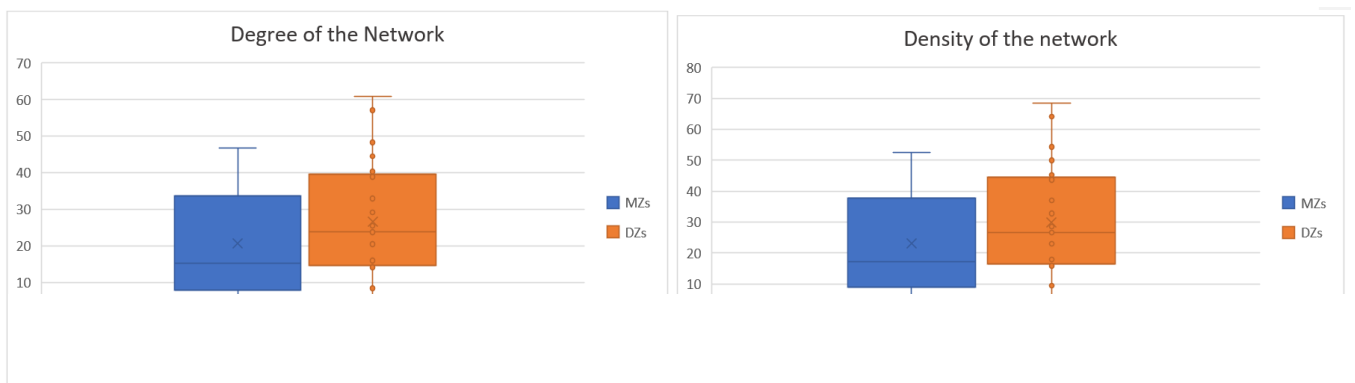


Figure 3.12, Boxplot of intra-pair difference in MZs and DZs, for the network-level parameters of Network Degree and Network Density

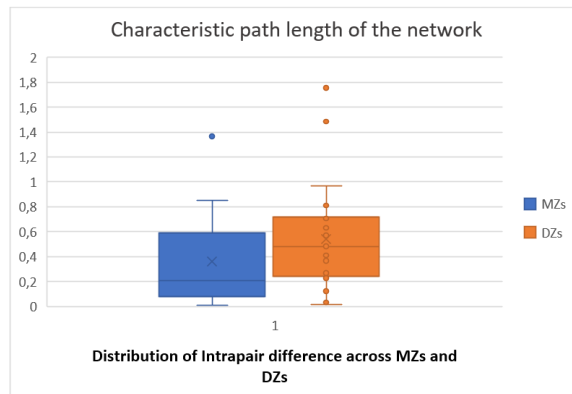


Figure 3.13, Boxplots of the distribution of the intra-pair difference of the network-level parameter of Characteristic path length of the network, across MZs and DZs

In the case of *node-level parameters*, we extract the *boxplots* which indicate the distribution of the intra-pair difference, between Twin 1 and Twin 2 in the couple, for the value of each node across MZs and DZs, calculated for each node-level parameter. We observe that the boxplots representing the distribution of intra-pair difference calculated for each of the **90 nodes is of difficult interpretation**, due to the high number of nodes represented along the horizontal axis. As result, we decide to calculate the *boxplots* which represents the distribution of the intra-pair difference estimated only *for the nodes* that result *suitable for ADE, ACE model* or are associated to *an Epistatic effect*. For example, in Figure 3.14 are reported the boxplots related to the parameter of *Node Degree*. Along the *y axis* is represented the distribution of the intra-pair difference of the nodes that result suitable for one of the three cases of ADE, ACE model or associated to Epistatic Effect. Along the *x axis* are represented the number of nodes for which we report the distribution of intra-pair difference along the y axis. For example, the two upper boxplots represent the distribution of the intra-pair difference (y axis) in each of the 10 nodes (x axis) which result associated to an Epistatic Effect.

From a visual inspection of the boxplots related to the nodes for which results suitable ADE, ACE or Epistatistic Effect, we can observe a *higher similarity of MZ twins with respect to DZ twins for the network-level parameter of Node Degree*. This higher similarity of MZs appears from the *lower median value* of the distribution of the intrainpair difference for MZs, which results closer to zero than the median value of the distribution of DZs. In addition, MZs result more similar, for the node-level parameter of Node Degree, because we can observe from the Figure that values of the MZs' boxplots are less scattered than the

values in DZs' boxplot. This last consideration indicates that the values of intra-pair difference of the parameter of Node Degree for MZ couples are similar to each other and are distributed close to the zero value, indicating a higher similarity (lower difference) between twins in MZ couples.

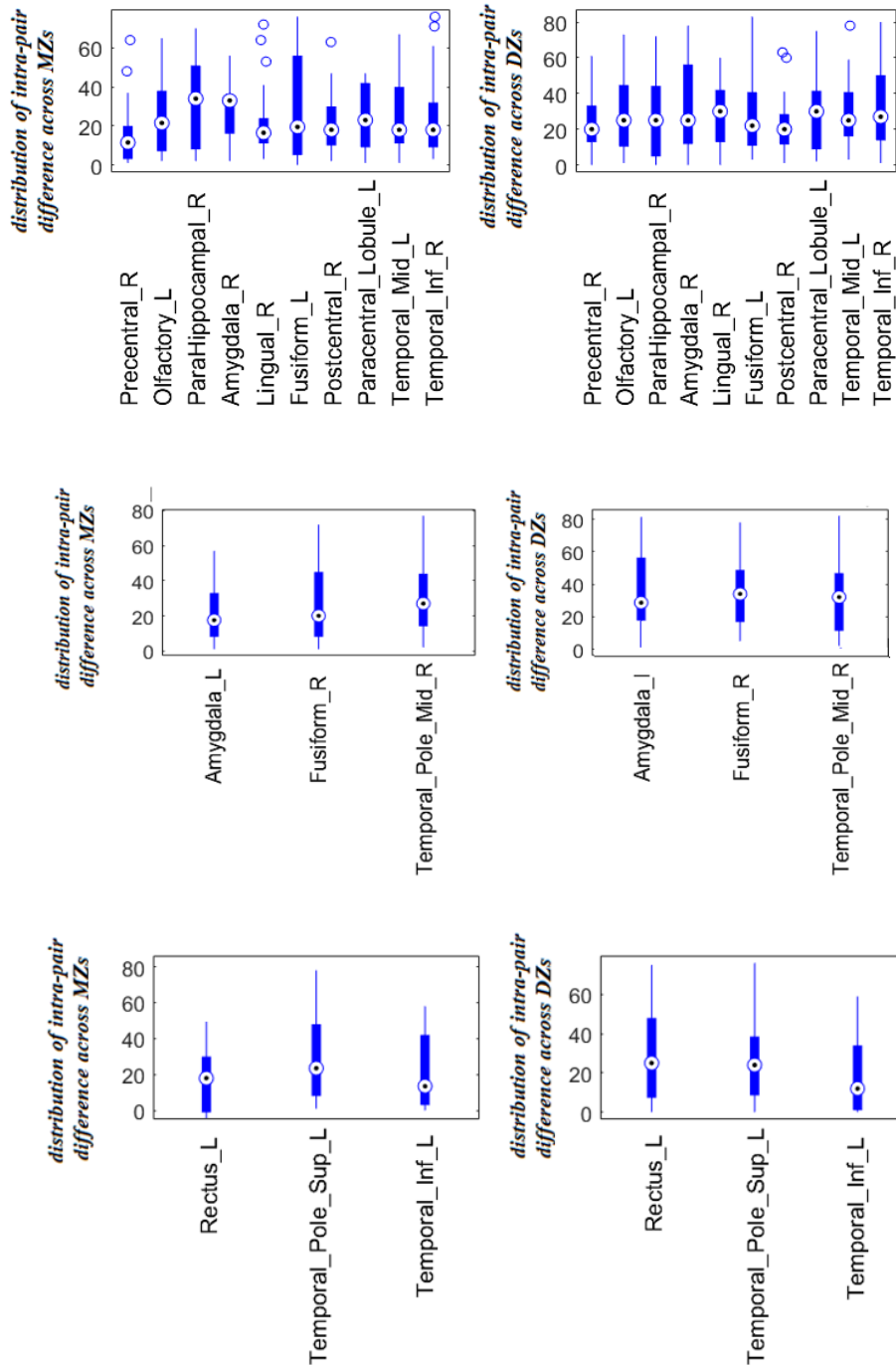


Figure 3.14, Boxplots of the distribution of intra-pair difference for the nodes (along x axis) suitable for ADE, ACE or associated to Epistatic Effect, calculated for the parameter of Node Degree.

3.2 Intra-pair similarity analysis based on correlation values of r_{MZ} and r_{DZ} of network-level and node-level parameters

Subsequently, we analyse the intra-pair similarity between MZs with respect to DZs using a correlation analysis.

The intra-pair correlation analysis is based on the estimation of the Spearman's intra-pair correlation coefficient in MZ and DZ twins separately, for the node-level and network-level topological parameter values. Then, these correlation values are compared between MZs and DZs.

The condition that need to be respected to compare the intra-pair correlation values between MZs and DZs and is also necessary for the analysis of Epistatic Effect, Twins model applicability and the quantitative analysis of the correlation difference ($r_{MZ} - r_{DZ}$) is the positivity of both intra-pair correlation coefficients r_{MZ} and r_{DZ} of MZs and DZs.

Unfortunately, we *did not find positive values of correlation* in DZs related to the *network-level parameters*, probably due to the small twin sample. Thus, network-level parameters were not subjected to the comparison of intra-pair similarity of MZs with respect to DZs based on the intra-pair correlation coefficients r_{MZ} and r_{DZ}

Regarding the *node-level parameters*, we extract the nodes associated with correlation values r_{MZ} and r_{DZ} , calculated across MZs and DZs, *that results positive and significant* in each node-level parameter. A correlation value is considered to be significant if the probability value associated to it is lower than 0.05. The Table reported below indicates the number of nodes for each node-level parameter that result associated positive and significant correlation values for MZs and DZs twins.

TABLE 3.2. NODES THAT RESULT ASSOCIATED TO SIGNIFICANT CORRELATION VALUES FOR MZs AND DZs TWINS

Node-Level Parameter	MZs	DZs
Nodal Strength of positive weights	3 nodes	0
Nodal Strength	3 nodes	0
Nodal Strength of negative weights	13 nodes	1 node
Node Degree	6 nodes	0
Local Efficiency	11 nodes	3 nodes
Clust-Coeff	12 nodes	2 nodes
Betweenness Centrality	6 nodes	7 nodes

For the node-level parameters of *Node Strength*, *Node Degree* and *Nodal strength of positive weights* evaluated for each nodes of the network we obtained a set of *positive and significant correlation values of r_{MZ} , only in MZ couples*.

The presence of positive and significant values of correlation only in MZ couples, underlines the idea that MZ twins are more similar than DZ twins, for the parameter of *Node Strength*, *Node Degree* and *Nodal strength of positive weights* in the relative ROI illustrated in Fig. 3.15, Fig. 3.16, Fig. 3.17. In addition, based on the hypothesis of the Twin Method, this suggests a *higher effect of Genetic factors* in the ROIs associated to these parameters. To correctly quantify the Genetic influence on the values of these parameters in that regions, in this work we have applied Twin Models to estimate the impact of Genetic effects. The results of the application of Twin Models are shown in *Paragraph 4*.

For the node-level measure of *Nodal strength of positive weights* and *Node Strength* emerge the same **3 nodes** ('Frontal_Inf_Orb_R', 'Amygdala_R' and 'Temporal_Pole_Mid_R') associated to positive and significant r_{MZ} . Regarding the

parameter *Node Degree* emerge **6 nodes** with positive and significant values for MZ couples.

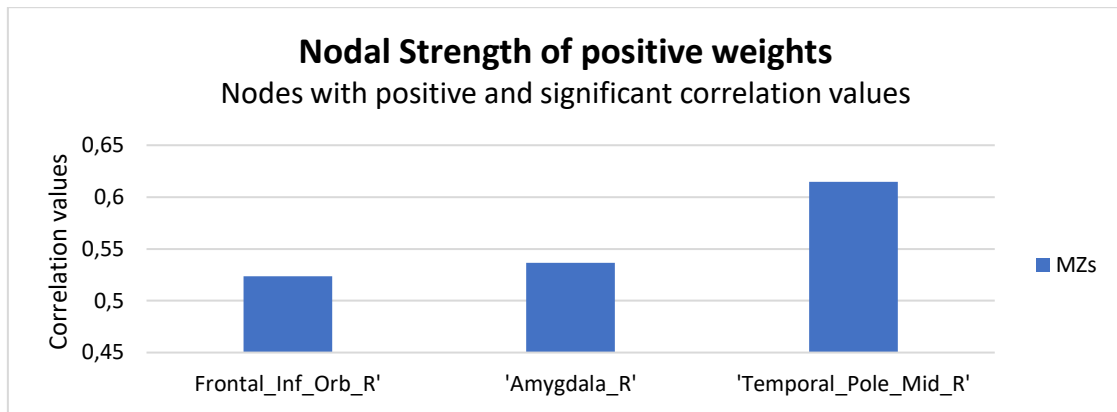


Figure 3.15, Correlation values of node-level Parameter of Total positive weight associated to specific nodes that results positive and significant

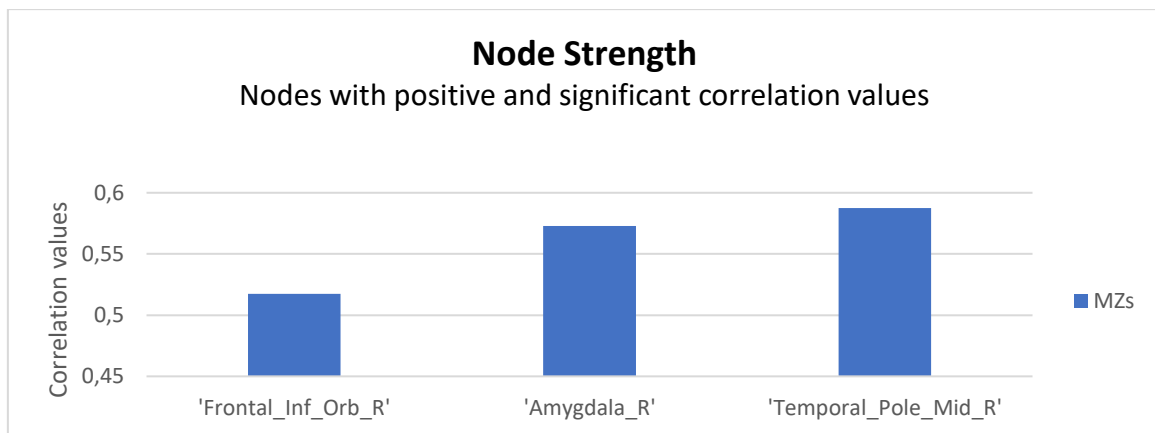


Figure 3.16, Correlation values of node-level parameter of Node Strength associated to specific nodes that results positive and significant

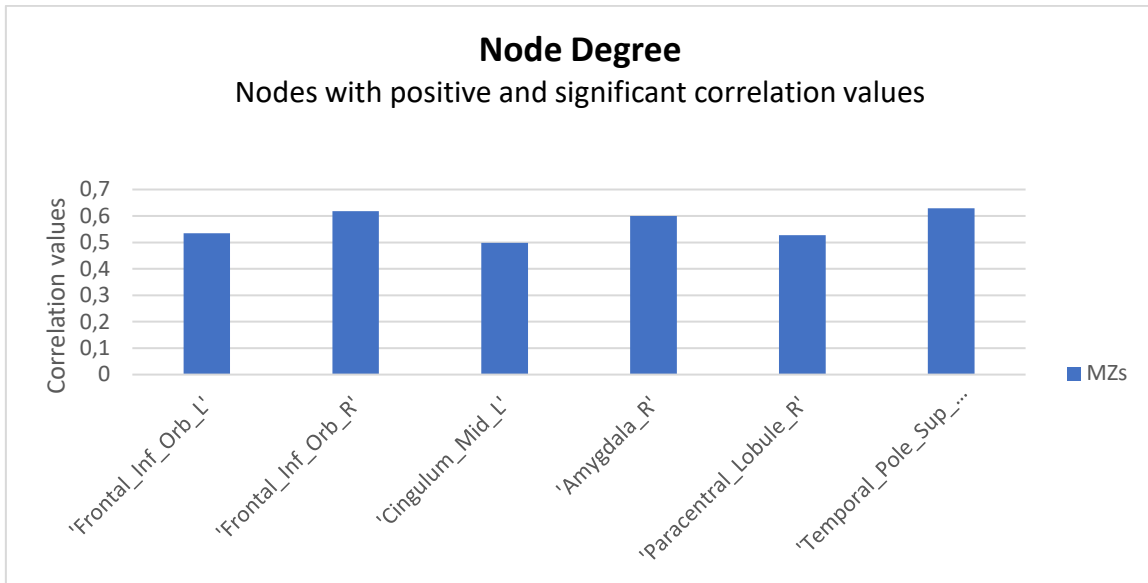


Figure 3.17, Correlation values of node-level Parameter of Node Strength associated to specific nodes that results positive and significant

Differently, analysing node-level parameters of **Nodal Strength of negative weights**, **Node Efficiency (Local Efficiency)**, **Clustering Coefficients** and **Betweenness centrality** calculated for each node we obtain, **in both MZ and DZ couples**, correlation values of r_{MZ} and r_{DZ} **positive and significant**.

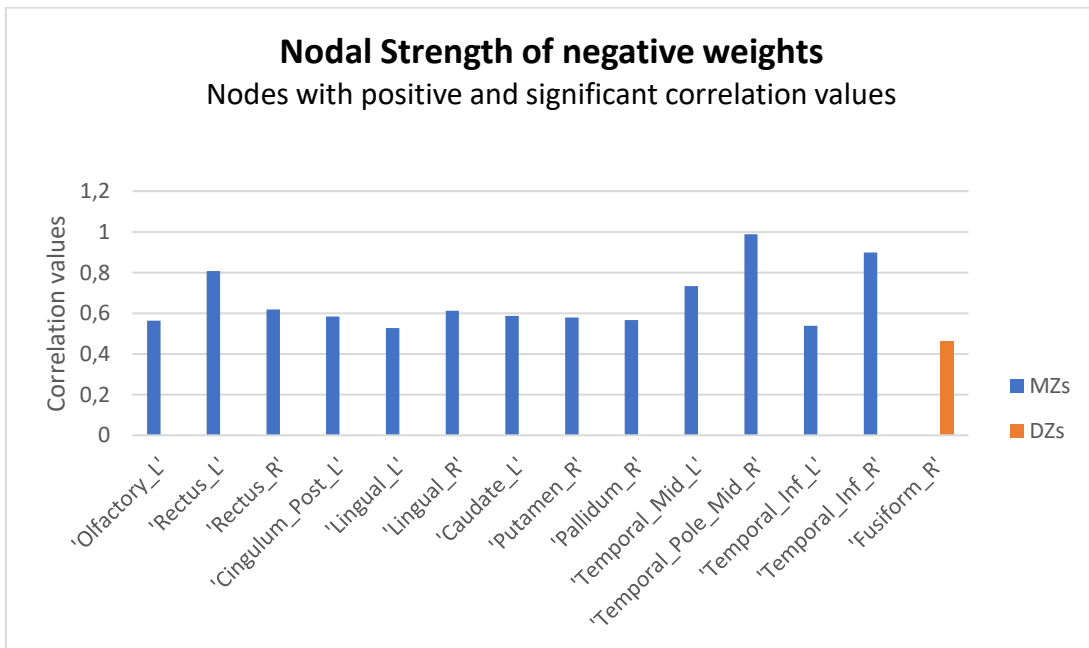


Figure 3.18, Correlation values of node-level Parameter of Total negative weight associated to specific nodes that results positive and significant

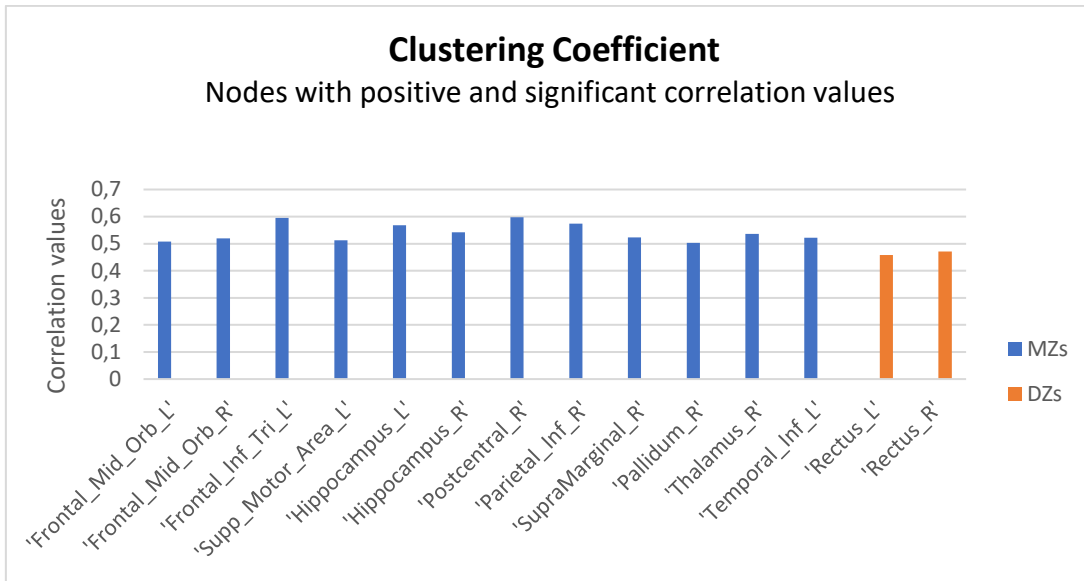


Figure 3.19, Correlation values of node-level Parameter of Clustering Coefficient associated to specific nodes that results positive and significant

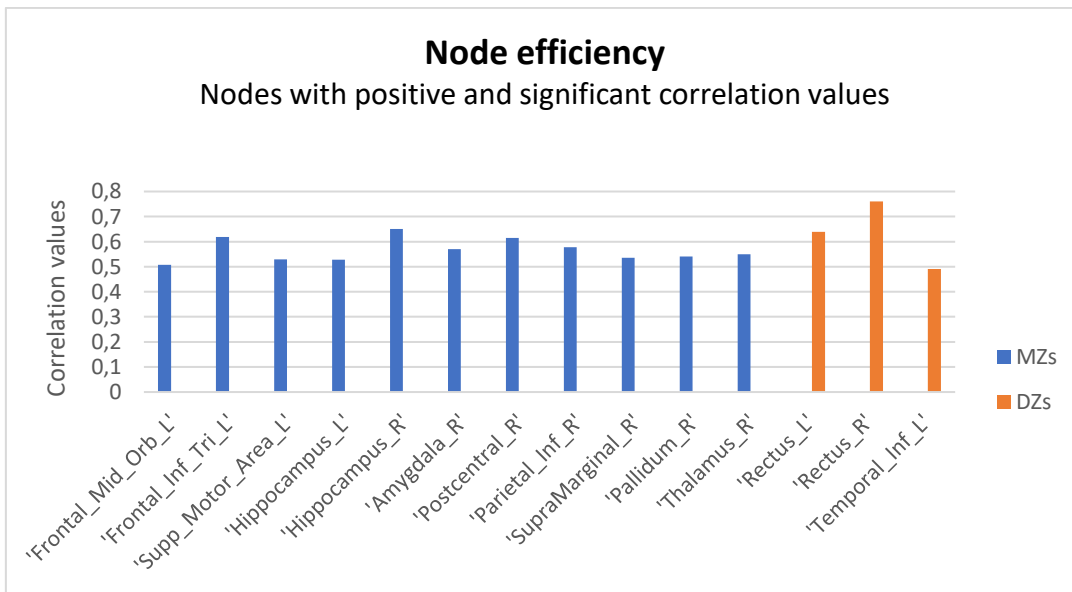


Figure 3.20, Correlation values of node-level Parameter of Node Efficiency (Local Efficiency) associated to specific nodes that results positive and significant

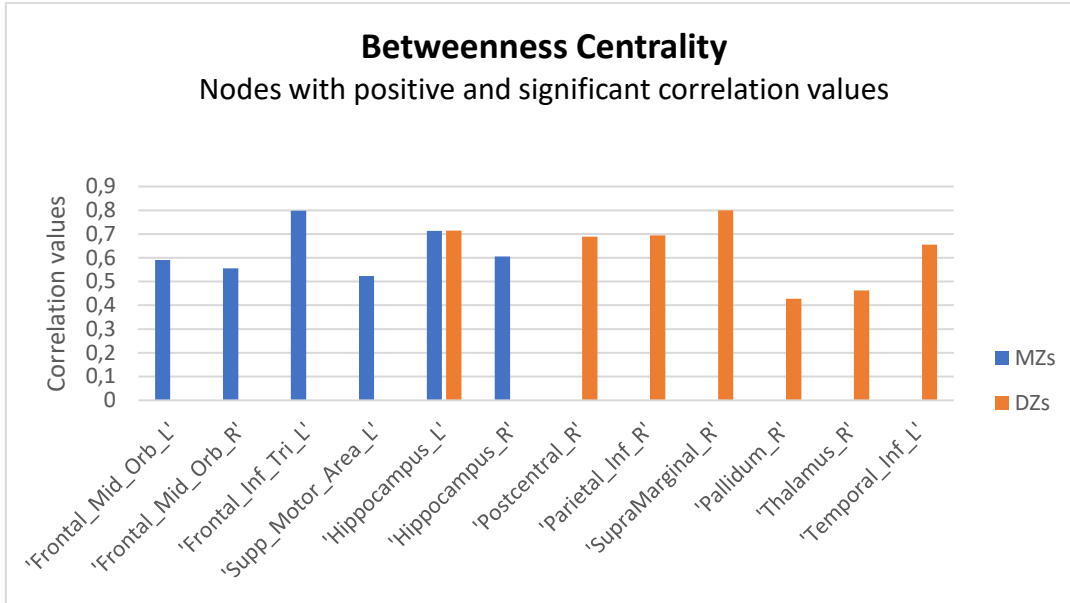


Figure 3.21, Correlation values of node-level Parameter of Betweenness Centrality associated to specific nodes that results positive and significant

In Fig. 3.18 and Fig.19, reporting the correlation values r_{MZ} and r_{DZ} which result *positive and significant* for the parameters of **Nodal strength of negative weights and Clustering Coefficient**, we can observe that the **correlation values r_{DZ} associated to DZ couples emerge to be lower than the correlation values r_{MZ} calculated across MZ couples**. This means that the similarity between Twin1 and Twin 2 in MZ couples is higher than the similarity between Twin1 and Twin2 in DZ couples. If exist a higher number of regions associated with significative correlation values in MZ couples, it suggests that the values of the parameters *Total negative weight* and *Clustering Coefficient* in that regions, are more influenced by Genetic effects.

For the node-level parameter of **Local Efficiency** of the node, the **correlation values of r_{DZ} , estimated in the related DZ couples' regions, result to have equal or higher values** with respect to r_{MZ} estimated in the regions for MZ couples. We can also observe also that MZ couples are associated to a higher number of regions with positive and significant values of correlation, with respect to DZ couples.

The higher number of regions with significant and positive correlation values of MZ couples suggests that the parameter of Local Efficiency is more similar in MZ couples and in these regions is more influenced by Genetic Effect. In the regions in which DZ couples have higher correlation value, we can suppose are associated to less Genetic Influence.

Lastly, for the parameter of *Betweenness Centrality* of the node, the *number of regions with positive and significant correlation values is higher in DZ couples*. The values of correlation in these regions result equal or higher than the correlation values estimated in the regions for MZ couples. For this parameter DZ couples are more similar than MZ couples. It suggests that the parameter of *Betweenness Centrality* is less influenced by Genetic Effects. As was introduced, the precise quantification of Genetic Effects on the value of the node-level parameters is estimated by applying Twin Model.

4. Analysis of Genetic and Environmental Effect on each Topological parameter

4.1 Topological Parameters associated to Epistatic Effect

Due to the fact that we obtain *network-level parameters* associated only to *negative correlation values* in MZ and DZ couples, we do not apply genetic analysis on the network-level parameters and so no Epistatic Effect is associated to them. This means that *network-level parameters are not genetically influenced by genetic factors created by genes at different loci*, that represent the Epistatic Effect.

The analysis of the Epistatic effect across the different *node-level parameters* underline for each nodal parameter the ROIs in which is present an Epistatic Effect, summarize in [Table 3.3](#). If the *Epistatic Effect* is present, this condition indicates that the *values of the specific node-level parameter in these ROIs are influenced by a Genetic Effect that is present at multiple loci*.

TABLE 3.3. EPISTATIC EFFECT EVALUATED IN EACH NODE-LEVEL PARAMETERS.

Node-level Parameters	ROIs associated to Epistatic Effect
<i>Nodal Strength of positive weights</i>	'Frontal_Inf_Orb_L'
	'Frontal_Inf_Orb_R'
	'Amygdala_R'
	'Occipital_Inf_L'
	'Paracentral_Lobule_L'

	'Paracentral_Lobule_R'
	'Heschl_L'
	'Temporal_Pole_Sup_R'
	'Temporal_Pole_Mid_L'
<i>Nodal Strength of negative weights</i>	'Cingulum_Ant_R'
	'Cingulum_Mid_L'
	'Cingulum_Mid_R'
	'Parietal_Inf_L'
	'Precuneus_L'
	'Temporal_Inf_R'
<i>Node Degree</i>	'Precentral_R'
	'Olfactory_L'
	'ParaHippocampal_R'
	'Amygdala_R'
	'Lingual_R'
	'Fusiform_L'
	'Postcentral_R'
	'Paracentral_Lobule_L'
	'Temporal_Mid_L'
	'Temporal_Inf_R'
<i>Node Strength</i>	'Frontal_Inf_Orb_L'
	'Amygdala_R'
	'Occipital_Inf_L'
	'Paracentral_Lobule_R'
	'Heschl_L'
	'Temporal_Pole_Sup_R'
	'Temporal_Pole_Mid_L'
	'Temporal_Pole_Mid_R'

Local Efficiency

'Rolandic_Oper_L'

'Insula_L'

'Temporal_Mid_L'

Clustering Coefficient

'Frontal_Mid_Orb_R'

'Rolandic_Oper_L'

'Insula_R'

'Cuneus_R'

'Paracentral_Lobule_L'

'Caudate_L'

Betweenness Centrality

'Frontal_Mid_Orb_R'

'Lingual_L'

'Parietal_Sup_R'

'Temporal_Pole_Sup_L'

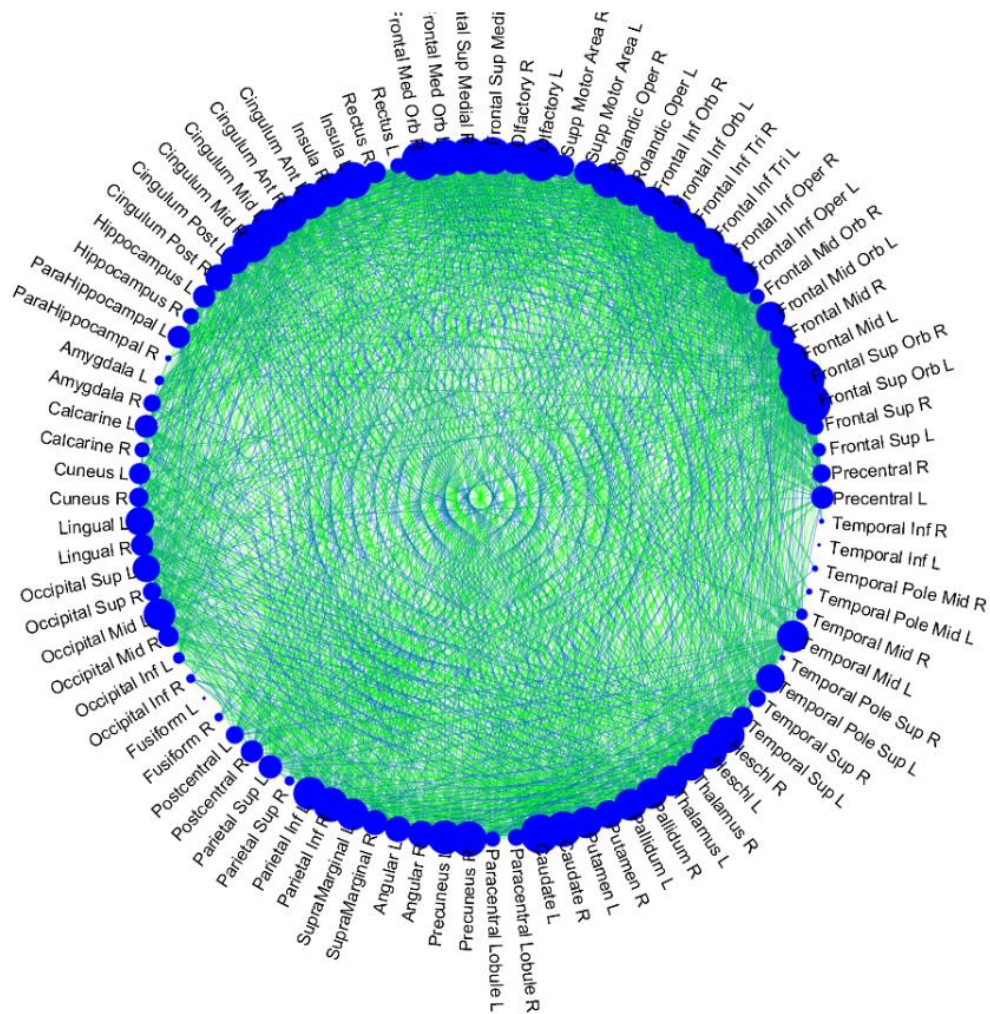


Figure 3.23, MI links that are associated to Epistatic Effect.

From Figure 3.22 and Figure 3.23 we can clearly observe the Epistatic Effect is highly present for all the functional connectivity links between region, for the MI and CC matrix. This means that the **Functional Connectivity matrix is highly influenced by the genetic effect created by genes at different loci.**

Regarding the CC matrix, the Epistatic Effect is present with less intensity in the links that involved nodes in the Hippocampus lobes. In Temporal and Frontal lobes, the Epistatic Effect is present with higher intensity. **Regarding the MI matrix,** the Epistatic Effect is present with less intensity in the links that involved nodes in the Inferior and Medium Temporal Pole, differently from the Frontal lobe in which we notice an Epistatic Effect with higher intensity. These means that the **functional connectivity that involves these regions of MI and CC matrix have less influence of genetic effect of Epistasis.**

4.2 Heritability analysis, ACE and ADE model results

In this chapter are reported the Heritability estimates obtain in the case of ACE or ADE suitable model, for each kind of topological parameters.

We consider ADE or ACE model applicable only when both correlation values r_{MZ} and r_{DZ} associated to the topological parameter result positives.

We do not find positive correlation values of r_{MZ} and r_{DZ} in the case of *network-level parameters*. So, for network-level parameters are not applied ACE model or ADE model analysis. As consequence, we do not calculate heritability estimates for network-level parameters. These indicates that network-level parameter has a value that is less influenced by genetic and environmental effects (described in the ADE or ACE model), with respect to node-level parameter or link-level parameter.

In the case of *node-level parameters*, we obtain a restricted number of nodes, for each node-level parameter, for which ADE and/or ACE model result suitable. In both cases of ADE or ACE suitable model, we extract heritability estimates associated to the specific nodes of the node-level parameters. In the Table 3.4 and Table 3.5 reported below are indicated the Nodes for which ADE or ACE model are considered to be suitable and for which we calculate the Heritability estimates using the Eq. 1.28, in the case of suitable ADE model, and Eq. 1.29, if ACE model is applied.

TABLE 3.4. NODES OF NODE-LEVEL PARAMETERS FOR WHICH IS APPLIED ADE MODEL AND THE CORRESPONDING HERITABILITY ESTIMATES.

Node-level Parameters	Nodes with Heritability Estimate for ADE model	Heritability Estimate for ADE model
Nodal Strength of positive weights	'Precentral_R'	0.1649
	'Lingual_R'	0.2290
	'Occipital_Mid_R'	0.1020
	'Occipital_Inf_R'	0.3796
	'Fusiform_L'	0.2408
	'Temporal_Pole_Sup_L'	0.1694
	'Temporal_Pole_Mid_R'	0.6145

Nodal Strength of negative weights	'Rectus_R'	0.6191
	'Occipital_Sup_L'	0.3207
Nodal Degree	'Amygdala_L'	0.0949
	'Fusiform_R'	0.4593
	'Temporal_Pole_Mid_R'	0.3763
Nodal Strength	'Precentral_R'	0.2032
	'Lingual_R'	0.2265
	'Occipital_Mid_R'	0.1298
	'Occipital_Inf_R'	0.3667
	'Postcentral_R'	0.1610
	'Temporal_Pole_Sup_L'	0.1712
Local Efficiency	'Calcarine_L'	0.2930
	'Cuneus_L'	0.1795
	'Lingual_L'	0.2823
	'Paracentral_Lobule_L'	0.2144
	'Caudate_L'	0.4008
	'Pallidum_R'	0.5404
	'Temporal_Pole_Mid_L'	0.3770
Clustering coefficient	'Insula_L'	0.3428
	'ParaHippocampal_L'	0.0906
	'Calcarine_L'	0.2818
	'Cuneus_L'	0.1798
	'Fusiform_R'	0.3816
	'Pallidum_R'	0.5024
	'Temporal_Pole_Mid_L'	0.3974
	'Temporal_Inf_L'	0.5218
Betweenness Centrality	'Putamen_L'	0.5226
	'Thalamus_R'	0.4925

TABLE 3.5. NODES OF NODE-LEVEL PARAMETERS FOR WHICH IS APPLIED ACE MODEL AND THE CORRESPONDING HERITABILITY ESTIMATES.

Node-level Parameters	Nodes with Heritability Estimate for ACE model	Heritability Estimate for ACE model
Nodal Strength of positive weights	'Rectus_L'	6.6677e-05
	'Rectus_R'	0.0451
	'Fusiform_R'	0.1625
	'Postcentral_R'	0.0608
	'Temporal_Inf_R'	0.3115
Nodal Strength of negative weights	'Frontal_Sup_R'	0.1631
	'Frontal_Mid_R'	0.1774
	'Fusiform_L'	0.2428
Nodal Degree	'Rectus_L'	0.0469
	'Temporal_Pole_Sup_L'	0.0848
	'Temporal_Inf_L'	0.1125
Nodal Strength	'Fusiform_L'	0.1408
	'Fusiform_R'	0.0159
	'Temporal_Inf_L'	0.0167
	'Temporal_Inf_R'	0.3359
Local Efficiency	'Insula_R'	0.3366
	'Cingulum_Post_R'	0.3095
	'ParaHippocampal_R'	0.0394
	'Occipital_Sup_L'	0.0059
	'Occipital_Sup_R'	0.0511
	'Fusiform_R'	0.2640
	'Postcentral_L'	0.2343
Clustering coefficient	'Cingulum_Post_R'	0.3193
	'ParaHippocampal_R'	0.0604
	'Occipital_Sup_L'	0.0090
	'Occipital_Sup_R'	0.0566
	'Postcentral_L'	0.2143
	'Temporal_Pole_Mid_R'	0.0161
Betweenness Centrality	'Frontal_Inf_Tri_R'	0.1025
	'Cingulum_Ant_L'	0.3357
	'Calcarine_L'	0.0023

From this two tables we can observe that the **“broad-sense” heritability estimates** obtained for the nodes ***in which is suitable ADE model***, are higher than the “narrow-sense” heritability estimates obtained for ACE-suitable nodes. This indicates that for the **majority of the nodes, of the node-level parameters that we estimate, the Dominant genetic effect (D) is actually present in the cases of application of the ADE genetic model**, since “narrow-sense” heritability is estimated by the coefficient A (Additive genetic effect) and “broad-sense” heritability is estimated by the sum of the coefficient A (Additive genetic effect) and D (Dominant genetic effect).

We can report **a maximum value of “broad-sense” heritability of 0.6 for ADE suitable nodes**, differently for ACE-suitable nodes related to a maximum value of “narrow sense heritability” of 0.3.

The **ADE-suitable nodes** that are **associated to the higher value of “broad-sense” heritability ($h^2 > 0.6$)** are:

- The Node 'Temporal_Pole_Mid_R', for the parameter of Nodal Strength of positive weights.
- The Node 'Rectus_R', for the parameter of Nodal Strength of negative weights.

Higher is the value of “broad-sense” heritability, higher is the **influence of Additive and Dominant genetic effect** on the node of the parameter, since h^2 is estimated as the sum of the coefficient A and D of the model.

For the nodes that result suitable for ACE or ADE model, we also quantify the **effect of each coefficients of the model** (A, D or E for ADE model, or A, C, or E for ACE model) **on each Nodes**.

In the case of ADE suitable model, for parameters of **Nodal Strength of positive weights, Node Strength, Clustering coefficients and Local Efficiency** the effect in the nodes of the unique environment (coefficient E) is clearly higher than the genetic influence (created by A and D). For all these node-level parameters, the coefficient E has a value always higher than 90%, that indicates that the other coefficients of A and D are characterized by a

common influence of 10%. In Figure 3.24 underline the few cases of nodes, in which the influence of the unique environment is lower than 50%. For the parameter of *LE the node “Pallidum_L”* and for the parameter *Clustering Coefficient the node “Pallidum_L” and “Temporal_Inf_L”* result associated to a unique environment influence lower than 50%. We can observe that in these nodes in which $E < 50\%$ the effect of the Dominant Genetic influence results higher.

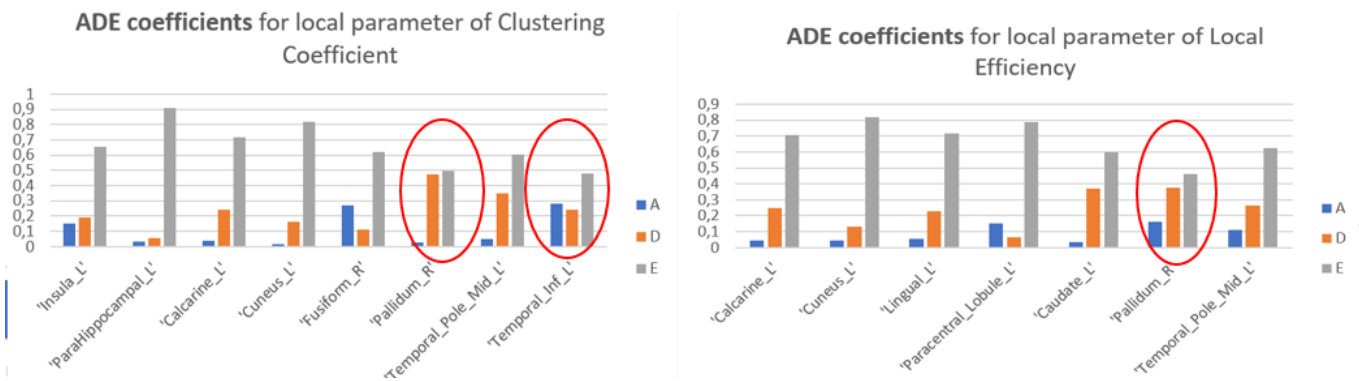


Figure 3.24, Nodes with unique environment influence lower than 50% and Dominant genetic effect higher than 20%.

For parameter of *Nodal strength of positive weights, Node degree and Betweenness centrality* we can observe also an additive and non-additive genetic effect (created by A and D), in some case comparable with the unique environmental effect. In these cases, the effect of the unique environment results for most of the nodes of this node-level parameter higher than 80%. In Figure 3.24 we illustrate the few nodes in which the influence of the unique environment is lower than 50% and we notice that in these nodes results at the same time higher than 40% the influence of the Additive Genetic Effect. These nodes are: “Rectus_L” for the parameter of *Nodal strength of negative weights* and “Putamen_L” for the parameter of *Betweenness centrality*.

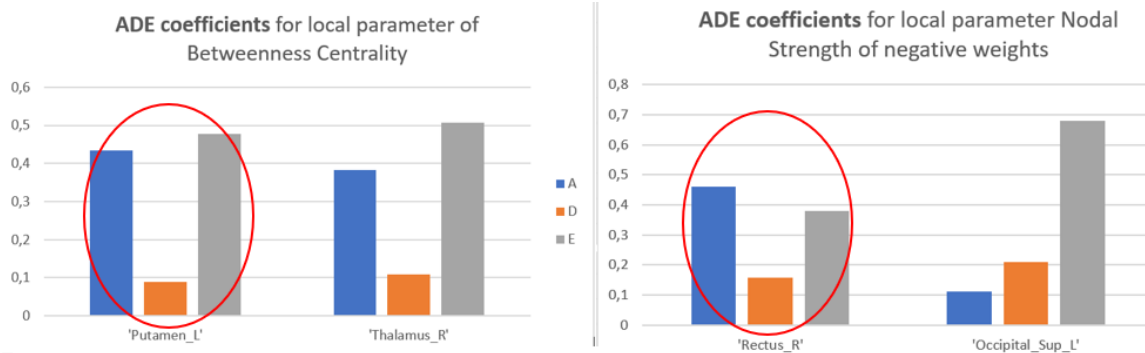


Figure 3.25, Nodes with unique environment influence lower than 50% and Additive genetic effect higher than 40%

In the case of ACE suitable model, for all node-level parameters we observe a clearly higher effect in the nodes of unique environment (coefficient E) with respect to the influence of shared environment (C) and additive genetic (A). We underline in Fig. 3.26 and 3.27 the cases of nodes in which the Common Environment influence is higher than 20%.

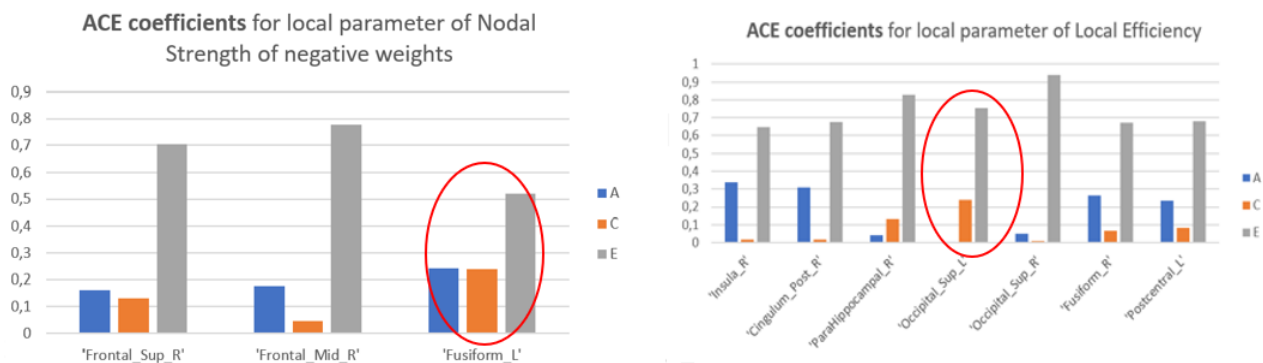


Figure 3.26, Nodes in which the Common environmental influences are higher than 20%

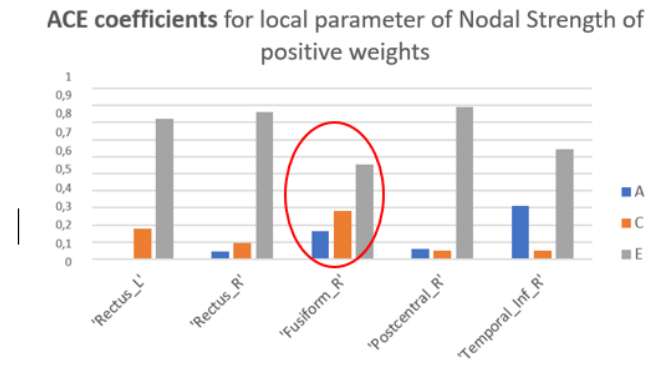


Figure 3.27, Nodes in which the Common environmental influences are higher than 20%

For link-level parameters, using the conditions of Paragraph 6 of Chapter 2 based on the correlation values of r_{MZ} and r_{DZ} , we evaluate if ADE or ACE model is suitable for each couple of ROIs in the Mutual Information and Cross-Correlation matrix. We also extract the heritability estimate of to the Mutual Information and Cross-Correlation associated to each couple of nodes. We decide to extract these heritability estimates for ADE or ACE-suitable model, only for the couple of ROIs that are associated to positive correlation values of r_{MZ} and r_{DZ} . In the Figure 3.28 are represented the links between couple of ROIs for which is applied ADE model (left panel) or ACE model (right panel) for the Functional Connectivity matrix of MI.

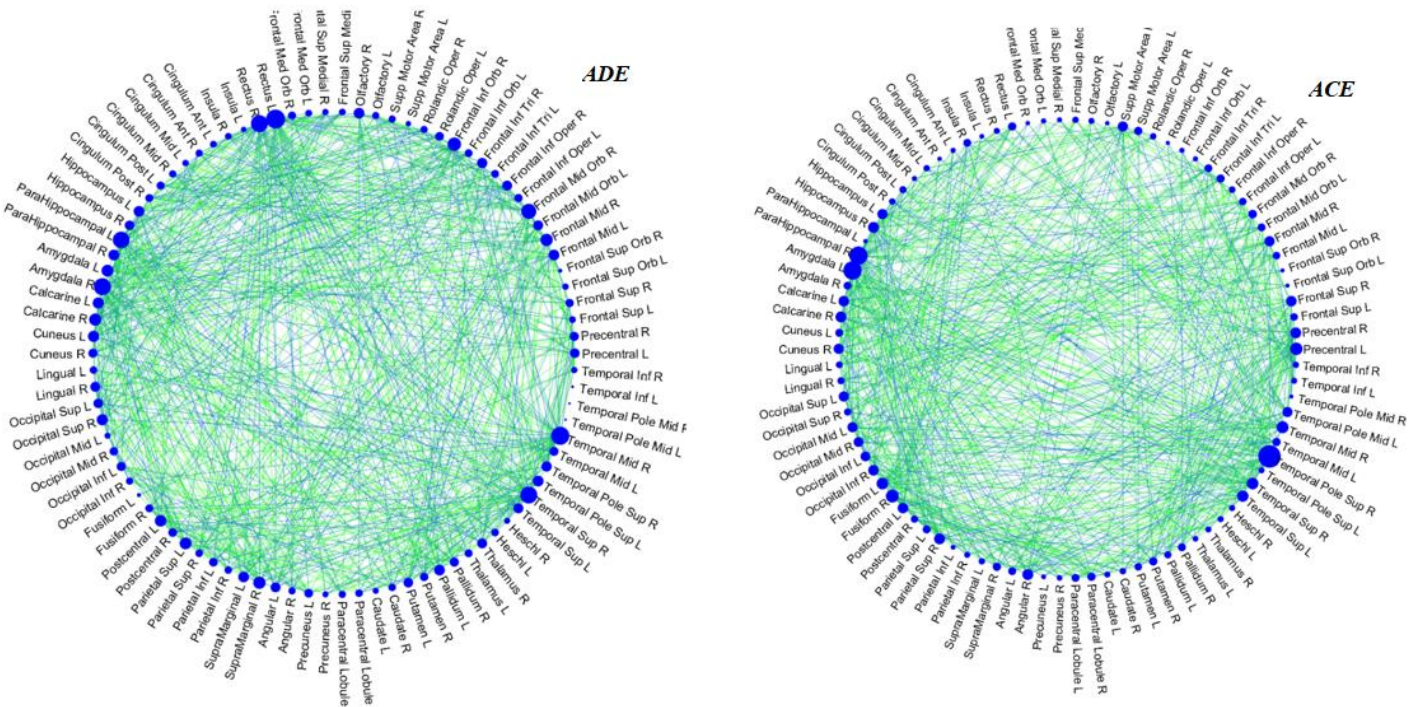


Figure 3.28, Links of functional connectivity between ROIs in which is applied ACE or ADE model for the MI matrix.

As we can observe from Figure 3.28, a higher number of functional connectivity link between couple of ROIs for MI matrix result suitable for ADE model with respect to ACE model. This indicates that these links are more influenced by Additive, Dominant genetic and unique environment influence. From Figure 3.28, we can observe that the functional connectivity links of CC matrix for which is applied ADE model involve node of Right Gyrus Amygdala and Right Medium Temporal Pole. On the other side, the links of CC for which is applied ACE model involve node in the Temporal lobes, Occipital lobes and Right Fusiform Gyrus. Both ADE and ACE models were less applied for the links that involve the node in the Frontal lobes.

In Figure 3.29, are represented the links between couple of ROIs for which is applied ADE model (left panel) or ACE model (right panel) for the Functional Connectivity matrix of CC.

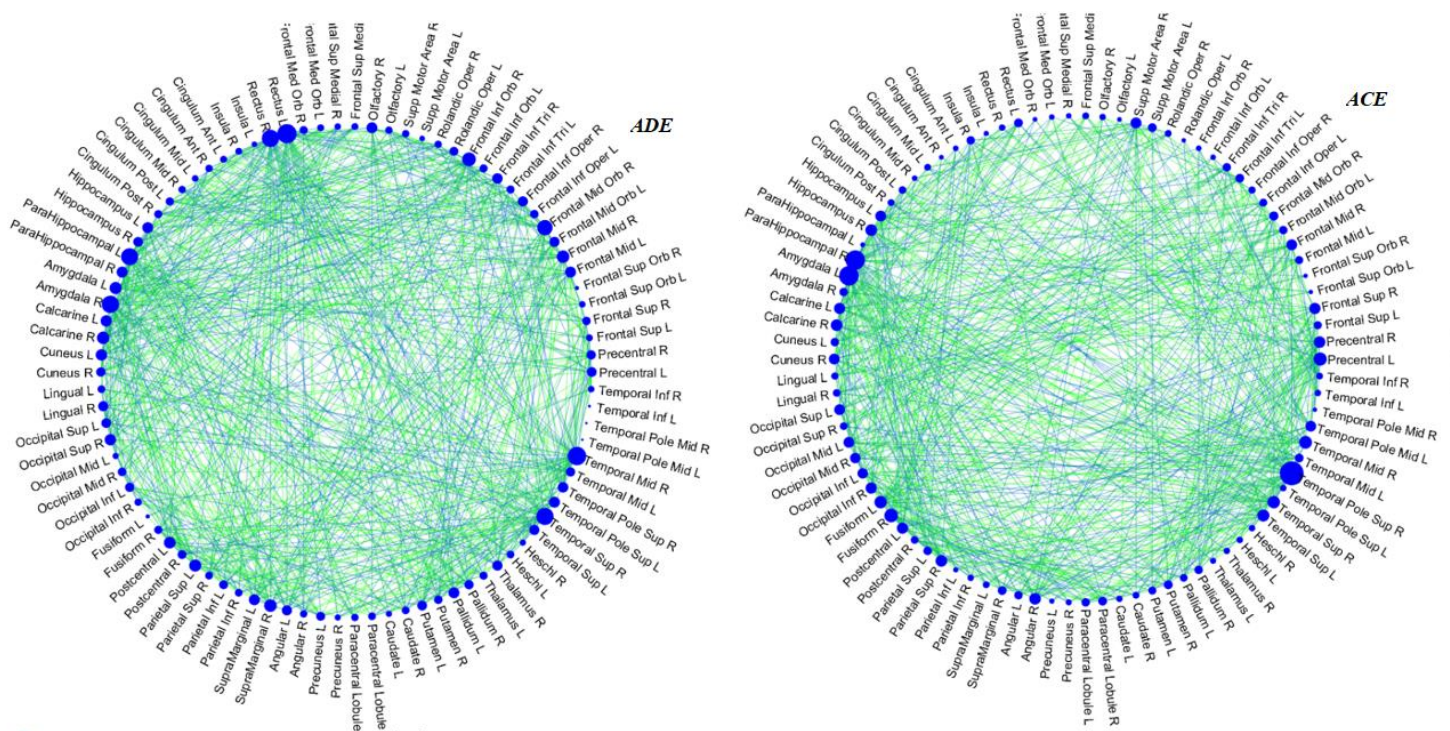


Figure 3.29, Links of functional connectivity between ROIs in which is applied ACE or ADE model for the CC matrix.

From Figure 3.29, we can observe that the functional connectivity links of MI matrix for which is applied ADE model involve pole node in the Medium and Superior Temporal Pole, in

the Medium Frontal Pole, Gyrus Rectus, Hippocampus, Para Hippocampus area and Right gyrus Amygdala. The links of MI for which is applied ACE model involve node in the Superior and Medium Temporal Pole, Right Para Hippocampus area and Left Gyrus Amygdala. Both ACE and ADE model were less applied in the links that involve the node in the Frontal lobes.

By comparing Fig.3.28 and Fig.3.29 we can observe that ***ACE or ADE models are applied more in the links of MI functional connectivity*** with respect to the links of CC functional connectivity matrix. By excluding the genetic and environmental influences described in ACE or ADE model, the remaining functional ***connectivity links of CC that result not suitable for ADE or ACE model could be associated to Epistatic effect or no genetic influence.***

We can observe that a ***higher number of functional connectivity links between couples of ROIs for MI matrix result suitable for ACE model with respect to ADE model.*** This indicates that these links are more influenced by Additive, Common environment and unique environment influence.

In the case of link-level parameters, we obtain a ***matrix of “broad-sense” heritability*** estimated in correspondence of the couple of ROIs for which is suitable ADE model, and a second ***matrix of “narrow-sense” heritability*** estimated for the couple of ROIs for which is suitable ACE model. In Figure 3.30 are represented the “broad-sense” matrix of heritability (when ADE model suitable), in the right panel, and “narrow sense” matrix of heritability (when ACE model suitable), in the left panel, evaluated for the link-level parameter of Mutual Information.

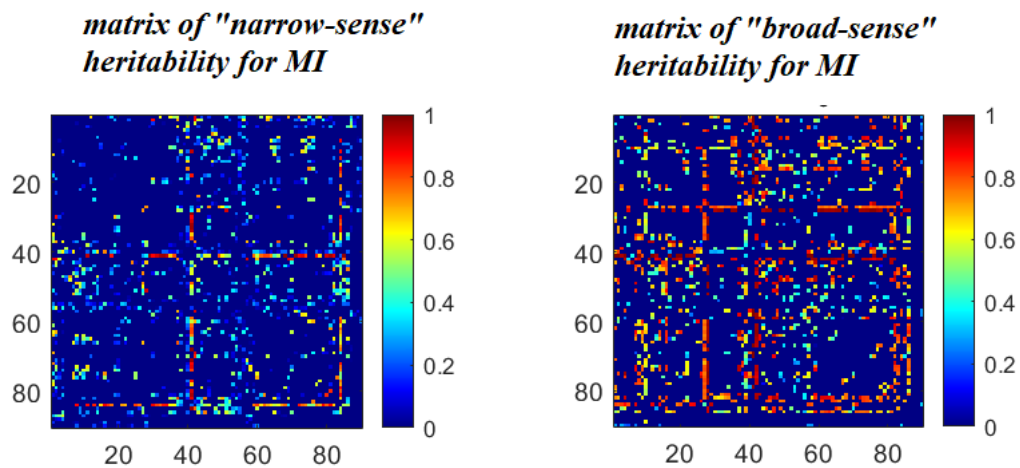


Figure 3.30, matrix of heritability when ACE (left panel) or ADE (right panel) model is suitable for link-level parameter of MI

In Figure 3.31 are represented the same matrices but evaluated for the link-level parameter of Cross-Correlation.

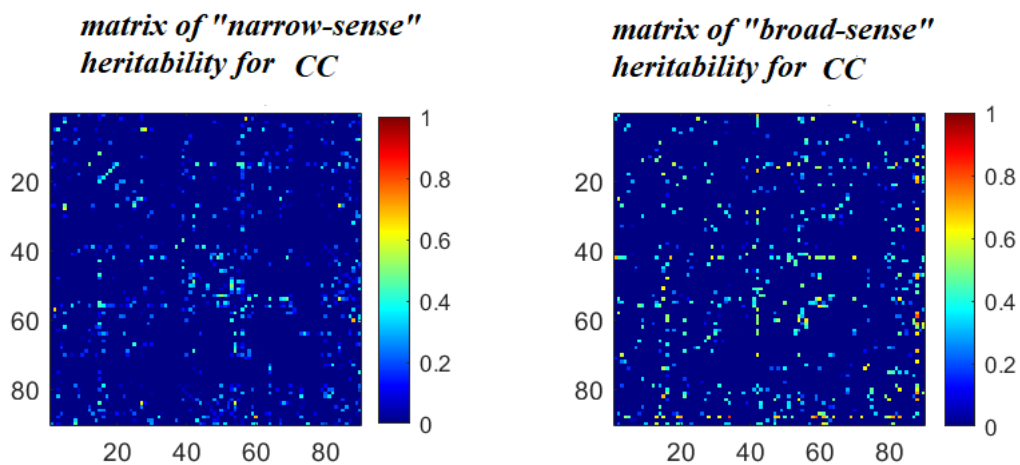


Figure 3.31, matrix of heritability when ACE (left panel) or ADE (right panel) model is suitable for link-level parameter of CC

We can observe from Figure 3.30 and Figure 3.31 that **Mutual Information links** in both cases of ADE or ACE suitable model is **associated to higher value of heritability with respect to Cross-Correlation links**. We can also notice that **for both MI and CC**, the **matrix of “broad sense” heritability**, estimated in the case of suitable ADE model for that couple of ROIs, is associated to **higher value of heritability with respect to the matrix of “narrow sense” heritability**, obtained if ACE model is suitable.

These indicates that the *Functional Connectivity between links of MI matrix are more influenced by Additive and Dominant genetic effects*, since the broad-sense heritability is calculated by the estimation of the sum of the coefficients A and D of the ADE mode.

5. Quantitative analysis on the difference $r_{MZ} - r_{DZ}$ based on the Z Fisher test

In this Paragraph we described the results associated to the *extraction of significant Z Fisher transformed value* for each topological parameter. The Z Fisher transformed value is proportional to the difference of correlation values in MZ and DZ couples, so it can be used to obtain a quantitative analysis of the difference ($r_{MZ} - r_{DZ}$).

We extracted *Z fisher transformed value* for the topological parameters in *three cases*: if the parameter is associated to Epistatic Effect, if is applied ADE model or if is applied ACE model. The other objective is also finding *the cases for which we obtain a higher number of significant Z fisher value*, that indicates significant difference $r_{MZ} - r_{DZ}$.

For *network-level parameters*, no significant Z Fisher transformed value is extracted due to the fact that we do not find positive values of correlation in MZs and DZs associated to the network-level parameters. *The Z Fisher test is performed only if these correlation values of r_{MZ} and r_{DZ} result both positive*. This indicates the presence of no difference of correlation values between MZs and DZs for the parameter calculated at the level of the network.

Regarding the *node-level parameters*, in Table 3.6 we report the Nodes, for each node-level parameter, in which the Z Fisher transformed value result significant. The Z transformed value is obtained considering the values of r_{MZ} and r_{DZ} associated to each node. The significant *Z fisher transformed values are obtained in correspondence of the Nodes for which is suitable ADE, ACE model or Epistatic effect*.

For a certain node-level parameter, if the Z fisher value is significant for a specific Node, it means that for that node-level parameter we find out a significant difference between correlation values of MZs and DZs in that specific Node.

This is a *quantitative analysis on the difference* ($r_{MZ} - r_{DZ}$), *in which a significant Z transformed value indicates a significant difference between the correlation values in MZ and DZ couples.*

TABLE 3.6. NODES OF NODE-LEVEL PARAMETERS FOR WHICH IS WE OBTAIN A SIGNIFICANT Z TRANSFORMED VALUE

Node-level Parameters	Nodes with significant Z value associated to Epistatic Effect	Significant Z values	Nodes with significant Z value suitable for ADE Model	Significant Z values
Nodal Strength of positive weights	'Frontal_Inf_Orb_R'	1.7323	'Temporal_Pole_Mid_R'	1.6632
Nodal Strength of negative weights	'Temporal_Inf_R'	4.2472		
Nodal Degree	'Amygdala_R'	2.0414		
Nodal Strength	'Amygdala_R'	1.7177	'Temporal_Pole_Mid_R'	1.7199
Local Efficiency				
Clustering coefficient	'Frontal_Mid_Orb_R'	1.6852		
Betweenness Centrality				

For node-level parameters *we obtain significant Z fisher transformed value*, which means significant difference $r_{MZ} - r_{DZ}$, *mainly for the nodes associated to Epistatic Effect*.

Only the node-level parameter of *Nodal strength of positive weights* has a significant difference $r_{MZ} - r_{DZ}$ for the *nodes associated to Epistatic Effect* and for one node for which is applied *ADE model*.

In the case of *link-level parameters of CC and MI*, we create a matrix for MI and for CC that contains the significant Z transformed values of each couple of ROIs in MI or CC matrix, obtained considering the r_{MZ} and r_{DZ} associated to this ROIs couple. If the Z transformed value of a couple of ROIs is significant, it means this ROIs couple is associated to a significant difference of correlation values. The significant Z fisher transformed values are obtained in correspondence of the couple of ROIs for which is suitable ADE, ACE model or Epistatic effect. In Figure 3.32 is represented the significant Z fisher value obtained for the couple of ROIs in MI matrix that result associated to Epistatic Effect (left panel), suitable for ADE model (middle panel) or suitable for ACE model (right panel). In Figure 3.33 the same matrices of Z-fisher values are reported for CC.

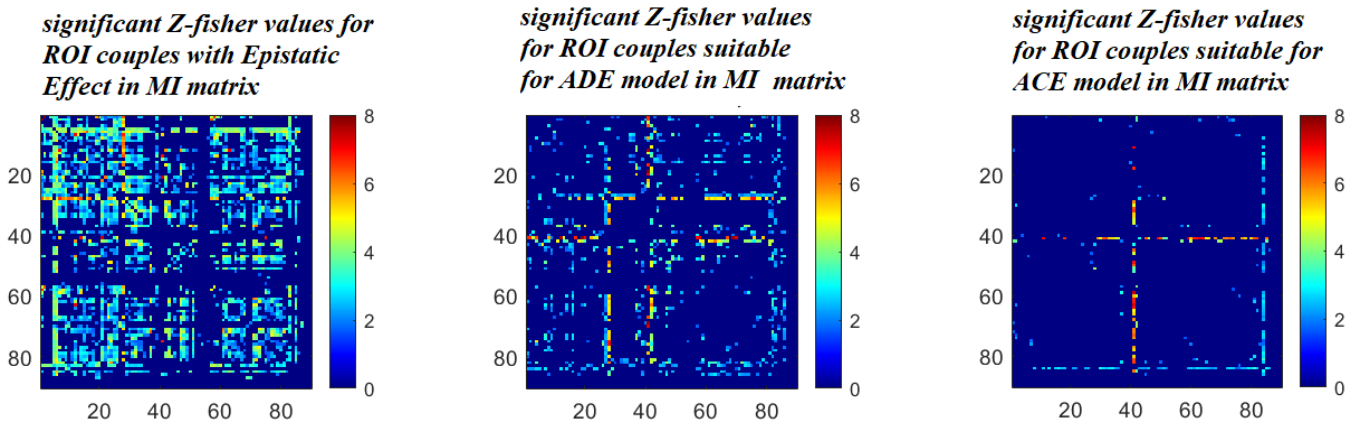


Figure 3.32, Significant Z-fisher values for ROI couples with Epistatic Effect (left panel), suitable for ADE model (middle panel), suitable ACE model (left panel) in MI matrix

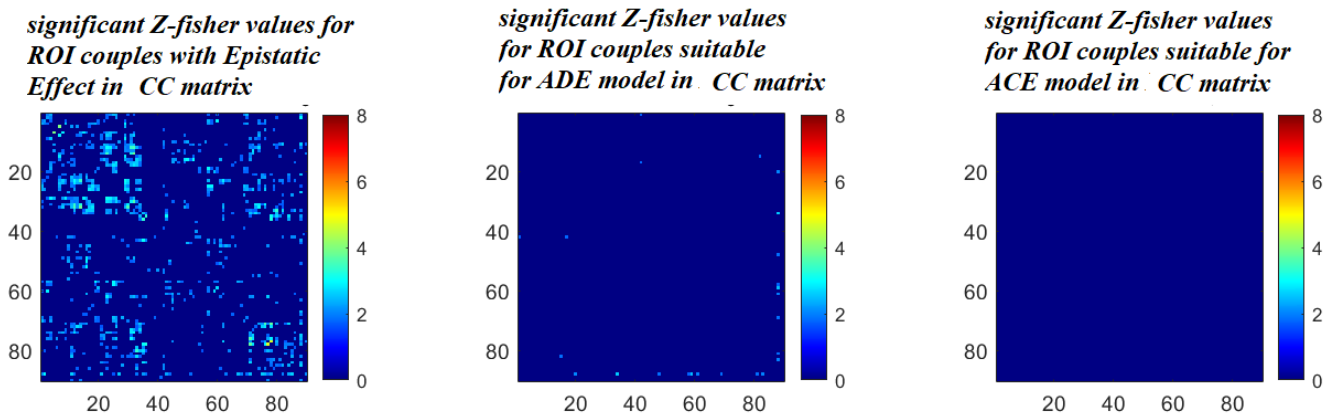


Figure 3.33, Significant Z-fisher values for ROI couples with Epistatic Effect (left panel), suitable for ADE model (middle panel), suitable ACE model (left panel) in CC matrix

For both link-level parameter of MI and CC result a **higher number of significant Z transformed values for the to links that are associated to an Epistatic Effect**, with respect to the ones suitable for ADE or ACE model. This means that the Functional connectivity values of MI and CC between couple of ROIs for which is present an Epistatic Effect are associated to a significant correlation difference between MZs and DZs.

In addition, the **Functional Connectivity of MI evaluated for the couple of ROIs** related to an Epistatic Effect, ADE or ACE suitable models **are characterized by a higher number of significant Z transformed values, with respect to the Cross-Correlation links**. This means that the MI values obtained between couple of ROIs are associated to higher number of significant correlation difference between MZs and DZs, with respect to Cross-Correlation parameter. CC parameter is associated to almost no significant Z fisher value (significant correlation difference between MZ and DZ) for the couple of ROIs suitable for ADE or ACE model.

6. Effects of Age and Sex on the intra-pair difference of the parameters

In this Paragraph are reported the results obtained after applying the function *partialcorr* to evaluate the *relative influence of the variable Age and Sex* on the *intra-pair difference* of the selected parameter in twins' couples, at the net of zygosity associated to the couples.

We analysed only the parameters that result associated to a significant partial correlation coefficient. For *node-level and network-level parameters*, a correlation coefficient is considered to be significant if the associated probability value is lower than 0.05.

Regarding the *link-level parameters*, a correlation coefficient needs to be associated to a probability value lower than a threshold, based on Bonferroni correction (Eq.2) applied on the total number of nodes of the network.

We obtain significant partial correlation coefficients only for some regions related to the *Node-level Parameters*. For *network-level and link-level parameters*, we do not obtain significant result of partial correlation which can describes significant effects of Age and Sex on the intrapair difference of network-level and link-level parameters.

This indicates that at the level of the link or network-level properties of the network does not exist any kind of effect of Age and Sex of the twins couple on the intra-pair difference of the value of this topological parameter between twins in a couple. *Network-level and Link-level parameters have an intra-pair difference value between twins in a couple, that is less significantly influenced by Age and Sex, with respect to node-level parameters.*

The *ROI* associated to a *significant effect of Age and Sex* on the intra-pair difference of the parameter in that ROI, at net of zygosity of the twin's couple considered, are reported in Table 3.7 and Table 3.8. In Table 3.7. are reported the significant partial correlation coefficient, and the relative probability value, between the variable age of the couples of twins and the intra-pair difference associated to a specific node-level parameter in a certain ROI, indicated by *r_Age_Delta* and *p_value_Age_Delta*. Differently, in Table 3.7 are reported the significant partial correlation coefficients (*r_Sex_Delta*) and probability value (*p_value_Sex_Delta*) that describe the effect of Sex on the intra-pair difference evaluated for a certain ROI, for a certain node-level parameter.

TABLE 3.7. SIGNIFICANT PARTIAL CORRELATION VALUES AND RELATIVES PROBABILITY VALUES ASSOCIATED TO THE EFFECT OF AGE ON INTRA-PAIR DIFFERENCE OF THE NODE-LEVEL PARAMETERS

<i>Node-level parameters</i>	<i>Nodes</i>	<i>r_Age_Delta</i>	<i>p_value_Age_Delta</i>
<i>Nodal Strength of positive weights</i>	'Calcarine_R	-0,35765	0,021689
	'Cuneus_R'	-0,33009	0,035054
	'Fusiform_R'	-0,33233	0,03376
<i>Nodal Strength of negative weights</i>	'Lingual_L'	-0,3149	0,044926
<i>Node Degree</i>	'Rolandic_Oper_L'	-0,38214	0,013679
	'Calcarine_R'	-0,30955	0,04889858
	'Fusiform_R'	-0,335	0,032273
<i>Node Strength</i>	'Calcarine_R	-0,35502	0,022745
	'Cuneus_R'	-0,33321	0,033263
	'Fusiform_R'	-0,30814	0,049991
<i>Local Efficiency</i>	'Putamen_L'	0,406876	0,00829
<i>Betweenness Centrality</i>	'Frontal_Sup_Medial_L'	0,317677	0.04297198

TABLE 3.8. SIGNIFICANT PARTIAL CORRELATION VALUES AND RELATIVES PROBABILITY VALUES ASSOCIATED TO THE EFFECT OF SEX ON INTRA-PAIR DIFFERENCE OF THE NODE-LEVEL PARAMETERS.

<i>Node-level parameters</i>	<i>Nodes</i>	<i>r_Sex_Delta</i>	<i>p_value_Sex_Delta</i>
<i>Local Efficiency</i>	'Lingual_L'	0,308275	0,049887
<i>Clustering Coefficient</i>	'Amygdala_R'	0,312015	0,047036
	'Lingual_L'	0,322652	0,039641
<i>Betweenness Centrality</i>	'Frontal_Sup_Orb_R'	0,348244	0,025665
	'Frontal_Inf_Oper_R'	0,370622	0,017061
	'Lingual_L'	0,318215	0,042601

'Heschl_R'	0,317928	0,042798
'Temporal_Pole_Sup_L'	0,314627	0,045124

From the Table 3.7 we can notice that the missing node-level parameter that are not associated to a significant effect of on the intra-pair difference of the parameter between twins, is the Clustering Coefficient. The *intra-pair difference of the Node-level parameter of Clustering Coefficient between twins in a couple is less influenced by the variable of Age.*

From the Table 3.7 we can observe that *most of the significant correlation coefficients r_{Age_Delta}* between the age of the twins couples and the intra-pair difference of the different node-level parameters *are negative*. These results indicate negative relationship between the variable age and the intra-pair difference of the node-level parameters. This means *if the age of the twins couples increases*, the intra-pair difference of the node-level topological parameters decreases and as consequence the *twins couple becomes more similar for these node-level parameters*. The only two positive values of significant correlation and intra-pair difference of the node-level parameter are associated to LE and Betweenness centrality, indicating that the twins couple become less similar for the parameter of LE and Betweenness centrality if the age of the twins couple increases. We decide to represent in the Figure 3.34 below the *scatterplot* which shows the relationship between the *intra-pair difference of the LE* in the region “Putamen_L”, evaluated for each of the 43 couple of twins, and the variable *age*, associated for each couple. From a visual inspection of the Figure 3.34, we can notice that the relationship between the two variables refers to a positive association (positive value of correlation $r_{Age_Delta} = 0.4$) and follow a straight-line relation (linear relationship). This means that the *intra-pair difference of LE in the “Putamen_L” increases by increasing the age of the twins’ pair*. As mentioned before, this might indicate that neurodevelopment is associated with a progressive decrease in twin-to-twin similarity of LE in the left Putamen.

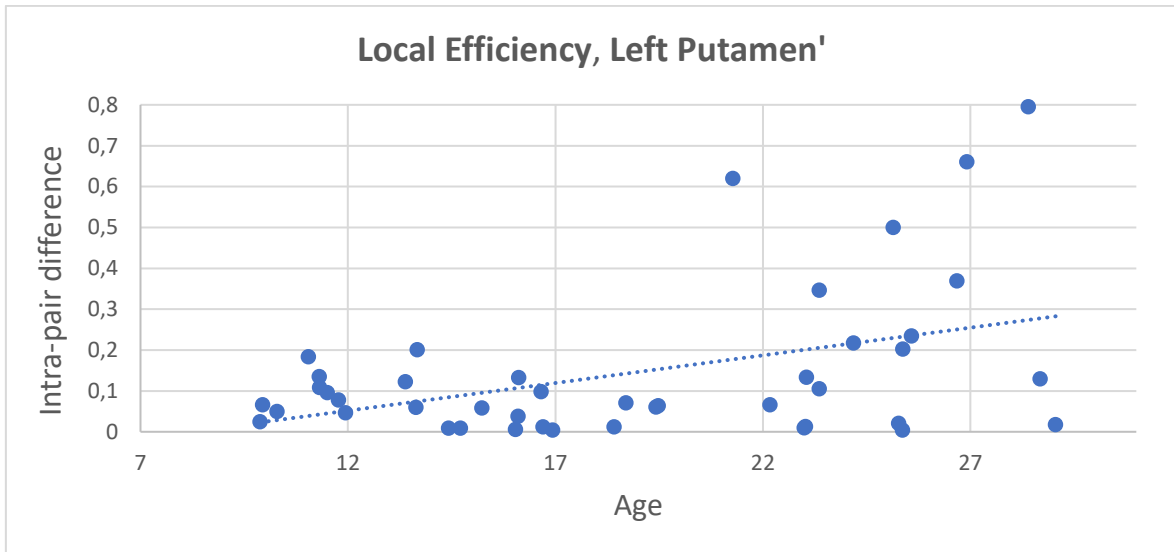


Figure 3.34, Significant Effect of Age, for the node-level parameter of Node efficiency, on the intra-pair difference evaluates in the “Putamen_L”.

In addition, we can also observe that most of the value of intra-pair difference evaluates for each couple of twins is close to zero. This indicates that the value of this LE parameter in this region is similar between twins in a couple, across the different twin’s pair.

From Table 3.8, we can notice that find significant correlation values between the sex and the intra-pair difference of the parameter for all Node-level parameters, except for *Nodal strength*, *Nodal Strength of positive and negative weights* and *Node Degree*.

Then, we decide to analyse which is the ***distribution of the intra-pair difference differentiated for “Male” and “Female” couple of twins***, based on the value of partial correlation coefficient obtained in Table 3.4.

We consider as before the partial correlation coefficients obtained for the parameter LE, in this case in the region “Lingual_L” ($r_{Sex_Delta} = 0.31$), which indicates the presence of significant effect of Sex on the intra-pair difference of the parameter in that region. In the Figure 3.35 is illustrated two boxplots, representing the distributions of the intra-pair differences of LE in this node, one for all “Male” couple of twins and one for all “Female” couple of twins.

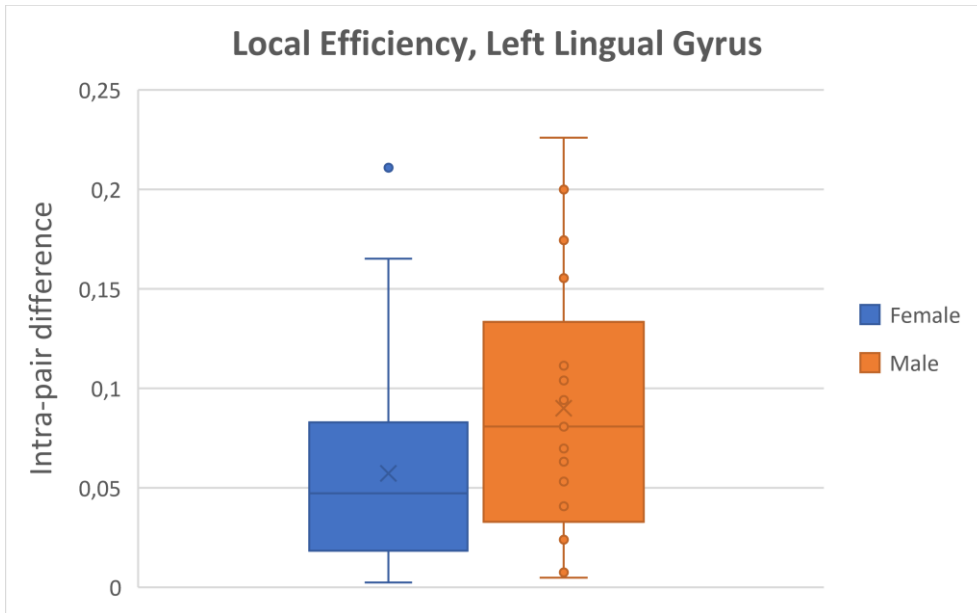


Figure 3.35, Boxplot of intra-pair differences in the region of “Lingual_L” for the parameter of LE, which shows a Significant Effect of Sex.

We can observe from the Figure 3.35 that the *female couples of twins are associated to a more similar value of LE in that region* with respect to male twin couples.

Chapter 4: Conclusion and Further Developments

Generally fMRI data are affected by many kinds of endogenous sources of noise, that are physiological noises created by the head-motion or for example the respiratory and cardiac cycle of the patient, or exogenous artefacts created by other sources that does not include the patient, for example the noise created by experimental instrumentation.

In this context is necessary to introduce a step of data-denoising used to identify the artefacts in the fMRI dataset and remove these components of noise. Independent Component analysis represents a common technique used to identify signal and noise-related patterns in the fMRI data, by using the blind source separation technique that allow to extract statistically independent and non-gaussian components that are linearly combined in the data.

In this work we propose a novel, fast and easy-to-use tool for subject-level ICA based classification of fMRI artefacts. The method relies on an automatic labelling procedure that is used to classify signal and noise-related ICs based on the parameter of Spatial Correlation and Relative percentage of Power Spectra, calculated between the test and the reference ICs. Despite being preliminary, our results associated to this novel tool suggest that the method is versatile and accurate in the classification of unknown ICs resulting from different fMRI protocols. Using a small set of reference ICs, we obtained good accuracy of classification in both task-based and resting-state datasets. Moreover, the method is less time-consuming compared to manual IC labelling and might represent a valid and faster alternative to machine learning techniques.

After testing and validating this tool, this method is applied on the resting-state fMRI twin dataset, obtaining a denoised fMRI dataset.

Starting from the resting-state data was applied a seed-based functional connectivity analysis to analyse the functional connectivity in the brain network. After the parcellation of the brain into ROIs, are estimated of the functional connectivity matrix of Cross-Correlation, based on linear metrics, and Mutual Information, sensible to non-linear variation, whose. These two matrices, indicating link-level parameter of the functional brain network indicate the functional connectivity established between couple of ROIs, regions, in the brain. Starting from the functional connectivity matrix of Cross-Correlation

were extracted the other Node-level and Network-level topological parameters of the brain network.

Subsequently, we have been applied a correlation and similarity analysis between resting-state connectivity patterns of the couples of monozygotic and dizygotic twins, at net of the age and sex associated to the twins couples. Our research is aimed to prove a higher similarity in MZs with respect to DZs, information that could be useful to predict the onset for example of a certain disease. This kind of analysis is called *cross-twin within-trait analysis*, in which the correlation between MZ and DZ twins for the same topological parameter have been computed. If the intra-pair correlation calculated for each topological parameter between MZs is higher than those of DZs, it is possible to assume that there is an influence of the genetic component in determining the parameter under investigation. This last consideration indicates only an assumption, that need to be verified by applying specific twin model to quantify genetic and environmental influences on the value of the topological parameters.

The general trend related to the intra-pair correlation analysis across MZs and DZs shows that for all of topological parameters, except for network-level parameter, we obtain a higher intra-pair correlation values between MZs, that confirms the assumption of a genetic influence on the value of these topological parameters. The functional connectivity based on Mutual Information shows a high intra-pair correlation between MZs for most of the couple of ROIs, with respect to the functional connectivity based on Cross-Correlation. This confirms the assumption of a high genetic influence on the functional connectivity between brain regions, calculated using the non-linear metrics of MI.

Network-level parameters were not suitable for genetic and environmental influences analysis, due to the negative values of intra-pair correlation between DZs, that can be due to the low sample size.

The analysis of genetic and environmental influences has been applied only on node-level and link-level parameters, associated to an intra-pair correlation value that result positive across MZs and also DZs couples. To quantify the relative influences created by different factors, in this thesis work has been applied analysis on the genetic and environmental influences by evaluating if each node and link-level parameter is influenced by an Epistatic effect, if is associated to an Additive, Dominant genetic effect and the factor of Non-shared

environment (ADE model) or if is influenced by the factors of Additive genetic effects, Common and Non-shared environment (ACE model).

The latter analysis shows that connectivity at the level of ROIs, for node-level parameters, and links between ROIs, for link-level parameters, is mostly associated with a high genetic influence created by the Epistatic Effects.

For a comparison between node-level and link-level parameters, considering that a node of the network summarizes the information associated with a certain number of links, we observe that the Epistatic effect is less present for node-level parameter with respect to the link-level parameters of functional connectivity. We can conclude that the majority of the links of functional connectivity, calculated using both MI or CC, established between couple of ROIs are associated to a genetic effect created by Epistasis. For the functional connectivity links of CC, the Epistatic Effect is present with higher intensity in the links that involve the node in the Frontal and Temporal lobe and with lower intensity in the links that involve the node of the Hippocampus. This indicates a higher genetic effect created by Epistasis associated to the functional connectivity links of CC created in the Frontal and Temporal lobe. Differently, we observe a higher genetic effect created by Epistasis in the functional connectivity links of MI created in the Frontal lobe and Hippocampus.

Regarding the application of twin models, it has been observed that for the nodes of node-level parameters that result suitable for ADE or ACE model show a high influence of Non-shared Environment (E), higher than 70% in most of the nodes, with respect to the influence of the Genetic Effects, represented by Additive and Dominant genetic effects for nodes suitable for ADE model and only Additive genetic effects in the case of ACE-suitable model.

In addition, we have noticed that the functional connectivity links of MI result to be more suitable for ADE and ACE model application with respect to the functional connectivity links of CC, indicating that the remaining links of CC for which were not applied ADE or ACE model could be present the effect created by Epistasis or the complete absence of genetic effect.

We also observe that for functional connectivity links of both MI and CC matrix, ADE and ACE model have been applied less in the links created in the Frontal lobes. This indicates

that Frontal lobes result to be less suitable for genetic and environmental analysis. In the case of ADE or ACE suitable model, it was applied respectively “broad-sense” or “narrow-sense” heritability estimation on the value of the node-level parameter and link-level parameter. We found that functional connectivity between ROIs based on MI results associated to higher “broad-sense” and “narrow-sense” heritability with respect to functional connectivity based on CC. Furthermore, for both case of functional connectivity based on MI or CC, the links result associated to higher “broad-sense” heritability than “narrow-sense” heritability. We conclude that “broad-sense” heritability is more present at the level of functional connectivity between brain regions.

Under the assumption of positive intra-pair correlation values of MZs and DZs couples, we performed also a quantitative analysis on the difference of correlation between MZs and DZs. This analysis was applied only on node and link-level parameters. Looking at the distribution of significant Z fisher values for nodes or links associated to Epistatic Effect, ADE or ACE model we found that a higher number of significant Z fisher values for the nodes and links associated to the Epistatic Effect. This indicates that the nodes and links associated to the genetic influence created by epistasis are mostly associated to significant difference of intra-pair correlation values between MZs and DZs.

The last analysis on the significant effect of age and sex on the intra-pair difference of the topological parameter between twins in a couple, has shown us that only some nodes of node-level parameter result associated to a significant effect of age and sex on the intra-pair difference between twins. No significant effect of age or sex is created on the intra-pair difference of Link-level parameters and Network-level parameters between twins. Looking at the nodes with intra-pair difference value significantly influenced by age, we found that most of the significant correlation coefficients between the age of the twins couples and the intra-pair difference of the different node-level parameters are negative. This indicates that for most of the node-level parameters, if the age of the twins couples increases, the intra-pair difference of the node-level topological parameters decrease and as consequence the twins couple become more similar for these node-level parameters of the network.

We believe that this work of thesis presents a novel spatio-temporal tool for the automatic classification of noise-related ICs that indicates an important starting point for an

improvement from a manual classification of ICs and might represent a valid alternative also to machine learning techniques. In future applications, there is the possibility to increase the performances by replacing the already provided reference dataset with ad hoc reference datasets selected and manually labelled by the user. Another future application associated to the introduction of this novel tool, regards the introduction of a third threshold, based on the time course of each Independent Component of the test set, to be used in addition to Spatial Correlation and Relative Percentage of power spectra to correctly classify unknown ICs associated to the subjects in the test set.

We believe that this work introduces important insights related to the functional connectivity methods, topological parameter analysis and heritability of the brain network patterns at the level of the node, link or network for the twin studies.

All the methods related to the analysis of genetic and environmental influences on different types of topological parameters introduce also important insights for the study of the different influences created by different kinds of genetic and environmental factors that affect the brain network during the growth from childhood to adulthood.

In future development, it could be useful to analyse also the Node-level and Network level parameters extracted from the functional connectivity matrix based on the non-linear metrics of Mutual Information, such that it could be possible to make a comparison with the results obtained from the parameter extracted from the functional connectivity matrix based on Cross-Correlation.

Bibliography

- [1] Vijay P.B. Grover, Joshua M. Tognarelli, Mary M.E. Crossey, I. Jane Cox, Simon D. Taylor-Robinson, and Mark J.W. McPhail. *Magnetic Resonance Imaging: Principles and Techniques: Lessons for Clinicians. Clin Exp Hepatol*, 5(3):246-255; 2015
- [2] Blair Mackiewicz. *Intracranial boundary detection and radio frequency correction in magnetic resonance images. Master's Thesis, University of British Columbia, 1995.*
- [3] Chen, J. E., Glover, G. H. *Functional magnetic resonance imaging methods. Neuropsychol Rev*, 25(3), 314, 2015.
- [4] Joseph P. Cousins Anthony T. Cacace, Talin Tasciyan. *Principles of functional magnetic resonance imaging: Application to auditory neuroscience. Journal of the American Academy Audiology*, 11(5):239-72, June 2000
- [5] R M Weisskoff, C S Zuo, J L Boxerman, B R Rosen. *Microscopic Susceptibility Variation and Transverse Relaxation: Theory and Experiment. Magn Reson Med.*, 31(6):601–610, June 1994
- [6] Edson Amaro Jr, Gareth J Barker. *Study Design in fMRI: Basic Principles. Brain Cogn.*, 60(3):220-32, Apr.2006.
- [7] M Poustchi-Amin , S A Mirowitz, J J Brown, R C McKinstry, T Li. *Principles and Applications of Echo-Planar Imaging: A Review for the General Radiologist. Radiographics*, 21(3):767-79, May-Jun 2001.
- [8] Gary H. Glover. *Overview of Functional Magnetic Resonance Imaging. Neurosurg Clin N Am.*, 22(2): 133–139, Apr 2011.
- [9] Kevin Murphy, Rasmus M Birn, Peter A Bandettini. *Resting-state fMRI Confounds and Cleanup. Neuroimage*, Oct 2013, 80:349-59
- [10] David A Leopold, Yusuke Murayama, Nikos K Logothetis. *Very Slow Activity Fluctuations in Monkey Visual Cortex: Implications for Functional Brain Imaging. Cereb Cortex*, 13(4):422-433, Apr 2003

- [11] *H Laufs, K Krakow, P Sterzer, E Eger, A Beyerle, A Salek-Haddadi, A Kleinschmidt. Electroencephalographic Signatures of Attentional and Cognitive Default Modes in Spontaneous Brain Activity Fluctuations at Rest. Proc Natl Acad Sci U S A, 100(19):11053-11058, Sep 2003.*
- [12] *Dietmar Cordes, Victor M. Haughton, Konstantinos Arfanakis, John D. Carew, Patrick A. Turski, Chad H. Moritz, Michelle A. Quigley and M. Elizabeth Meyerand. Frequencies Contributing to Functional Connectivity in the Cerebral Cortex in “Resting-state” Data. American Journal of Neuroradiology, 22 (7) 1326-1333, August 2001*
- [13] *Martijn P. van den Heuvel, Hilleke E. Hulshoff Pol. Exploring the brain network: A review on resting-state fMRI functional connectivity. European Neuropsychopharmacology, 20(8):519-234, August 2010*
- [14] *Kaiming Li, Lei Guo, Jingxin Nie, Gang Li, and Tianming Liu. Review of methods for functional brain connectivity detection using fMRI. Comput Med Imaging Graph, 33(2): 131–139, March 2009*
- [15] *Calhoun V.D., Pekar J.J., McGinty V.B., Adali T., Watson T.D., Pearlson G.D. Different activation dynamics in multiple neural systems during simulated driving. Human Brain Mapping, 16(3):158-67, 2002.*
- [16] *McKeown MJ, Jung TP, Makeig S, Brown G, Kindermann SS, Lee TW, Sejnowski TJ. Spatially independent activity patterns in functional MRI data during the stroop color-naming task. Proc Natl Acad Sci USA, 95(3):803-10, Feb 1998.*
- [17] *Anthony J. Bell, Terrence J. Sejnowski. An Information-Maximization Approach to Blind Separation and Blind Deconvolution. Neural Comput., 7(6):1129-59, 1995.*
- [18] *A. Hyvarinen. Fast and robust fixed-point algorithms for independent component analysis. IEEE Transactions on Neural Networks, 10(3):626-634, 1999.*

- [19] Martin J. McKeown, Scott Makeig, Greg G. Brown, Tzyy-Ping Jung. *Analysis of fMRI Data by Blind Separation Into Independent Spatial Component. Human Brain Mapping, 6:160–188, December 1998*
- [20] Moritz CH, Rogers BP, Meyerand ME. *Power spectrum ranked independent component analysis of a periodic fMRI complex motor paradigm. Hum Brain Mapp., 18:111–122, 2003.*
- [21] Bordier C., Dojat M., Lafaye de Micheaux P. *Temporal and Spatial Independent Component Analysis for fMRI data sets embedded in a R package. Journal of statistical software, 44(9),2010*
- [22] Hyvarinen A, Karhunen J, Oja E. *Independent component analysis. Wiley Interscience, p.267, 2001*
- [23] Calhoun VD, Adali T, Pearlson GD, Pekar JJ. *Spatial and temporal independent component analysis of functional MRI data containing a pair of task-related waveforms. Hum Brain Mapp., 13(1):43-53, 2001*
- [24] Michael D. Greicius, Gaurav Srivastava, Allan L. Reiss, and Vinod Menon. *Default-mode network activity distinguishes Alzheimer's disease from healthy aging: Evidence from functional MRI. Proc Natl Acad Sci U S A.,101:4637–42, 2004.*
- [25] Kiviniemi V., Kantola J., Jauhiainen J., Hyvarinen A. and Tervonen O. *Independent component analysis of nondeterministic fMRI signal sources. Neuro Image, 19(2 Pt 1):253-260, 2003*
- [26] Beckmann C.F., Smith S.M. *Probabilistic Independent Component Analysis for Functional Magnetic Resonance Imaging. IEEE Transactions on Medical Imaging, 23(2):137-52, 2004*
- [27] Ma L., Wang B., Chen X., Xiong J. *Detecting functional connectivity in the resting brain: a comparison between ICA and CCA. Magnetic Resonance Imaging, 25(1):47-56, Jan 2007.*
- [28] Christian F. Beckmann. *Modelling with independent components. NeuroImage, 62(2):891-901, August 2012*

- [29] *Jussi Tohka, Karin Foerde, Adam R. Aron, Sabrina M. Tom, Arthur W. Toga, and Russell A. Poldrack. Automatic Independent Component Labeling for Artifact Removal in fMRI. Neuroimage, 39(3), 1227-124, 2008*
- [30] *Federico De Martino, Francesco Gentile, Fabrizio Esposito, Marco Balsi. Classification of fMRI independent components using IC-fingerprints and support vector machine classifiers. Neuroimage, 34(1), 177-194. 2007.*
- [31] *Gholamreza Salimi-Khorshidi, Gwenaëlle Douaud, Christian F Beckmann, Matthew F Glasser, Ludovica Griffanti, and Stephen M Smith. Automatic Denoising of Functional MRI Data: Combining Independent Component Analysis and Hierarchical Fusion of Classifiers. NeuroImage, 90:449-68, Apr 2014.*
- [32] *Christian F Beckmann, Marilena DeLuca, Joseph T Devlin, Stephen M Smith. Investigations Into Resting-State Connectivity Using Independent Component Analysis. Philos Trans R Soc Lond B Biol Sci., 360(1457):1001-13, May 2005.*
- [33] *Michael D Greicius, Kaustubh Supekar, Vinod Menon, Robert F Dougherty. Resting-state Functional Connectivity Reflects Structural Connectivity in the Default Mode Network. Cereb Cortex, 19(1):72-8, Jan 2009.*
- [34] *David M. Cole, Stephen M. Smith and Christian F. Beckmann. Advances and pitfalls in the analysis and interpretation of resting-state FMRI data. Front Syst Neurosci., 4: 8, 2010*
- [35] *Kiviniemi, V., Starck, T., Remes, J., Long, X., Nikkinen, J., Haapea, M., Veijola, J., Moilanen, I., Isohanni, M., Zang, Y. F., and Tervonen, O. Functional Segmentation of the Brain Cortex Using High Model Order Group PICA. Hum.Brain.Mapp., 30(12):3865-86, Dec 2009.*
- [36] *Cao J, Worsley KJ. The geometry of correlation fields, with an application to functional connectivity of the brain. The Annals of Applied Probability, 9(4):1021-1057, 1999.*

- [37] Felice T. Sun, Lee M. Miller, and Mark D'Esposito. *Measuring interregional functional connectivity using coherence and partial coherence analyses of fMRI data. NeuroImage, 21(2):647–658, 2004.*
- [38] Bugli C., Lambert P. *Comparison between Principal Component Analysis and Independent Component Analysis in Electroencephalograms Modelling. Biometrical Journal, 49(2):312-27, Apr 2007.*
- [39] Catherine M. Barker. *Sample size in twin studies. Master's thesis, Emporia State University, 1988.*
- [40] Arija G. Jansen, Sabine E. Mous, Tonya White, Danielle Posthuma, and Tinca J. C. Polderman. *What twin studies tell us about the heritability of brain development, morphology, and function: A review. Neuropsychology Review, 25(1):27-46, 2015.*
- [41] Jay Joseph. *The Equal Environment Assumption of the Classical Twin Method: A Critical Analysis. The Journal of Mind and Behavior, 19(3):325-358, 1998.*
- [42] Eleonora Maggioni, Letizia Squarcina, Nicola Dusia, Vaibhav A. Diwadkar, Paolo Brambilla. *Twin MRI studies on genetic and environmental determinants of brain morphology and function in the early lifespan. Neuroscience and Biobehavioral Reviews, 109 (2020) 139–149, 2020.*
- [43] Andellini, M., Cannata, V., Gazzellini, S., Bernardi, B., Napolitano, A. *Test-retest reliability of graph metrics of resting state MRI functional brain networks: a review. J Neurosci Methods, 253:183-92, Sep 2015.*
- [44] John S. Witte, John B. Carlin, and John L. Hopper. *Likelihood based approach to estimating twin concordance for dichotomous traits. Genetic Epidemiology, 16(3):290-304, 1999*
- [45] Corrado Fagnani, Sonia Brescianini, Emanuela Medda e Maria Antonietta Stazi. *Metodi statistici per lo studio dei gemelli. Ann. Ist. Super. Sanità, 42(1)-86-93, 2006*

- [46] Daniëlle Posthuma, A. Leo Beem, Eco J. C. de Geus, G. Caroline M. van Baal, Jacob B. von Hjelmberg, Ivan Iachine, and Dorret I. Boomsma. *Theory and Practice in Quantitative Genetics*. *Twin Res.* 6(5):361-376, 2003
- [47] Paul H. Soloff, Richard White, Amro Omari, Karthik Ramaseshan and Vaibhav A. Diwadka. *Affective context interferes with brain responses during cognitive processing in borderline personality disorder: fMRI evidence*. *Psychiatry Res*, 233(1): 23–35, 2015.
- [48] Zhiqiang Ge. *Process Data Analytics via Probabilistic Latent Variable Models: A Tutorial Review*. *Industrial & Engineering Chemistry Research*, 57(38): 12646-12661, 2018.
- [49] Griffanti L, Douaud G, Bijsterbosch J, et al. *Hand classification of fMRI ICA noise components*. *Neuroimage*, 154:188-205, 2017
- [50] Shannon CE, Weaver W. *A mathematical theory of communications*. *Bell System Technical Journal*, 27(2):632–656, 1948